Natural gas sweetening using ionic liquids

Natural Gas Sweetening Using Ionic Liquids

PROEFSCHRIFT

ter verkrijging van de graad van doctor aan de Technische Universiteit Eindhoven,
op gezag van de rector magnificus prof.dr.ir. C.J. van Duijn, voor een commissie
aangewezen door het College voor Promoties, in het openbaar te verdedigen
op donderdag 27 november 2014 om 16:00 uur

door

Mamoun A. M. Althuluth

geboren te Beit Iba, Palestina

Dit proefschrift van het proefontwerp is goedgekeurd door de promotoren en de samenstelling van de promotiecommissie is als volgt:

voorzitter:	prof.dr.ir. J.C. Schouten
1e promotor:	prof.dr.ir. C.J. Peters (The Petroleum Institute, Abu Dhabi)
2e promotor:	prof.dr.ir. M.C. Kroon
leden:	prof.dr. J. Meuldijk
	prof.dr.ir. T.J.H. Vlugt (TU Delft)
	prof.dr. Ing. A.P. Fróba (University of Erlangen-Nuremberg)
	prof.dr. F. Banat (The Petroleum Institute, Abu Dhabi)
	prof.dr.ir. M. van Sint Annaland

A catalogue record is available from the Eindhoven University of Technology Library.

ISBN: 978-90-386-3728-0

Printed by Printservice, Eindhoven University of Technology, The Netherlands.

Cover design by Paul Verspaget, http://www.verspaget-bruinink.nl/

The project was funded by the Gas Research Center of the Petroleum Institute in Abu Dhabi, UAE.

Summary

Natural Gas Sweetening Using Ionic Liquids

The most common technologies for carbon dioxide (CO_2) removal from natural gas streams (natural gas sweetening) are absorption processes with chemical (amine-based) solvents or with physical absorbents. However, these absorption processes have several drawbacks. For instance, amine-based processes suffer from: (i) corrosion, (ii) amine degradation, (iii) solvent losses and iv) highly energy intensive regeneration. On the other hand, physical absorbents have the following drawbacks: (i) the solvents show a high affinity to heavy hydrocarbons, which are removed together with the CO_2, resulting in hydrocarbon losses, (ii) only suitable for feed streams with a sufficiently high CO_2 partial pressure, and (iii) physical solvents can only be used for bulk acid gas removal. As the demand for natural gas has significantly increased in recent years, the need has arisen to develop more effective methods for CO_2 removal from natural gas streams.

This thesis focuses on the applicability of ionic liquids (ILs) as alternative absorbents in natural gas sweetening. The unique properties of ILs include their non-volatility, high thermal stability and high absorption capacity for various gases (e.g., CO_2), making them good candidates for natural gas sweetening processes.

The solubility of CO_2 in the IL 1-ethyl-3-methylimidazolium tris(pentafluoroethyl) trifluorophosphate ([emim][FAP]) was determined by measuring bubble point pressures at different temperatures and compositions using Cailletet equipment. It is shown that CO_2 is more soluble in this IL than in any other IL sharing the same cation. Under gas sweetening operating conditions, [emim][FAP] is thermally stable avoiding contamination of the gas stream with degradation products. Furthermore, [emim][FAP] combines a high CO_2 solubility with a low absorption capacity for small hydrocarbons such as methane (CH_4), ethane (C_2H_6), propane (C_3H_8) and butane (C_4H_{10}) as indicated by high solubility selectivities that can be achieved for e.g., $S_{CO2/CH4}$ = 5.77 to 11.58, depending on the operating conditions. Maximum selectivities for CO_2 removal from small hydrocarbons are achieved at lower temperatures and found to be higher than selectivities in other ILs and physical solvents. This observation confirms that [emim][FAP] is a promising candidate that can compete with commercially available physical solvents for gas sweetening processes.

The absorption behavior of the heavier aliphatic hydrocarbons (hexane, heptane) and aromatic hydrocarbons (benzene, toluene, ethylbenzene and xylene, collectively called BTEX) in [emim][FAP] IL has been studied. This information is of utmost importance, because of the severe problems that BTEX can cause in the sulfur recovery unit, during natural gas liquefying, and also as emissions. It was observed that the solubility of aliphatic hydrocarbons in [emim][FAP] is relatively low, thus they will remain in the natural gas stream. This is an advantage because these compounds have a high heating value and they can be liquefied for various commercial and industrial applications. The solubility of the BTEX compounds in [emim][FAP] IL is high. This is desirable, because the BTEX compounds will be removed from the natural gas together with the acid gases, so that plugging problems in the liquefying units, which can be caused by BTEX will be minimized. However, full recovery of the BTEX compounds from the acid gas stream (without any emissions) is required in order to protect the catalyst bed in the sulfur recovery unit from coking that could be caused by BTEX components.

The experimental measurements of phase equilibria of mixtures with ILs are expensive and time-consuming. Therefore, the Peng Robinson equation of state (PR-EoS), combined with quadratic mixing rules was used to correlate the experimental gas solubility data over a wide temperature range (293- 363K) and pressures up to 11 MPa. This research established that the experimental data of all binary mixtures of small hydrocarbons such as CH_4, C_2H_6, C_3H_8 or C_4H_{10} + [emim][FAP] could be accurately correlated by using only one linearly temperature-dependent binary interaction parameter with an average absolute deviation (*AAD*) less than 1%, while, on the other hand, the solubility data of the binary mixture CO_2 + [emim][FAP] required two binary interaction parameters to yield the *AAD* of less than 3%. Ternary liquid-liquid equilibrium data of aliphatic + aromatic + IL systems were also correlated using the NRTL (Non-Random Two Liquid) model.

The IL [emim][FAP] was also incorporated in a supported ionic liquid membrane (SILM), because it has several advantages over conventional absorption, such as lower capital cost (less IL needed), and simpler process equipment. For that purpose, [emim][FAP] was impregnated successfully in the γ-alumina layers of a tubular porous asymmetric membrane. The pure gas permeability of natural gas components, such as CO_2, CH_4, C_2H_6 and C_3H_8 were tested through the SILM at a trans-membrane pressure of 0.7 MPa and at a temperature of 313 K. The following trend of pure gas permeability was observed for the SILM in this study:

$P_{CO2} > P_{CH4} > P_{C2H6} > P_{C3H8}$. Moreover, the CO_2/CH_4 ideal permselectivity was calculated. Mixed gas permeabilities and permselectivities for the binary mixture of CO_2/CH_4 (50/50%, v/v) were also measured. The mixed gas permselectivity (α = 1.15) was found to be much lower than the ideal permselectivity (α = 3.12). The performance of the SILM was negatively affected by the presence of water, which is also generally present in natural gas. Therefore, the natural gas stream should be dehydrated before it is fed into the SILM. Even though [emim][FAP] is an excellent alternative absorbent with high CO_2 absorptive capacity and selectivity (e.g., $S_{CO2/CH4}$ = 9.69), the incorporation of this IL in a SILM is less promising for the removal of CO_2 from natural gas streams, because the permselectivity for CO_2/CH_4 is low (α = 1.15) in that case.

Samenvatting

Verzoeten van aardgas middels ionische vloeistoffen

De meest gebruikelijke technologie voor koolstofdioxide (CO_2) verwijdering uit aardgas (gaswassen, verzoeten ofwel het verwijderen van zure gassen) is gebaseerd op absorptie, waarbij gebruik wordt gemaakt van chemische (aminegasbehandeling) of fysische absorbentia. Echter, deze absorptieprocessen hebben een aantal nadelen. In het geval van amines zijn dit: i) corrosie, ii) afbraak van de amines, iii) verliezen van het oplosmiddel en iv) een zeer energie intensieve regeneratieproces. Fysische absorbentia hebben de volgende nadelen: i) het oplosmiddel heeft hoge affiniteit voor zware koolwaterstoffen, die samen worden verwijderd met CO_2 wat resulteert in verspilling van koolwaterstoffen, ii) ze zijn alleen geschikt voor voedingsstromen met een voldoende hoge CO_2 druk en iii) de fysische oplosmiddelen kunnen alleen toegepast worden voor de bulk zure gassen afscheidingen. De laatste jaren is de behoefte naar aardgas toegenomen en is daarmee ook de vraag gerezen voor de ontwikkeling van meer efficiënte methoden waarbij CO_2 uit de aardgasstromen wordt verwijderd.

Dit proefschrift richt zich op de toepassing van ionische vloeistoffen als alternatieve absorbentia voor het verzoeten van aardgas. De unieke eigenschappen van ionische vloeistoffen, onder andere de extreem lage dampdruk, hoge thermische stabiliteit en hoge absorptiecapaciteit voor verschillende gassen (bijv. CO_2) maken van ionische vloeistoffen goede kandidaten voor gaswasprocessen.

De oplosbaarheid van CO_2 in de ionische vloeistof 1-ethyl-3-methylimidazolium tris (pentafluoroethyl) trifluorfosfaat ([emim][FAP]) werd gemeten door de kooklijn te bepalen bij verschillende temperaturen en samenstellingen door middel van de Cailletet-apparatuur. Het is aangetoond dat de CO_2 beter oplosbaar is in deze ionische vloeistof dan in enige andere ionische vloeistof met hetzelfde kation.

Onder de operationele condities waarbij gaswassing plaatsvindt is [emim][FAP] thermisch stabiel. Hierdoor wordt voorkomen dat de gasstroom verontreinigd wordt met de ionische vloeistof. Bovendien combineert [emim][FAP] een hoge CO_2 oplosbaarheid met een lage absorptiecapaciteit voor vluchtige koolwaterstoffen zoals methaan (CH_4), ethaan (C_2H_6). Propaan (C_3H_8) en butaan (C_4H_{10}). Dit kan ook worden afgeleid uit de hoge absorptie selectiviteit (bijv. $S_{CO2/CH4}$ =5.77-11.58), afhankelijk van de operationele condities. De

hoogste selectiviteit voor CO_2 verwijdering uit vluchtige koolwaterstoffen wordt bereikt bij lagere temperaturen en dit bleek hoger te zijn dan in andere ionische vloeistoffen en fysische oplosmiddelen. Dit bevestigt des temeer dat [emim][FAP] een veelbelovende kandidaat is die kan concurreren met de bestaande commerciële fysische oplosmiddelen die toegepast worden in gaswassing.

Het absorptiegedrag van de zwaardere alifatische koolwaterstoffen (hexaan, heptaan) en aromatische koolwaterstoffen (benzeen, tolueen, ethylbenzeen en xyleen, gezamenlijk BTEX genoemd) in [emim][FAP] is vervolgens bestudeerd. Deze kennis is van groot belang vanwege de schade die BTEX kunnen veroorzaken in de zwavelterugwinninginstallatie, bij het vloeibaar maken van aardgas en als uitstoot op zich. De metingen geven aan dat de oplosbaarheid van de alifatische koolwaterstoffen in [emim][FAP] laag is. Dit houdt in dat deze stoffen in de gasstroom blijven. Dit heeft zijn voordelen. Deze stoffen hebben namelijk een hoog calorische waarde; zij kunnen vloeibaar gemaakt worden voor verschillende commerciële en industriële toepassingen. De oplosbaarheid van de BTEX verbindingen in [emim][FAP] is hoog. Dit is wenselijk, omdat BTEX tegelijkertijd met de zure gassen uit aardgas worden verwijderd zodat het verstopt raken van de procesinstallaties bij het vloeibaar maken van aardgas geminimaliseerd worden. Echter, volledige terugwinning van de BTEX verbindingen uit de zure gasstroom (zonder emissies) is vereist om het katalysatorbed in de zwavelterugwinningsinstallatie te beschermen tegen cokesvorming, die kan worden veroorzaakt door de BTEX componenten.

De experimentele metingen van de fasenevenwichten zijn duur en tijdrovend. Deswege is de Peng-Robinson toestandsvergelijking met kwadratische mengregels gebruikt om de experimentele data te correleren over een breed temperatuurbereik (293K-363K) en drukken tot 11 MPa. In dit onderzoek is vastgesteld dat de experimentele data van alle binaire mengsels met vluchtige koolwaterstoffen zoals CH_4, C_2H_6 of C_3H_8 + [emim][FAP] nauwkeurig konden worden gecorreleerd met behulp van slechts één lineair temperatuur afhankelijke binaire interactie parameter (AAD minder dan 1%). De correlatie van de oplosbaarheden van het binaire mengsel CO_2 + [emim][FAP] vereiste echter twee binaire interactie parameters om een AAD van minder dan 3% te realiseren. Ternaire vloeistof-vloeistof evenwicht data van alifatische + aromatische + ionische vloeistof-systemen werden gecorreleerd met behulp van het NRTL model.

De ionische vloeistof [emim][FAP] werd ook opgenomen in een ‘supported ionic liquid membrane (SILM)’. Dit heeft een aantal voordelen ten opzichte van het conventionele absorptieproces, zoals lagere kapitaalkosten (minder ionische vloeistof nodig) en eenvoudigere procesapparatuur. [Emim][FAP] was met succes geïmpregneerd in de γ-alumina lagen van een buisvormig poreus asymmetrisch membraan. De zuivere gaspermeabiliteit van aardgas bestanddelen, zoals CO_2, CH_4, C_2H_6 en C_3H_8 werden bepaald in de SILM bij een transmembraan druk van 0,7 MPa en bij een temperatuur van 313 K. In deze studie werd geconstateerd dat de zuivere gas permeabiliteit in de SILM het hoogst is voor CO_2 en het laagst voor C_3H_8: $P_{CO2} > P_{CH4} > P_{C2H6} > P_{C3H8}$. Daarnaast werd de ideale permeabiliteit van CO_2/CH_4 berekend. Verder werden de gemengde gaspermeabiliteit en permselectiviteit voor het binaire mengsel van CO_2/CH_4 (50/50%, v/v) gemeten. De gemengde gas permselectiviteit ($\alpha = 1.15$) was veel lager dan de ideale permselectiviteit ($\alpha = 3.12$). De prestaties van SILM werden negatief beïnvloed door de aanwezigheid van water, dat doorgaans ook aanwezig is in aardgas. Daarvoor moet de aardgasstroom eerst worden gedroogd alvorens deze in contact wordt gebracht met de SILM. Ofschoon [emim][FAP] een uitstekende alternatieve absorptiemiddel is met hoge absorptiecapaciteit en selectiviteit (bijv. $SCO_2/CH_4 = 9.69$) voor CO_2, is het impregneren van deze ionische vloeistof in een SILM minder veel belovend voor de verwijdering van CO_2 uit aardgasstromen, omdat de permselectiviteit voor CO_2/CH_4 ($\alpha = 1.15$) in dat geval laag is.

Table of Contents

Chapter 1

Introduction

1.1 Problem definition

It is widely accepted that global climate change is caused by anthropogenic (produced by human activities) emissions of greenhouse gases (GHGs) into the atmosphere. Carbon dioxide (CO_2) is the most important greenhouse gas (Figure 1.1a). The combustion of fossil fuels is the main source of CO_2 emissions. When these fuels are burned, the carbon stored is released mainly as CO_2. Figure 1.1a shows that CO_2 emissions account for about 80 % of all GHGs emissions. Therefore, they contribute in large extend to global warming, even though CO_2 has the lowest global warming potential of all GHGs and a relatively short life-time in the atmosphere [1]. Largest CO_2 emission result from the energy supply sector, which is responsible for 26 % of the global GHGs emissions, see Figure 1.1b.

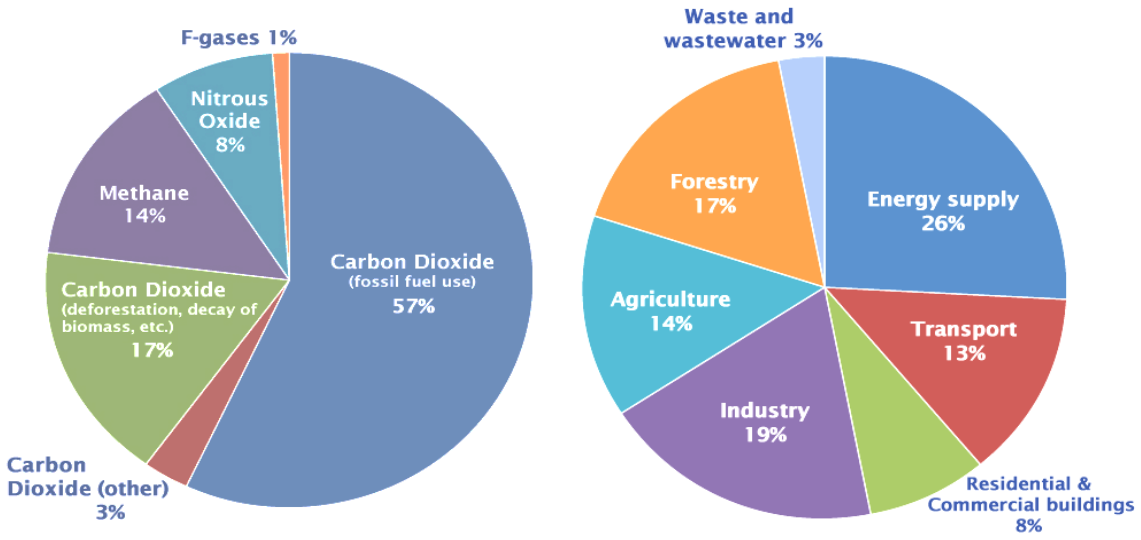

Figure 1.1: a) Global greenhouse gas emissions by gas, b) Global greenhouse emissions by sector [2].

Up to now, the global energy supply is mainly dependent on fossil fuels, such as coal, oil and natural gas. These fuels offer more than 85% of the world energy demand. Figure 1.2 shows that petroleum liquids are the most consumed fuels followed by coal and natural gas. From future projections it can be noticed that the global energy demand will continue to rise and that fossil fuels will remain the dominant source of energy worldwide in the next decades as a result of their low cost, availability, and existing reliable infrastructure and technology for energy production. Therefore, CO_2 emissions from the energy supply sector are expected to increase at a rate of 2.1% per year [3]. Thus, the capture of CO_2 is becoming increasingly important.

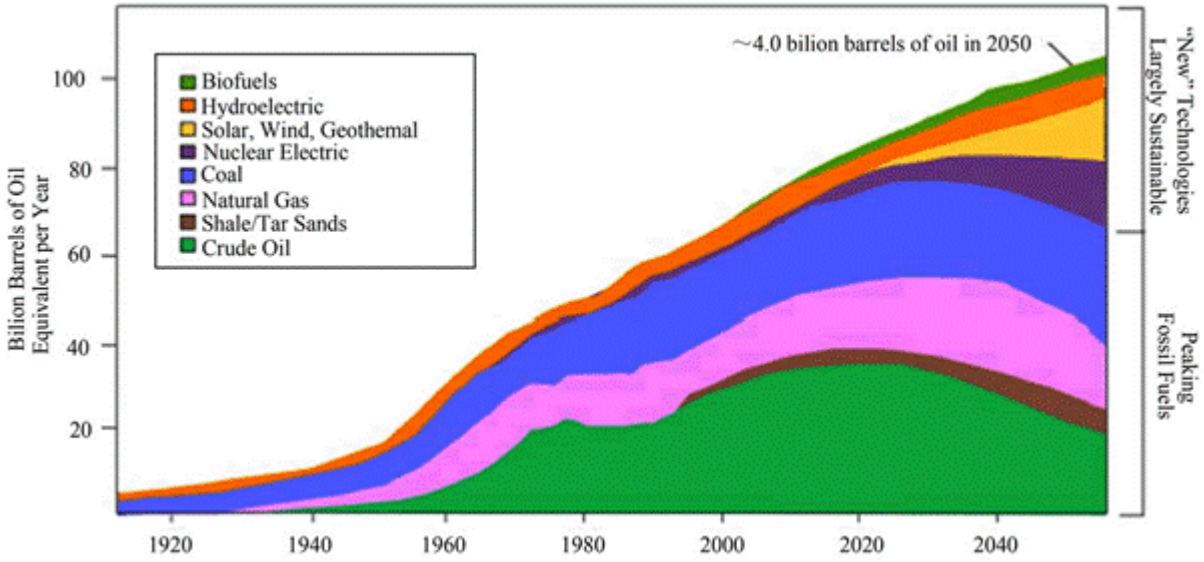

Figure 1.2: World energy demand by fuel type [4].

A number of CO_2 capture technologies have been tested to reduce CO_2 emission from fossil fuels combustion. After capture, the CO_2 must be transported to a location where it is safely stored, typically in appropriate geologic formations [5]. There are three technological methods that can be used for CO_2 capture: (i) pre-combustion capture, (ii) post-combustion capture, and (iii) oxy-combustion capture.

Pre-Combustion Capture

In pre-combustion capture, CO_2 is removed from the fuel before combustion (Figure 1.3).

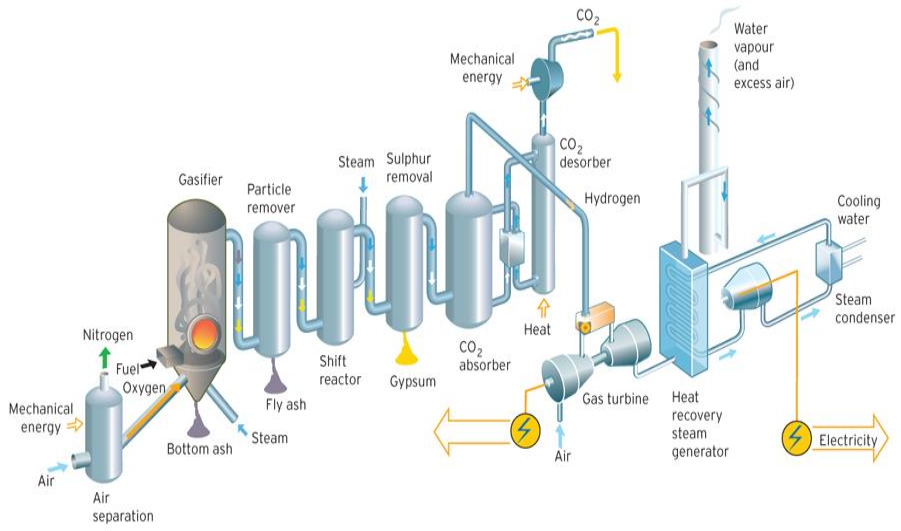

Figure 1.3: Simplified scheme of pre-combustion capture system [6].

In this configuration, the coal is first gasified with oxygen (O_2) to produce syngas, which is a mixture of CO and H_2. The syngas with added steam is then sent to a shift converter where the water-gas-shift reaction ($CO + H_2O \rightarrow CO_2 + H_2$) takes place to produce more hydrogen. Therefore, CO_2 is present in high concentrations in the stream leaving the shift converter. This CO_2 is removed by physical absorption and the hydrogen will continue to the combustion turbine to be used as a fuel. When natural gas (instead of coal) is used as fuel, the gasification step is replaced by a reforming stage to produce the syngas [6].

Post-Combustion Capture

Post-combustion capture involves the removal of CO_2 from flue gases produced by the combustion of fuels (Figure 1.4)

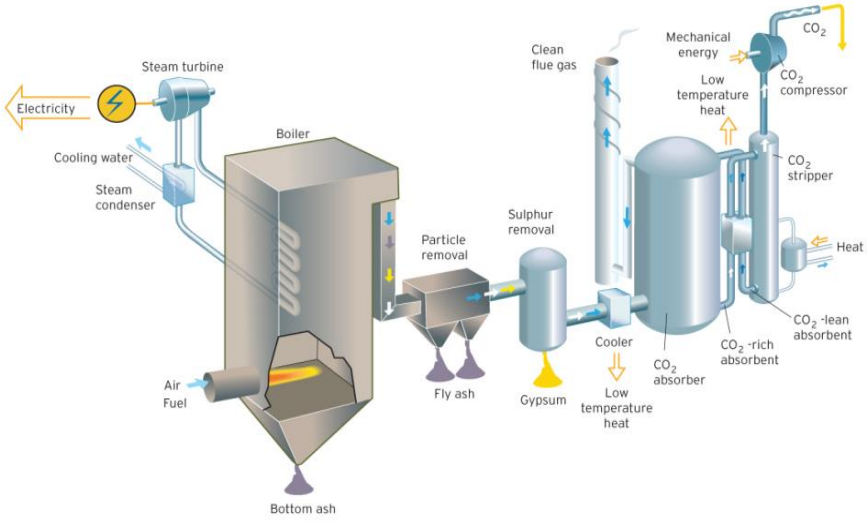

Figure 1.4: Simplified scheme of the post-combustion capture system [6].

Aqueous amine solutions (e.g., a 30% monoethanolamine solution in water) are mainly used to chemically absorb the CO_2 from flue gases after the combustion process [6]. Chemical absorbents are able to capture CO_2 from streams with very low CO_2 concentrations, because of the strong interaction with CO_2. Afterwards, the CO_2 is stripped from the amine solution, compressed and transported to the storage site. This regeneration step costs a lot of energy.

Oxy-Combustion Capture

Oxy-combustion capture is an alternative post-combustion capture process, whereby the CO_2 is captured from the flue gas. However, the flue gas does not contain nitrogen, because pure oxygen (instead of air) is used as oxidant in the combustion step (Figure 1.5).

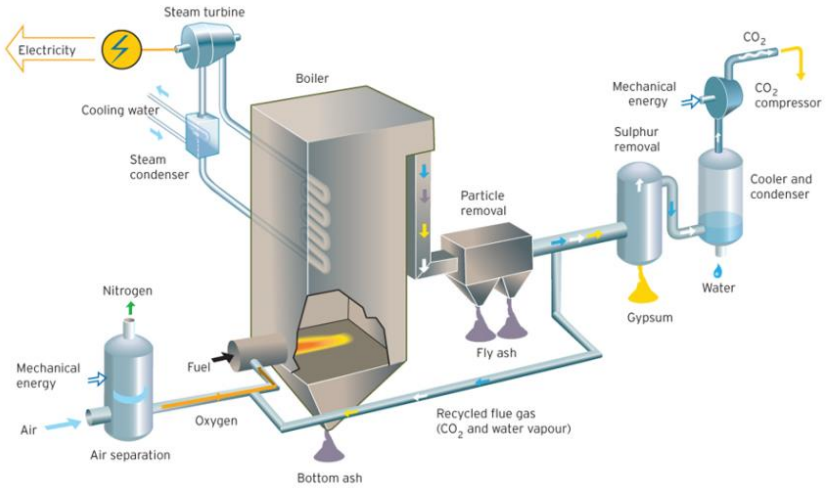

Figure 1.5: Simplified scheme of oxy-combustion capture system [6].

Oxy-combustion results in a flue gas mainly consisting of CO_2 and water vapor. The water vapor can be condensed to give a highly concentrated CO_2 stream for transport and storage.

Up to now, the CO_2 capture technologies have been found to be technically challenging and they are not cost-effective technologies to be commercialized at a large scale [7]. In addition, it takes time to reduce the dependency on fossil fuels and to switch to other (sustainable) energy sources, which generally have a lower energy conversion efficiency. For these reasons, the worldwide demand for natural gas as a cleaner and more efficient fuel is still increasing. Natural gas is considered as the most environmentally friendly fossil fuel, because natural gas combustion leads to negligible sulfur dioxide (SO_2) emissions, low nitrous oxide (N_2O) emissions, and low CO_2 emissions in comparison to coal or oil [8], see Table 1.1.

Table 1.1: Kilograms of air pollutants produced per billion kJ of energy.

Pollutant	Natural gas	Oil	Coal
Carbon Dioxide	53,070	74,389	94,347
Carbone Monoxide	18	15	94
Nitrogen Oxides	41	203	207
Sulfur Dioxides	0.27	504	1,175
Particulates	3	38	1,245
Formaldehyde	0.34	0.100	0.100
Mercury	0.00	0.003	0.007

Nevertheless, natural gas processing is challenging because of the contamination with undesired components. Natural gas mainly consists of methane (CH_4), but it also contains undesired acid gases such as carbon dioxide (CO_2) and hydrogen sulfide (H_2S). The removal of CO_2 from natural gas streams in a so-called sweetening process is crucial, not only for environmental concerns, but also because the presence of CO_2 may cause problems during transportation, such as gas hydrate formation that can clog pipelines [2], and corrosion in equipment and pipelines [9]. In addition, high amounts of CO_2 in the natural gas stream for electricity generation reduce the efficiency of power plants, because the presence of CO_2 reduces the heating value of natural gas [10].

Chemical and physical absorption processes are the most commonly used techniques for natural gas sweetening [11]. The advantages of chemical absorption using aqueous amine solutions are the high effectivity for CO_2 removal at various conditions to low concentration levels, the negligible hydrocarbon loss and the low price of the amine. However, aqueous amine processes have several disadvantages: corrosion, amine degradation, solvent losses and a highly energy-intensive regeneration. The main advantages of physical absorption using physical solvents (e.g., Selexol) are the simple regeneration (by pressure release) and the much lower amount of regeneration energy required compared to chemical absorption. However, physical processes also have several disadvantages: (i) the solvent shows high affinity to hydrocarbons, which are removed together with the CO_2 and result in hydrocarbon losses, (ii) it is only suitable for feed streams with a sufficiently high CO_2 pressure, and (iii) the physical solvent can only be used for bulk acid gas removal; low concentration levels of CO_2 cannot be reached [12]. Therefore, it is desirable to seek new solvents with favorable characteristics.

The requirements of an alternative absorbent

- High CO_2 loading capacity resulting in low circulation rates [13];
- Low co-absorption of hydrocarbons [14];
- High absorption and desorption rates [15];
- Low energy requirement for regeneration [14];
- Low vapor pressure preventing solvent losses, saving make-up volume and avoiding contamination of the gas stream [14];
- High degradation resistance allowing a wide range of operation temperatures [13];

- Non-corrosive nature of the solvent [13].

It is anticipated that ionic liquids (ILs) could fulfill the requirements mentioned above. Ionic liquids are molten salts composed of bulky organic cations, and organic or mostly inorganic anions. It was found that the solubility of CO_2 in many ILs is high [16], while ILs cannot evaporate and contaminate the gas stream, because their vapor pressure at room temperature is negligibly [17]. The amount of energy required for regeneration is also expected to be low. Therefore, ILs are potentially interesting solvents for carbon capture as long as the co-absorption of heavy hydrocarbons is low, the absorption/desorption kinetics are fast, the degradation resistance is high and the corrosivity is low. In this thesis, these requirements will be addressed.

1.2 Aim of the research

The aim of this research is to study the potential of using ionic liquids (ILs) as absorption solvents for CO_2 removal from natural gas streams. The first objective is to investigate the absorption capacity of the IL 1-ethyl-3-methylimidazolium tris(pentafluoroethyl)trifluoro phosphate ([emim][FAP]) for most important natural gas components including carbon dioxide (CO_2), methane (CH_4), ethane (C_2H_6), propane (C_3H_8), butane (C_4H_{10}), benzene (C_6H_6), toluene (C_7H_8), ethylbenzene (C_8H_{10}) and *o*-xylene (C_8H_{10}). The second objective is to investigate the absorption rates in the same IL. The knowledge of both aspects (thermodynamics and kinetics) is of great importance for the design of natural gas sweetening processes, either in a conventional absorption set-up or in a novel IL membrane unit in which less IL is needed.

1.3 The outline of the research

After a brief introduction and background to the central themes, the thesis is organized as follows:

Chapter two summarizes the most common technologies used in natural gas sweetening processes. In addition, applications, advantages and disadvantages of these techniques were discussed in detail. Chapter two also reports on the properties of a novel class of solvents (ionic liquids) and their potential application in gas separation

In chapter three, the IL ([emim][FAP]) was characterized, the physical properties such as density, viscosity and surface tension were measured at several temperatures. Further, solubility of CO_2 in the studied IL was determined using Cailletet equipment over a wide range of temperatures, pressures and compositions. The solubilities of CO_2 in [emim][FAP] compared to the solubilities of CO_2 at the same temperature in other ILs sharing the same cation. The use of [emim][FAP] results in highest absorptive capacity, which makes this IL an attractive solvent for gas separation processes as long as solubility of CH_4 is low. Therefore, the solubility of CH_4 in [emim][FAP] has been investigated in detail in the next chapter.

In chapter four, solubility of CH_4 in [emim][FAP] was determined using Cailletet equipment at various conditions. The obtained solubilities of CH_4 were compared with solubilities of CO_2 in the same IL in order to calculate CO_2/CH_4 selectivities. The high solubility of CO_2 compared to CH_4 in [emim][FAP] indicates the possibility of using this IL in separating CO_2 from the natural gas.

Besides CH_4, natural gas also contains significant amounts of C_2H_6, some C_3H_8, C_4H_{10}, and other higher hydrocarbons. In natural gas treating, the loss of small hydrocarbons to the CO_2-rich stream is a concern. Therefore, the solubilities of the small hydrocarbons C_2H_6, C_3H_8 and C_4H_{10} in the same IL were experimentally determined **in chapter five,** and compared to the CO_2 and CH_4 solubilities in [emim][FAP].

Since experimental measurements of phase equilibria of mixtures with ILs are expensive and time-consuming, the Peng-Robinson EoS (PR-EoS) was used to model the gas solubility of CO_2, CH_4, C_2H_6, C_3H_8 and C_4H_{10} in [emim][FAP] IL over wide ranges of pressure, temperature and composition and is presented in **chapter six.**

In chapter seven, the solubility of heavy hydrocarbons in the studied ionic liquid is presented. It is highly desirable to remove the heavy hydrocarbons from acid gas, specifically aromatics compounds (benzene, toluene, ethylbenzene and xylene, collectively called BTEX). BTEX are known to cause problems in sulfur recovery, they are difficult to burn and can cause coking in the catalyst beds, thus frequent replacement of catalyst. Further, BTEX compounds are known as air pollutants that must be limited to certain level emissions. For this reason, heavy aliphatic hydrocarbons and BTEX solubilities in the [emim][FAP] IL have been studied.

In chapter eight, In addition to importance of absorption capacities of ILs, knowledge of absorption rate of gases in ILs is also very important for the design and development of gas separation processes. The permeabilities of pure CO_2, CH_4, C_2H_6 and C_3H_8 through a SILM consisting a γ-alumina impregnated with the IL [emim][FAP] were measured. These measurements were used to calculate the permselectivity and diffusivity. Also, diffusivities were measured and correlated using a suitable model.

In chapter nine, conclusions and recommendations for future work are presented.

1.4 References

[1] CO_2 Capture and Storage: A VGB Report on the State of the Art, VGB PowerTech e.V., Essen, (2004).

[2] Contribution of Working Group III to the Fourth Assessment Report of the Intergovernmental Panel on Climate Change, Cambridge University Press, Cambridge, United Kingdom and New York, USA, (2007).

[3] F. Karadas, M. Atilhan, S. Aparicio, Review on the Use of Ionic Liquids (ILs) as Alternative Fluids for CO_2 Capture and Natural Gas Sweetening, Energy & Fuels, 24 (2010) 5817-5828.

[4] A. Bolonkin, Production of Freshwater and Energy from Earth's Atmosphere, 2 (2011) 86-98.

[5] P. Viebahn, D. Vallentin, S. Höller, Prospects of carbon capture and storage (CCS) in India's power sector – An integrated assessment, Applied Energy, 117 (2014) 62-75.

[6] Vattenfall, www.vattenfall.com, (2014).

[7] M. Ramdin, T.W. de Loos, T.J.H. Vlugt, State-of-the-Art of CO_2 Capture with Ionic Liquids, Industrial & Engineering Chemistry Research, 51 (2012) 8149-8177.

[8] Natural Gas : Issues and Trends, Energy Information Administration., Washington, D.C., DOE/EIA-0560(98), (1998).

[9] S. Ma'mun, V.Y. Dindore, H.F. Svendsen, Kinetics of the Reaction of Carbon Dioxide with Aqueous Solutions of 2-((2-Aminoethyl)amino)ethanol, Industrial & Engineering Chemistry Research, 46 (2006) 385-394.

[10] K. Simons, K. Nijmeijer, M. Wessling, Gas–liquid membrane contactors for CO_2 removal, Journal of Membrane Science, 340 (2009) 214-220.

[11] B.D. Bhide, A. Voskericyan, S.A. Stern, Hybrid processes for the removal of acid gases from natural gas, Journal of Membrane Science, 140 (1998) 27-49.

[12] A.-L. Revelli, F. Mutelet, J.-N.l. Jaubert, High Carbon Dioxide Solubilities in Imidazolium-Based Ionic Liquids and in Poly(ethylene glycol) Dimethyl Ether, The Journal of Physical Chemistry *B*, 114 (2010) 12908-12913.

[13] A. Chakma, A.K. Mehrotra, B. Nielsen, Comparison of chemical solvents for mitigating CO_2 emissions from coal-fired power plants, Heat Recovery Systems and CHP, 15 (1995) 231-240.

[14] D. Chinn, D. Vu, M. Driver, L. Boudreau, CO_2 removal from gas using ionic liquid absorbents, Google Patents, (2005).

[15] J. Tang, H. Tang, W. Sun, H. Plancher, M. Radosz, Y. Shen, Poly(ionic liquid)s: a new material with enhanced and fast CO_2 absorption, Chemical Communications, (2005) 3325-3327.

[16] L. Duchet, J.C. Legeay, D. Carrié, L. Paquin, J.J. Vanden Eynde, J.P. Bazureau, Synthesis of 3,5-disubstituted 1,2,4-oxadiazoles using ionic liquid-phase organic synthesis (IoLiPOS) methodology, Tetrahedron, 66 (2010) 986-994.

[17] E.D. Bates, R.D. Mayton, I. Ntai, J.H. Davis, CO_2 Capture by a Task-Specific Ionic Liquid, Journal of the American Chemical Society, 124 (2002) 926-927.

Chapter 2

Background

2.1 Introduction

This chapter summarizes the most common technologies used in natural gas sweetening processes. In addition, applications, advantages and disadvantages of these techniques will be discussed in detail. This chapter also reports on the properties of a novel class of solvents (ionic liquids) and their potential application in gas separation.

2.2 What is natural gas?

Natural gas exists in nature under pressure in rock reservoirs in the earth's crust. The main component of the natural gas is methane (CH_4). Among methane, natural gas contains other components such as ethane (C_2H_6), propane (C_3H_8), butane (C_4H_{10}), carbon dioxide (CO_2), hydrogen sulfide (H_2S), and may contain trace quantities of other components too. The composition of natural gas can vary widely depending on the location of the field. Table 2.1 presents a typical composition of natural gas prior to treatment.

Table 2.1: Typical composition of natural gas [1].

Name	Formula	Volume (%)
Methane	CH_4	> 85
Ethane	C_2H_6	3-8
Propane	C_3H_8	1-2
Butane	C_4H_{10}	<1
Pentane	C_5H_{12}	<1
Carbon dioxide	CO_2	1-2
Hydrogen sulfide	H_2S	<1
Nitrogen	N_2	1-5
Helium	He	<0.5

When natural gas contains significant amounts of acid gases, i.e. CO_2 and H_2S, removal of these components from natural gas streams is therefore crucial. It is not only because of environmental issues but also because these gases may cause many problems during transportation such as gas hydrate formation that may clog pipelines [2]. Furthermore, the presence of acid gases leads to corrosion in equipment and pipelines [3], significantly reducing the lifetime of the facilities. In addition, high amounts of CO_2 in natural gas stream for power generation reduce the efficiency of power plants because the presence of CO_2 reduces the heating value of natural gas [4]. The removal of acid gases such as CO_2, H_2S and other sulfur-containing components like, for instance, mercaptans, from the natural gas is

referred to as gas sweetening process. As the demand for natural gas has increased in recent years, the need has arisen to develop highly effective technology for acid gas removal.

2.2.1 Gas treating technologies

There are many technologies available for treating gas streams such as absorption, adsorption and membrane technology. Figure 2.1 shows a brief overview of these technologies.

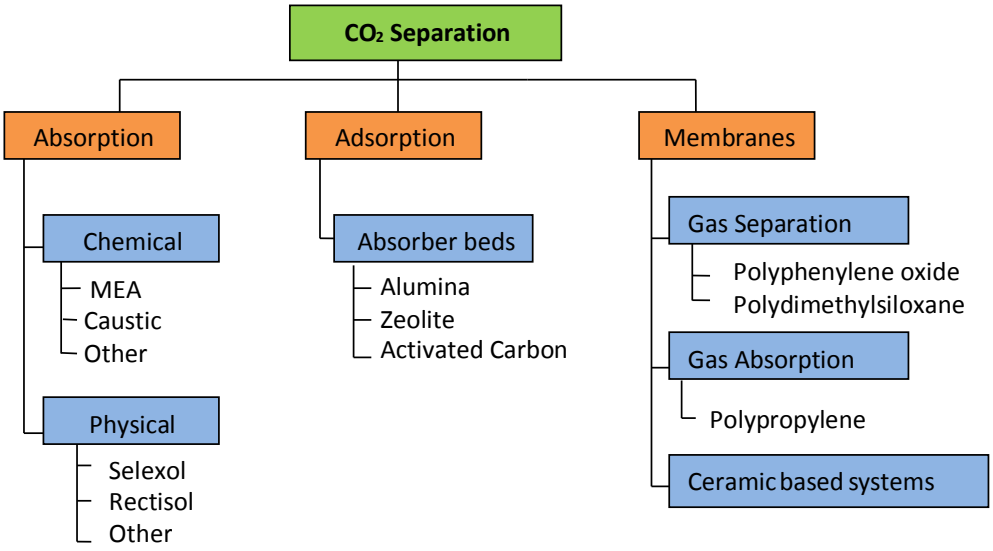

Figure 2.1: The technologies used for CO_2 separation [5].

At present gas absorption processes represent about 70% of the techniques used for treating natural gas [6]. Absorption processes generally can be divided into two categories;

- Processes where the solvent chemically reacts with the dissolved gas which are referred to as chemical absorption processes. For these processes; alkanolamines are commonly used as reactive absorbents.
- Physical absorption processes are processes where the solvent only interacts physically with the dissolved gas. The most commonly used physical solvents are glycol ethers (Selexol Process).

Chemical absorption

Nowadays the most common technology for CO_2 removal is absorption with amine-based absorbents such as MEA, DEA and MDEA [7]. The typical amine natural gas sweetening process used in industry is shown in Figure 2.2.

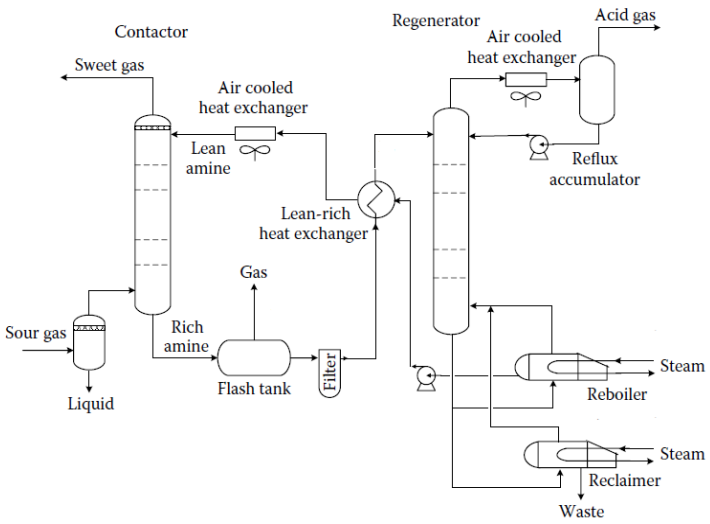

Figure 2.2: Flow diagram of a typical amine treating process used in industrial plants [8].

Sour gas enters into the absorber at a pressure of 7 MPa and a temperature in range of 290 – 320 K; When the gas stream contains CO_2, the CO_2 reacts with the amine-solution via two different mechanisms. The first mechanism, the reaction of CO_2 with primary or secondary amines forms carbamate species. The CO_2 reacts with one primary or secondary amine molecule to form the carbamate intermediate, which reacts with a second amine molecule to form the carbamate formation. The overall reaction is given by Eq.1.

$$CO_2 + R_1R_2NH \rightleftharpoons R_1R_2N^+HCOO^- \qquad \text{Eq.1a}$$

$$R_1R_2N^+HCOO^- + R_1R_2NH \rightleftharpoons R_1R_2NCOO^- + R_1R_2H_2N^+ \qquad \text{Eq.1b}$$

$$CO_2 + 2R_1R_2NH \rightleftharpoons R_1R_2H_2N^+R_1R_2NCOO^- \qquad \text{Eq.1}$$

The second mechanism for the reaction of CO_2 with amines, the tertiary amine does not form carbamate. In this case, the amine reacts with CO_2 via hydrolysis as CO_2 hydrolyzes in water to form carbonic acid, followed by a slow dissociation to bicarbonate. Finally, the bicarbonate reacts with the amine, leading to the overall reaction shown by Eq. 2:

$$CO_2 + H_2O \rightleftharpoons H_2CO_3 \text{ (carbonic acid)} \qquad \text{Eq.2a}$$

$$H_2CO_3 \rightleftharpoons H^+ + HCO_3^- \text{(bicarbonate)} \qquad \text{Eq.2b}$$

$$H^+ + R_1R_2R_3N \rightleftharpoons R_1R_2R_3NH^+ \qquad \text{Eq.2c}$$

$$CO_2 + H_2O + R_1R_2R_3N \rightleftharpoons R_1R_2R_3NH^+HCO_3^- \qquad \text{Eq.2}$$

Although the reaction is shown for a tertiary amine, however, it applies to primary and secondary amines as well. The above reactions are also reversible where the original amine can be recovered by supplying heat [9]. The amine solution rich with CO_2 is sent to a stripper where it is reheated up to a temperature of 350 – 370 K to release the CO_2. The amine solution is then recycled to the absorber. The gas stream from the amine regenerator column is sent to the sulfur recovery unit or vented to the atmosphere depending on the sulfur content. In case of the gas stream from the amine regenerator contains H_2S, the gas stream is fed into furnace in the sulfur recovery unit (see Figure 2.3), while the air is fed into furnace as well to react with the H_2S, along with any other combustibles, such as hydrocarbons and mercaptans. But, aromatic compounds such as benzene, toluene, ethylbenzene and xylene are difficult to burn in the furnace and can cause catalyst coking thus limiting the catalyst life in the sulfur recovery unit [10].

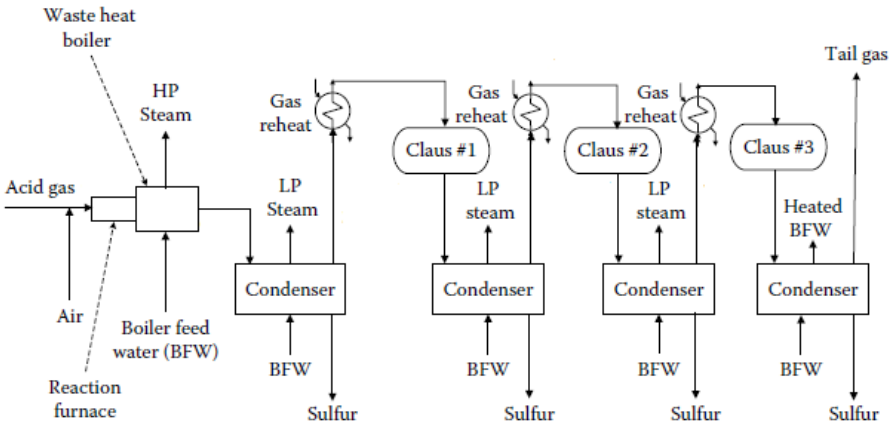

Figure 2.3 : Straight-through Claus unit [8].

The H_2S is oxidized to form H_2O and sulfur dioxide (SO_2) according to the following reaction:

$$H_2S + \frac{3}{2}O_2 \rightleftharpoons H_2O + SO_2 \qquad \text{Eq.3}$$

Thereafter, the combustion products pass through a series of catalytic converters. The following reaction occurs:

$$2H_2S + SO_2 \rightleftharpoons 2H_2O + \left(\frac{3}{x}\right)S_x \qquad \text{Eq.4}$$

The catalytic converters are followed by condensers to remove the sulfur.

The sweetened gas exits from the top of the absorber, it must be dehydrated typically with a glycol system, before further processing can take place. The operation of a glycol unit is very similar to the amine unit (Figure 2.4).

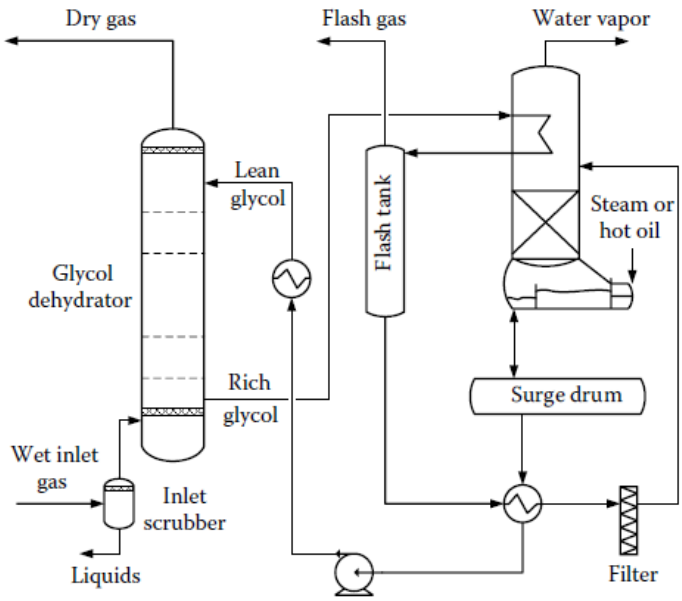

Figure 2.4: Schematic of typical glycol dehydrator unit [8].

The wet gas enters the bottom of the glycol contactor. Water in the gas is absorbed into the glycol, and the dry gas exits at the top of the absorber. Rich glycol exits the bottom of the column and is sent through a regeneration system to remove any dissolved hydrocarbons including BTEX and water [8, 11].

The major advantages of the amine treatment:

i) It is a widely commercialized technology;
ii) The hydrocarbon loss is almost negligible;

iii) Furthermore the aqueous amine solutions are effective to remove CO_2 from natural gas under a variety of conditions.
iv) Aqueous solutions of amines can reduce the CO_2 level to low concentrations.

Nevertheless, processes using aqueous amine solutions also have several disadvantages [7, 12] :

i) Intensive energy required during the regeneration step as the heating energy is needed to break the chemical bonds between the absorbed CO_2 and the solvent. For example, strong amines (e.g. MEA) require a significant amount of energy, leading to higher operating costs. Furthermore, application of the aqueous amine process is highly energy intensive, which is a consequence of the thermodynamic properties (e.g. heat capacity) of water;
ii) Amines can corrode low alloy steel. Therefore, diluted solutions are used to minimize corrosion. However, this diluted solution needs higher circulation rates to achieve the required CO_2 removal;
iii) Because amines react with CO_2, they degrade to form non-reversible products;
iv) Amines can degrade thermally as well;
v) Amines can be oxidized when it is used for flue gas treatment;
vi) Solvent losses.

Physical absorption

Physical absorption processes use organic solvents such as dimethylether or polyethylene glycol, methanol, propylene carbonate, sulfolane, N-formylmorpholine and N-methylpyrrolidone. They physically absorb acid gas components. The process description is shown in Figure 2.5.

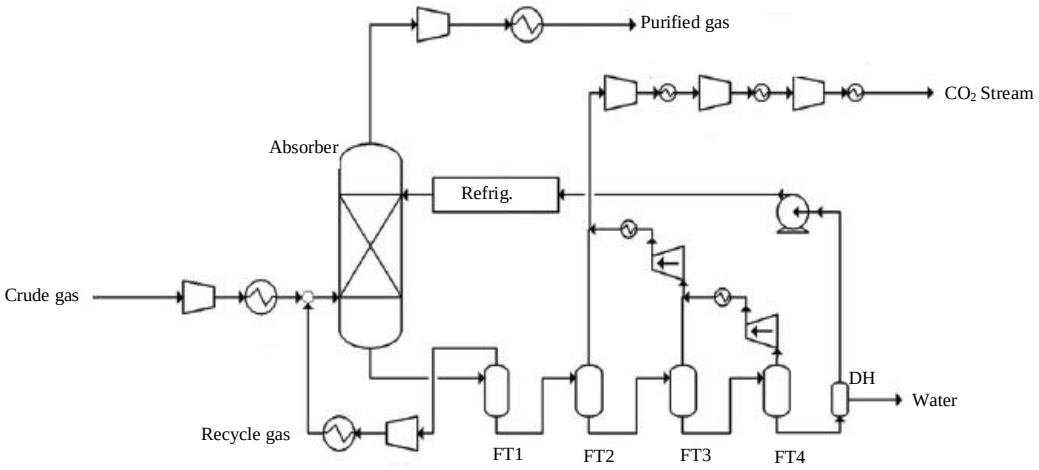

Figure 2.5: Flow diagram of Selexol process for CO_2 removal from natural gas [13].

Removal of CO_2 from natural gas by physical absorption processes are based on the solubility of CO_2 within the solvent. The solubility of CO_2 depends on the partial pressure and on the temperature of the feed gas. Higher CO_2 partial pressure and lower temperature increases the solubility of CO_2 in the solvent. After absorption, the enriched solvent with CO_2 by the absorber is regenerated by reduction of the pressure in four flashes. The CO_2-rich solvent leaves from the bottom of the absorber and enters flash tank (FT1). The Selexol solvent leaving the absorber also contains a small amount of CH_4 and other hydrocarbons (C_2H_6, C_3H_8, etc). These compounds are mostly released from the Selexol in (FT1), with some remaining CO_2. Subsequently, the released gas is recycled and mixed with the crude gas. The solvent leaving the FT1 is further depressurized through a sequence of the flash stages (FT2-FT4) to desorb the remaining CO_2 from the solvent. The lean solvent leaving FT4 goes to a dehydrator (DH) to remove the water, followed by recycling of the Selexol to the absorber. The CO_2 stream released from FT2-FT4 is delivered to the next process step, for instance to the sulfur recovery plant if the stream contains H_2S. Purified gas that exits from the top of the absorber is compressed and then cooled down.

The main advantage of the physical solvents over amine solutions is that less energy for regeneration is required. However, physical absorption processes also have several disadvantages:

i) Often the solvents have a high affinity to hydrocarbons which will be removed with the CO_2 and essentially resulting into hydrocarbon losses;
ii) The partial pressure of the CO_2 in the feed has to be high to achieve a reasonable solubility level;

iii) Physical solvents are only used for bulk acid gas removal,

iv) Solvent losses as some physical solvents have a significant vapor pressure, e.g. methanol [14].

In general, physical solvents are effective when the acid gas pressure is high. On the other hand, chemical solvents are more favored when the acid gas pressure in the gas stream is low (Figure 2.6).

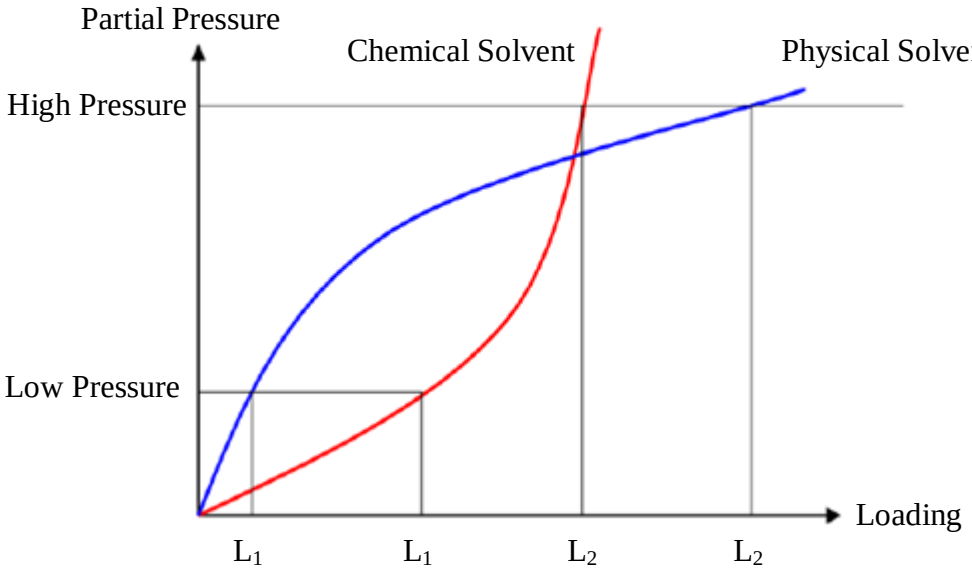

Figure 2.6: Physical versus chemicals solvents [15].

In natural gas sweetening processes, it is desirable to achieve high absorption rates, high acid gases capacity into the solvent, low hydrocarbons capacity, easy solvent regeneration and the solvent should have a low own vapor pressure at the process conditions.

2.3 Ionic liquids

Ionic liquids (ILs) are salts composed of bulky organic cations and organic or inorganic anions. They have melting points lower than 373 K and most of them have melting points around or below room temperature [16]. Compared to conventional solvents, the unique properties of ILs and the possibility to tune their properties by changing the anion-cation combination favor their application in many processes [17-19].

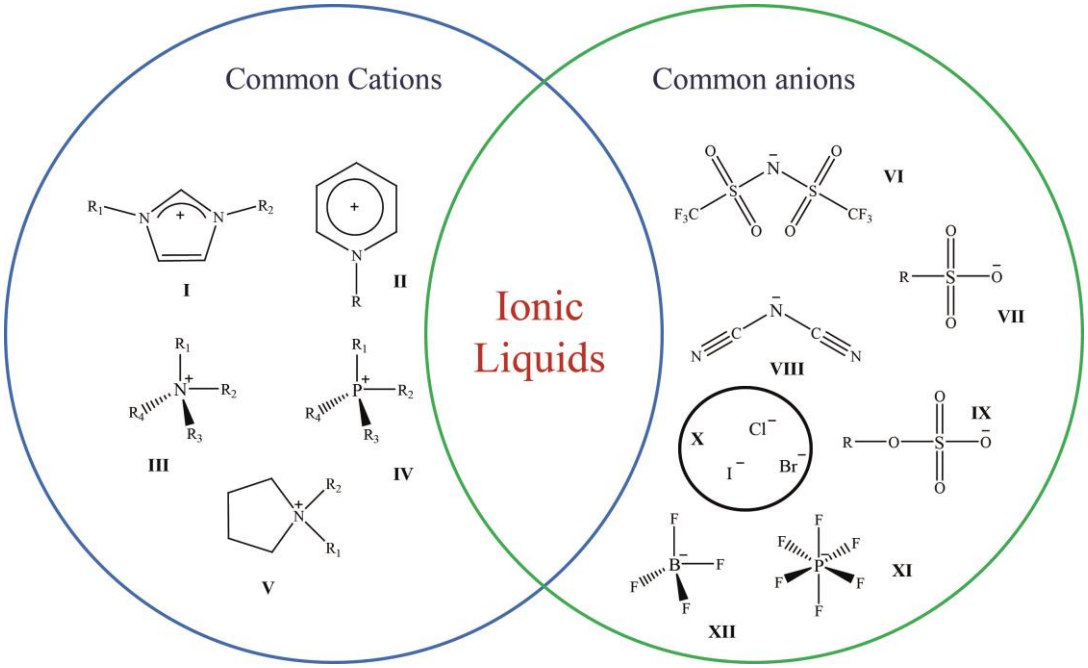

Figure 2.7: Common cations and anions of RTILs. **I**: 1,3-dialkylimidazolium; **II**: N-alkylpyridinium; **III**: tetraalkylammonium; **IV**: tetraalkylphosphonium; **V**: N,N-dialkylpyrrolidinium; **VI**: bis(trifluoromethanesulfonyl)imide; **VII**: alkylsulfonate; **VIII**: dicyanimide; **IX**: alkylsulfates; **X**: chloride, bromide, iodide; **XI**: hexafluorophosphate; **XII**: tetrafluoroborate. adapted from source [20].

Figure 2.7 presents the common cations and anions found in the literature. However, these are only a limited selection of an almost infinite number of possible cations and anions that will form ILs.

The introduction of structural functionalities in the cation or anion enables to synthesize task-specific ILs. The types of ILs available have been extended to include new generations of ILs (see, Figure 2.8) with targeted and specific properties.

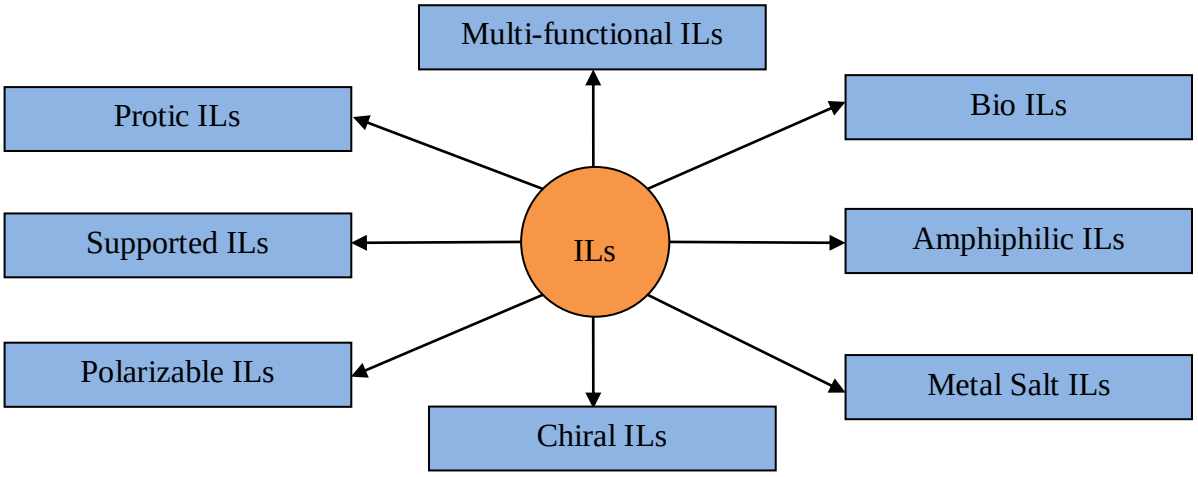

Figure 2.8: Various categories of ILs [21].

2.3.1 Ionic Liquid Properties

There is a great interest in ILs because of their unique properties. Their physical properties such as melting point, viscosity, water-miscibility, density and hydrophobicity can be tailored to suit the requirements of a particular process. The properties can be varied by simple changes to the structure of the ions by the variation of the cation or anion family or by the length and branching of the alkyl groups incorporated in the cation [22].

Melting point: ILs different from other salts by the fact that most of them remain liquid at room temperature, since their ions do not pack very well and thus reduces the lattice energy [23, 24].

Volatility: ILs display a negligibly low volatility at room temperature caused by strong coulombic interactions. This aspect of ILs prevent pollution of the air [25] and contamination of industrial gas streams, making them excellent alternatives for volatile organic compounds.

Viscosity: ILs have higher viscosities than the conventional organic solvents. Organic solvents have viscosities ranging from 0.2 to 10 mPa.s, while ILs have a wider range of viscosities, typically ranging from 10 to 10^4 mPa.s [26]. The high viscosities of ILs are related to their high molecular weights as well as their intermolecular interactions (H-bonding, dispersive and electrostatic interactions) [27]. The viscosity of IL increases with an increase in anion size. In addition, its shape also has an effect on the viscosity. It was reported that the flat shape of the anion contributes to a lower viscosity of the ILs [28]. Also a higher

degree of fluorination of the anions contributes to a reduction van der Waals interactions and hydrogen bonding, which leads to lower viscosities of ILs [28]. The viscosities of the same class of ILs (with the same anion) increase if the alkyl group in the cation is increased. This is due to the stronger van der Waals forces between cations, leading to an increase in the energy required for molecular motion [29]. The viscosity of ILs depends not only on the cation and anion but also on the water content and chloride impurities [30]. It was found that the presence of very low concentrations of chloride in the IL sample drastically increases the viscosity, whereas the presence of water reduces the viscosity. The viscosity is an important factor to be taken into consideration to select a suitable IL for a separation process, e.g. in a gas absorption process, ILs with a high viscosity lead to low absorption and desorption rates. In general, all ILs show a significant decrease in viscosity as temperature increases [31].

Thermal stability: In general, most ILs have a high thermal stability; they begin to decompose around 673 K [32]. The stability of ILs is found to be more dependent on anions than on the cations [27]. The thermal decomposition strongly depends on the structure of the IL. The onset of thermal decomposition decreases as the anion hydrophilicity increases, while, on the other hand, the stability increases as the anion size increases. Halide anions reduce the relative thermal stability compared to ILs without halide anions. The following order in stability has been identified: $[PF_6^-] > [Tf_2N^-] \sim [BF_4^-] >$ halides [32].

Toxicity and biodegradability: As mentioned already, ILs cause insignificant air pollution compared to the typical volatile organic solvents. However, this is not enough to refer to the IL to be "a green solvent''. Any release of ILs from industrial processes into an aquatic environment may lead to water pollution. The most commonly used ILs [bmim][PF_6] and [bmim][BF_4] are known to decompose in the presence of water to form hydrofluoric and phosphoric acids [24]. The impact of ILs on aquatic ecosystems was studied for two imidazolium-based ILs with [PF_6^-] and [BF_4^-] anions. Both ILs are equally toxic to ecosystems as benzene, but much less toxic than ammonia, chlorine, and phenol [24]. Furthermore, it was found that the toxicity of ILs increases with increasing alkyl chain length of the cation and branching incorporated into cation ring [24]. However, toxicological data in literature are still very limited. Therefore, further investigations and studies are needed in order to judge the toxicity of ILs in its applications. Readily biodegradable ILs are defined as ILs that reach a biodegradation level higher than 60 % within 28 days. The biodegradability of imidazolium-, phosphonium- and pyridinium-based ILs have been investigated and

documented in literature [33, 34]. The results confirmed that pyridinium-based ILs have a higher biodegradability than imidazolium and phosphonium ILs. The biodegradability was shown to improve with incorporating an ester group in the alkyl side-chain of the cations of imidazolium and pyridinium. The biodegradability of phosphonium ILs did not improve with incorporating an ester functional group. Garcia, *et al.* [35] studied the biodegradability of imidazolium based ILs with various anions. The effect of the anion on the biodegradability of ILs was minor, except for ILs with an octylsulfate anion the biodegradability enhanced significantly. Nicholas *et. al.* [36] reported the first readily biodegradable ILs contain an imidazolium cation with a propyl- or pentyl-ester side-chain together with an octylsulfate anion.

Corrosivity: Some studies have shown a certain corrosion of ILs towards some metals and alloys, especially at high temperatures. Moreover, certain impurities present in IL samples, such as halides, may increase the corrosive ability of these ILs [37-39].

Other properties are:
- They are highly polar [40].
- They are feasible to recycle and repeatedly reuse them [24].

2.3.2 Ionic Liquid Applications

The possibility of concisely tuning the properties of ILs by changing the anion-cation combination is one of the biggest advantages of these systems. Considering the aim of this thesis, this section will focus on the application of ILs in gas separation.

Gas separation

Recently, the use of ILs for gas separation processes has attracted much attention because of the high solubility of different gaseous species in ILs. The most widely investigated binary IL + gas systems are their mixtures with CO_2 [41-45].
It was found that the anion predominantly determines the CO_2 solubility in ILs. ILs with fluorinated anions, e.g., ($[Tf_2N^-]$), ($[BF_4^-]$) and ($[PF_6^-]$) show the highest CO_2 solubility [46]. On the other hand, it was found that ILs with non-fluorinated anions, such as alkanoates and sulfates, have a much lower CO_2 solubility [47].

The solubility of CO_2 in an IL is less strongly influenced by the type of the cation. However, the CO_2 solubility in ILs having fluorinated cations is higher in comparison to ILs with non-fluorinated cations [47]. It was also observed that an increase in the alkyl chain length of the cation slightly increases the CO_2 solubility in the IL [48], which could be a consequence of the decrease of the IL density. Thus, longer alkyl chain creates a greater free volume in ILs that allows accommodating more CO_2.

Kazarian *et al.* [49] used ATR-FTIR spectroscopy to analyze the specific interactions between CO_2 and the ILs [bmim][BF_4] and [bmim][PF_6]. They observed the existence of weak Lewis acid-base interactions between CO_2 molecules and the fluorinated anions, where the anion acts as a Lewis base. This type of interactions can be enhanced by addition of basic functionalities such as amino and fluorine groups in the IL [50]. Seki *et al.* [51] showed that the interaction of CO_2 with [BF_4^-] and [PF_6^-] anions based ILs are stronger than those with [Tf_2N^-] anions based ILs. However, the solubility of CO_2 in [Tf_2N^-] anions based ILs is higher. Thus, the strength of these interactions cannot only be responsible for the solubility of CO_2 in these ILs. Also the available free volume in the ILs could play a significant role in the CO_2 solubility in the these ILs. Baltus *et al.* [52] mentioned that the larger size of the [Tf_2N^-] anion compared with other ones leads to weakening of the cation-anion interactions, which increases the available free volume in the IL and, consequently, allowing to accommodate more CO_2 in the IL.

Although fluorine-containing ILs are generally good solvents for CO_2, they are less stable with respect to moisture and air, especially at high temperatures when hydrofluoric acid (HF) can be formed [53]. Moreover, most of the imidazolium and ammonium salts are hydrophilic, which means that these ILs can dissolve significant amounts of water. It was reported that the hygroscopic character of ILs is strongly influenced by the anion size, where the stability with respect to moisture increases with increasing anion size in the order [PF_6^-] < [BF_4^-] < [Tf_2N^-] [54].

From previous studies it was demonstrated that ILs have a high absorption capacity for CO_2. However, for CO_2 removal from flue gas or natural gas, solubilities of other gases in the same ILs are also crucial to consider. A good solvent should on the one hand show a high CO_2 absorption capacity with, on the other hand, a high selectivity for other components. Therefore, the solubilities of various gases in ILs were determined to estimate the

selectivities. This information is of crucial interest for a better judgment of the applicability of ILs in gas separation processes. Generally, ILs were found to show high CO_2 solubilities [41-45], where CH_4 solubilities were much lower [55-60]. Therefore, ILs could be attractive absorbents for gas separations.

Carvalho and Coutinho [61] reported that CO_2/CH_4 and H_2S/CH_4 ideal selectivities increase as polarity of ILs increases. The reason is that the CH_4 solubility in ILs is related to polarity of ILs. CH_4 is a non-polar compound which dissolves better in ILs with lower polarities.

Hert *et al.*[62] reported that the presence of CO_2 and CH_4 in the mixed gas increases the CH_4 solubility in [hmim][Tf_2N] IL in comparison to solubility of pure CH_4, this makes gas separation more challenging. Using molecular simulations, Maginn *et al.* [63] showed that the mixed gas solubilities are nearly ideal, with little enhancement for mixtures of CO_2/O_2 and SO_2/N_2. Toussaint *et al.* [64] showed that addition of CO_2 to the binary system of H_2 and [bmim][BF_4] increases the H_2 solubility at low temperatures while an inverse behavior was observed at higher temperatures.

Solubilities of hydrocarbons such as ethane, propane, butane and etc. have been studied in ILs [65-67]. In natural gas treating, the loss of small hydrocarbons to the CO_2-rich stream is a concern. It is desirable to maintain these compounds in the CH_4-rich stream, because of their economic value. Solubilities of hydrocarbons in many ILs were found to be low which is favorable in natural gas sweetening processes. However, it was found that as the alkyl chain of ILs increases, the solubilities of hydrocarbons in theses ILs also increases, thus reducing the CO_2/hydrocarbon selectivity.

Besides the importance of the absorption capacities of ILs, also the knowledge on diffusivities of gases in ILs is most important for the design and development of absorption processes, i.e. for natural gas sweetening processes. Recently, new ILs were synthesized with a much higher absorbtion rate for CO_2 [68-70]. For example, polymerized-ILs took only 4 min to reach their 90% of absorption capacities and about 30 min to reach their full capacities [68]. Moreover, CO_2 absorption in protic ILs could be almost completed within 5 min [69]. In mixed IL + aqueous amine solutions 90% of the absorption capacity was reached within 15 min, and the chemisorption was completed after 25 min [70]. However, it takes about 3 hrs to reach equilibrium for most other ILs to absorb CO_2 physically [71]. The properties of ILs, specifically the viscosity, have an effect on the gas absorption rate. Morgan *et al.* [72]

reported that the diffusivity of gases is inversely related to the viscosity of ILs according to the following equation:

$$D_{12} = 3.7 \times 10^{-3} \frac{1}{\eta_2^{0.59} V_1 \rho_2^2} \qquad \text{Eq.5}$$

Where η_2 is the viscosity, ρ_2 is the density of the IL respectively and V_1 is liquid molar volume of the solute (gas) [9]. Thus, ILs with a high viscosity lead to low absorption and desorption rates in comparison to conventional chemical absorbents, e.g., aqueous amine solutions and physical absorbents (e.g., Selexol). However, it is important to note that IL viscosities show a strong sensitivity to temperature. Furthermore, Ahosseini et al. [73] reported that the viscosity of ILs decreases drastically with the CO_2 concentration. A lower viscosity of the IL results in higher gas diffusivities.

In general, ILs are more expensive than conventional solvents. Therefore, it can be difficult to apply ILs in conventional absorption columns. For this reason, researchers have given much attention to create new cost-effective technologies using small amount of low-viscous ILs.

There has been a growing interest in the use of ILs in supported liquid membranes (SILM). SILM is produced by impregnating a porous membrane with a small amount of IL. Traditional liquid membranes suffer from non-stability due to evaporation of the solvent at higher temperatures in time [74]. However, SILMs do not have this problem, as the ILs show extremely low volatility that will minimize solvent losses from the membrane [71].

Park *et al*. [75] used supported ionic liquid membranes (SILMs) for the removal of CO_2 and H_2S from crude natural gas. The reported results showed a good performance for the studied membranes with high selectivities for both CO_2/CH_4 and H_2S/CH_4. These SILMs could not withstand the higher pressures required for natural gas sweetening. Therefore, Barghi *et al.* [76] studied CO_2/CH_4 selectivity using [bmim][PF_6] IL supported on an alumina membrane, showing that permeability and solubility of CO_2 is much higher than that of CH_4. Furthermore, this membrane can provide a higher selectivity for CO_2/CH_4 in comparison to traditional polymer membranes. The permselectivity factor (α_{AB}) is defined as the ratio of the permeances of gases A and B through a membrane:

$$\alpha_{AB} = \frac{P_A}{P_B} = \frac{D_A \times S_A}{D_B \times S_B} \qquad \text{Eq.6}$$

where P is permeability in mol·m/m^2·sPa, S is the solubility coefficient in mol/m^3·Pa and D is the diffusivity in m^2/s of the gas molecule in the IL [77]. As shown by Equation 6, the permselectivity depends on both transport properties (diffusion) and thermodynamic equilibria (solubilities).

2.4 References

[1] S. Mokhatab, W.A. Poe, J.G. Speight, Handbook of Natural Gas Transmission and Processing, First ed., Elsevier Science, 2011.

[2] F. Karadas, M. Atilhan, S. Aparicio, Review on the Use of Ionic Liquids (ILs) as Alternative Fluids for CO_2 Capture and Natural Gas Sweetening, Energy & Fuels, 24 (2010) 5817-5828.

[3] S. Ma'mun, V.Y. Dindore, H.F. Svendsen, Kinetics of the Reaction of Carbon Dioxide with Aqueous Solutions of 2-((2-Aminoethyl)amino)ethanol, Industrial & Engineering Chemistry Research, 46 (2006) 385-394.

[4] K. Simons, K. Nijmeijer, M. Wessling, Gas–liquid membrane contactors for CO_2 removal, Journal of Membrane Science, 340 (2009) 214-220.

[5] A.B. Rao, E.S. Rubin, A Technical, Economic, and Environmental Assessment of Amine-Based CO_2 Capture Technology for Power Plant Greenhouse Gas Control, Environmental Science & Technology, 36 (2002) 4467-4475.

[6] B.D. Bhide, A. Voskericyan, S.A. Stern, Hybrid processes for the removal of acid gases from natural gas, Journal of Membrane Science, 140 (1998) 27-49.

[7] B.R. Strazisar, R.R. Anderson, C.M. White, Degradation Pathways for Monoethanolamine in a CO_2 Capture Facility, Energy & Fuels, 17 (2003) 1034-1039.

[8] A.J. Kidnay, W.R. Parrish, D.G. McCartney, Fundamentals of Natural Gas Processing, Second ed., CRC PressINC, 2011.

[9] G.F. Versteeg, W.P.M. van Swaaij, On the kinetics between CO_2 and alkanolamines both in aqueous and non-aqueous solutions—I. Primary and secondary amines, Chemical Engineering Science, 43 (1988) 573-585.

[10] J.A. Bullin, W.G. Brown, hydrocarbons and BTEX pickup and control from amines systems, 83rd Annual Convention of the Gas Processors Association, Texas (2004).

[11] J. Collie, M. Hlavinka, A. Ashoworth, An Analysis of BTEX emissions from Amine Sweetening and Glycol Dehydration Facilities,: Laurance Reid Gas Conditioning Conference Proceedings, Oklahoma, (1998).

[12] D. Chinn, D. Vu, M. Driver, L. Boudreau, CO_2 removal from gas using ionic liquid absorbents, Google Patents, (2005).

[13] W. Guo, F. Feng, G. Song, J. Xiao, L. Shen, Simulation and energy performance assessment of CO_2 removal from crude synthetic natural gas via physical absorption process, Journal of Natural Gas Chemistry, 21 (2012) 633-638.

[14] A.-L. Revelli, F. Mutelet, J.-N.l. Jaubert, High Carbon Dioxide Solubilities in Imidazolium-Based Ionic Liquids and in Poly(ethylene glycol) Dimethyl Ether, The Journal of Physical Chemistry *B*, 114 (2010) 12908-12913.

[15] G. Hochgesand, Rectisol and Purisol, Industrial & Engineering Chemistry, 62 (1970) 37-43.

[16] K. Marsh, A. Deev, A.-T. Wu, E. Tran, A. Klamt, Room temperature ionic liquids as replacements for conventional solvents – A review, Korean Journal of Chemical Engineering, 19 (2002) 357-362.

[17] P. Scovazzo, J. Kieft, D.A. Finan, C. Koval, D. DuBois, R. Noble, Gas separations using non-hexafluorophosphate [PF_6] anion supported ionic liquid membranes, Journal of Membrane Science, *238* (2004) 57-63.

[18] M.V.B. Zanoni, E.I. Rogers, C. Hardacre, R.G. Compton, The electrochemical reduction of the purines guanine and adenine at platinum electrodes in several room temperature ionic liquids, Analytica Chimica Acta, 659 (2010) 115-121.

[19] N. Fontanals, S. Ronka, F. Borrull, A.W. Trochimczuk, R.M. Marcé, Supported imidazolium ionic liquid phases: a new material for solid-phase extraction, Talanta, 80 (2009) 250-256.

[20] M.D. Joshi, J.L. Anderson, Recent advances of ionic liquids in separation science and mass spectrometry, RSC Advances, 2 (2012) 5470-5484.

[21] H. Olivier-Bourbigou, L. Magna, D. Morvan, Ionic liquids and catalysis: Recent progress from knowledge to applications, Applied Catalysis A: General, 373 (2010) 1-56.

[22] R.D. Rogers, K.R. Seddon, Ionic Liquids--Solvents of the Future?, Science, 302 (2003) 792-793.

[23] J.F. Brennecke, E.J. Maginn, Ionic liquids: Innovative fluids for chemical processing, AIChE Journal, 47 (2001) 2384-2389.

[24] S. Keskin, D. Kayrak-Talay, U. Akman, Ö. Hortaçsu, A review of ionic liquids towards supercritical fluid applications, The Journal of Supercritical Fluids, 43 (2007) 150-180.

[25] J.F. Wishart, Energy applications of ionic liquids, Energy & Environmental Science, 2 (2009) 956-961.

[26] H. Shirota, E.W. Castner, Why Are Viscosities Lower for Ionic Liquids with −CH2Si(CH3)3 vs −CH2C(CH3)3 Substitutions on the Imidazolium Cations?, The Journal of Physical Chemistry B, 109 (2005) 21576-21585.

[27] S. Raeissi, C.J. Peters, A potential ionic liquid for CO_2-separating gas membranes: selection and gas solubility studies, Green Chemistry, 11 (2009) 185-192.

[28] Z.-B. Zhou, H. Matsumoto, K. Tatsumi, Structure and Properties of New Ionic Liquids Based on Alkyl- and Alkenyltrifluoroborates, ChemPhysChem, 6 (2005) 1324-1332.

[29] A.K.N. Virendra V. Singh, Anil K. Nigam, Mannan Boopathi, Mannan Boopathi, Rajagopalan Vijayaraghavan, Applications of Ionic Liquids in Electrochemical Sensors and Biosensors, International Journal of Electrochemistry, 2012 (2012).

[30] R. Seddon Kenneth, A. Stark, M.-J. Torres, Influence of chloride, water, and organic solvents on the physical properties of ionic liquids, in: Pure and Applied Chemistry, (2000) pp. 2275.

[31] O.O. Okoturo, T.J. VanderNoot, Temperature dependence of viscosity for room temperature ionic liquids, Journal of Electroanalytical Chemistry, 568 (2004) 167-181.

[32] J.G. Huddleston, A.E. Visser, W.M. Reichert, H.D. Willauer, G.A. Broker, R.D. Rogers, Characterization and comparison of hydrophilic and hydrophobic room temperature ionic liquids incorporating the imidazolium cation, Green Chemistry, 3 (2001) 156-164.

[33] K. Docherty, J. Dixon, C. Kulpa Jr, Biodegradability of imidazolium and pyridinium ionic liquids by an activated sludge microbial community, Biodegradation, 18 (2007) 481-493.

[34] F. Atefi, M.T. Garcia, R.D. Singer, P.J. Scammells, Phosphonium ionic liquids: design, synthesis and evaluation of biodegradability, Green Chemistry, 11 (2009) 1595-1604.

[35] M.T. Garcia, N. Gathergood, P.J. Scammells, Biodegradable ionic liquids Part II. Effect of the anion and toxicology, Green Chemistry, 7 (2005) 9-14.

[36] N. Gathergood, P.J. Scammells, M.T. Garcia, Biodegradable ionic liquids Part III. The first readily biodegradable ionic liquids, Green Chemistry, 8 (2006) 156-160.

[37] M. Uerdingen, C. Treber, M. Balser, G. Schmitt, C. Werner, Corrosion behaviour of ionic liquids, Green Chemistry, 7 (2005) 321-325.

[38] I. Perissi, U. Bardi, S. Caporali, A. Lavacchi, High temperature corrosion properties of ionic liquids, Corrosion Science, 48 (2006) 2349-2362.

[39] A.B. Tolstoguzov, U. Bardi, S.P. Chenakin, Study of the corrosion of metal alloys interacting with an ionic liquid, Bull. Russ. Acad. Sci. Phys., 72 (2008) 605-608.

[40] T. Welton, Room-Temperature Ionic Liquids. Solvents for Synthesis and Catalysis, Chemical Reviews, 99 (1999) 2071-2084.

[41] L.A. Blanchard, Z. Gu, J.F. Brennecke, High-Pressure Phase Behavior of Ionic Liquid/CO_2 Systems, Journal Physical Chemistry *B*, 105 (2001) 2437-2444.

[42] J. Kumelan, Á. Pérez-Salado Kamps, D. Tuma, G. Maurer, Solubility of CO_2 in the ionic liquid [hmim][Tf_2N], Journal of Chemical Thermodynamics, 38 (2006) 1396-1401.

[43] Y. Chen, S. Zhang, X. Yuan, Y. Zhang, X. Zhang, W. Dai, R. Mori, Solubility of CO_2 in imidazolium-based tetrafluoroborate ionic liquids, Thermochimica Acta, 441 (2006) 42-44.

[44] A.M. Schilderman, S. Raeissi, C.J. Peters, Solubility of carbon dioxide in the ionic liquid 1-ethyl-3-methylimidazolium bis(trifluoromethylsulfonyl)imide, Fluid Phase Equiliria, 260 (2007) 19-22.

[45] A.N. Soriano, B.T. Doma, M.-H. Li, Solubility of Carbon Dioxide in 1-Ethyl-3-methylimidazolium Tetrafluoroborate, Journal of Chemical & Engineering Data, 53 (2008) 2550-2555.

[46] C. Cadena, J.L. Anthony, J.K. Shah, T.I. Morrow, J.F. Brennecke, E.J. Maginn, Why Is CO_2 So Soluble in Imidazolium-Based Ionic Liquids?, Journal of the American Chemical Society, 126 (2004) 5300-5308.

[47] R.E. Baltus, B.H. Culbertson, S. Dai, H. Luo, D.W. DePaoli, Low-Pressure Solubility of Carbon Dioxide in Room-Temperature Ionic Liquids Measured with a Quartz Crystal Microbalance, The Journal of Physical Chemistry *B*, 108 (2003) 721-727.

[48] S.N.V.K. Aki, B.R. Mellein, E.M. Saurer, J.F. Brennecke, High-Pressure Phase Behavior of Carbon Dioxide with Imidazolium-Based Ionic Liquids, The Journal of Physical Chemistry B, 108 (2004) 20355-20365.

[49] S.G. Kazarian, B.J. Briscoe, T. Welton, Combining ionic liquids and supercritical fluids: ATR-IR study of CO dissolved in two ionic liquids at high pressures, Chemical Communications, (2000) 2047-2048.

[50] E. Torralba-Calleja, J. Skinner, D. rrez-Tauste, CO_2 Capture in Ionic Liquids: A Review of Solubilities and Experimental Methods, Journal of Chemistry, 2013 (2013) 16.

[51] T. Seki, J.-D. Grunwaldt, A. Baiker, In Situ Attenuated Total Reflection Infrared Spectroscopy of Imidazolium-Based Room-Temperature Ionic Liquids under "Supercritical" CO_2, The Journal of Physical Chemistry *B*, 113 (2008) 114-122.

[52] R.E. Baltus, B.H. Culbertson, S. Dai, H. Luo, D.W. DePaoli, Low-Pressure Solubility of Carbon Dioxide in Room-Temperature Ionic Liquids Measured with a Quartz Crystal Microbalance, The Journal of Physical Chemistry *B*, 108 (2003) 721-727.

[53] I. Minami, M. Kita, T. Kubo, H. Nanao, S. Mori, The Tribological Properties of Ionic Liquids Composed of Trifluorotris(pentafluoroethyl) Phosphate as a Hydrophobic Anion, Tribology Letters, 30 (2008) 215-223.

[54] J. Huddleston, A. Visser, M. Reichert, H. Willauer, G. Broker, R. Rogers, Characterization and comparison of hydrophilic and hydrophobic room temperature ionic liquids incorporating the imidazolium cation, Green Chemistry, 3 (2001) 156-164.

[55] A. Finotello, J.E. Bara, D. Camper, R.D. Noble, Room-Temperature Ionic Liquids: Temperature Dependence of Gas Solubility Selectivity, Industrial & Engineering Chemistry Research , 47 (2007) 3453-3459.

[56] J. Jacquemin, P. Husson, V. Majer, M.F.C. Gomes, Low-pressure solubilities and thermodynamics of solvation of eight gases in 1-butyl-3-methylimidazolium hexafluorophosphate, Fluid Phase Equilibria , 240 (2006) 87-95.

[57] S. Raeissi, C.J. Peters, High pressure phase behaviour of methane in 1-butyl-3-methylimidazolium bis(trifluoromethylsulfonyl)imide, Fluid Phase Equilibria, 294 (2010) 67-71.

[58] J.L. Anthony, J.M. Crosthwaite, D.G. Hert, S.N.V.K. Aki, E.J. Maginn, J.F. Brennecke, Phase Equilibria of Gases and Liquids with 1--butyl-3-Methylimidazolium Tetrafluoroborate, in: R.D. Rogers, K.R. Seddon (Eds.) Ionic Liquids as Green Solvents, American Chemical Society, Washington, (2003) 110-120.

[59] J.L. Anthony, E.J. Maginn, J.F. Brennecke, Solubilities and Thermodynamic Properties of Gases in the Ionic Liquid 1-n-Butyl-3-methylimidazolium Hexafluorophosphate, Journal Physical Chemistry *B*, 106 (2002) 7315-7320.

[60] J. Kumełan, Á. Pérez-Salado Kamps, D. Tuma, G. Maurer, Solubility of the Single Gases Methane and Xenon in the Ionic Liquid [hmim][Tf_2N], Industrial & Engineering Chemistry Research , 46 (2007) 8236-8240.

[61] P.J. Carvalho, J.A.P. Coutinho, The polarity effect upon the methane solubility in ionic liquids: a contribution for the design of ionic liquids for enhanced CO_2/CH_4 and H_2S/CH_4 selectivities, Energy & Environmental Science, 4 (2011) 4614-4619.

[62] D.G. Hert, J.L. Anderson, S.N.V.K. Aki, J.F. Brennecke, Enhancement of oxygen and methane solubility in 1-hexyl-3-methylimidazolium bis(trifluoromethylsulfonyl) imide using carbon dioxide, Chemical Communications, (2005) 2603-2605.

[63] W. Shi, E.J. Maginn, Molecular Simulation and Regular Solution Theory Modeling of Pure and Mixed Gas Absorption in the Ionic Liquid 1-n-Hexyl-3-methylimidazolium Bis(Trifluoromethylsulfonyl)amide ([hmim][Tf_2N]), The Journal of Physical Chemistry *B*, 112 (2008) 16710-16720.

[64] V.A. Toussaint, E. Kühne, A. Shariati, C.J. Peters, Solubility measurements of hydrogen in 1-butyl-3-methylimidazolium tetrafluoroborate and the effect of carbon dioxide and a selected catalyst on the hydrogen solubility in the ionic liquid, The Journal of Chemical Thermodynamics, 59 (2013) 239-242.

[65] L.J. Florusse, S. Raeissi, C.J. Peters, High-Pressure Phase Behavior of Ethane with 1-Hexyl-3-methylimidazolium Bis(trifluoromethylsulfonyl)imide, Journal of Chemical & Engineering Data, 53 (2008) 1283-1285.

[66] B.-C. Lee, S.L. Outcalt, Solubilities of Gases in the Ionic Liquid 1-n-Butyl-3-methylimidazolium Bis(trifluoromethylsulfonyl)imide, Journal of Chemical & Engineering Data, 51 (2006) 892-897.

[67] G. Hong, J. Jacquemin, M. Deetlefs, C. Hardacre, P. Husson, M.F. Costa Gomes, Solubility of carbon dioxide and ethane in three ionic liquids based on the bis{(trifluoromethyl)sulfonyl}imide anion, Fluid Phase Equilibria, 257 (2007) 27-34.

[68] J.B. Tang, W.L. Sun, H.D. Tang, M. Radosz, Y.Q. Shen, Enhanced CO_2 absorption of poly(ionic liquid)s, Macromolecules, 38 (2005) 2037-2039.

[69] C. Wang, H. Luo, D.-e. Jiang, H. Li, S. Dai, Carbon Dioxide Capture by Superbase-Derived Protic Ionic Liquids, Angewandte Chemie International Edition, 49 (2010) 5978-5981.

[70] D. Camper, J.E. Bara, D.L. Gin, R.D. Noble, Room-Temperature Ionic Liquid−Amine Solutions: Tunable Solvents for Efficient and Reversible Capture of CO_2, Industrial & Engineering Chemistry Research, 47 (2008) 8496-8498.

[71] E.D. Bates, R.D. Mayton, I. Ntai, J.H. Davis, CO_2 Capture by a Task-Specific Ionic Liquid, Journal of the American Chemical Society, 124 (2002) 926-927.

[72] D. Morgan, L. Ferguson, P. Scovazzo, Diffusivities of Gases in Room-Temperature Ionic Liquids: Data and Correlations Obtained Using a Lag-Time Technique, Industrial & Engineering Chemistry Research, 44 (2005) 4815-4823.

[73] A. Ahosseini, E. Ortega, B. Sensenich, A.M. Scurto, Viscosity of n-alkyl-3-methyl-imidazolium bis(trifluoromethylsulfonyl)amide ionic liquids saturated with compressed CO_2, Fluid Phase Equilibria, 286 (2009) 72-78.

[74] H. Yang, Z. Xu, M. Fan, R. Gupta, R.B. Slimane, A.E. Bland, I. Wright, Progress in carbon dioxide separation and capture: A review, Journal of Environmental Sciences, 20 (2008) 14-27.

[75] Y.-I. Park, B.-S. Kim, Y.-H. Byun, S.-H. Lee, E.-W. Lee, J.-M. Lee, Preparation of supported ionic liquid membranes (SILMs) for the removal of acidic gases from crude natural gas, Desalination, 236 (2009) 342-348.

[76] S.H. Barghi, M. Adibi, D. Rashtchian, An experimental study on permeability, diffusivity, and selectivity of CO_2 and CH_4 through [bmim][PF_6] ionic liquid supported on an alumina membrane: Investigation of temperature fluctuations effects, Journal of Membrane Science, 362 (2010) 346-352.

[77] J.J. Close, K. Farmer, S.S. Moganty, R.E. Baltus, CO_2/N_2 separations using nanoporous alumina-supported ionic liquid membranes: Effect of the support on separation performance, Journal of Membrane Science, 390–391 (2012) 201-210.

Chapter 3

Solubility of Carbon Dioxide in the Ionic Liquid [emim][FAP]

This chapter is adapted from the following publication: M. Althuluth, M.T. Mota-Martinez, M.C. Kroon, C.J. Peters, J. Chem. Eng. Data, 57 (2012) 3422-3425.

3.1 Introduction

In the last two decades, ILs were recognized as novel solvents for gas separation processes [1]. Reason is that the solubility of various gases (e.g., CO_2) in ILs is high, while ILs cannot evaporate and contaminate the gas stream, because their vapor pressure at room temperature is negligibly low [2]. Therefore, ILs can be used in gas absorption processes e.g., as solvents for carbon capture [2, 3]. Especially for the design of separation processes involving ILs, the phase behavior of IL systems is of great importance.

The most widely investigated binary IL + gas systems are their mixtures with CO_2 [4-8]. The CO_2 solubility in an IL is generally high at lower pressures, but a nearly infinite bubble-point slope is present at a specific maximum concentration of CO_2, beyond which increasing the external pressure hardly increases the CO_2 solubility in the IL. According to Huang *et al.*[9], the reason for this sharp pressure increase at a certain maximum CO_2 concentration is that at this point all cavities in the IL phase are occupied by CO_2, so that further insertion of CO_2 would require "breaking" the cohesive structure of the IL.

It was found that the anion predominantly determines the CO_2 solubility in the ILs. ILs with fluorous anions e.g., [Tf_2N^-], [BF_4^-] and [PF_6^-] show highest CO_2 solubility [10]. On the contrary, it was found that ILs with non-fluorous anions such as alkanoates and sulfates have a much lower CO_2 solubility [11]. The solubility of CO_2 in an IL is less strongly influenced by the type of the cation. However, the CO_2 solubility in ILs having fluorinated cations is higher as compared to ILs with non-fluorinated cations [11]. It was also observed that an increase in the alkyl chain length on the cation slightly increases the CO_2 solubility in the IL [12].

Although fluorine-containing ILs are generally good solvents for CO_2, they are less stable with respect to moisture and air, especially at high temperatures when hydrofluoric acid (HF) can be formed [13]. Moreover, most of the imadazolium and ammonium salts are hydrophilic, which means that these ILs can dissolve significant amounts of water. It was reported that the hygroscopic character of ILs is strongly influenced by the anion size, where the stability with respect to moisture increases with increasing anion size in the order [PF_6^-] < [BF_4^-] < [Tf_2N^-] [14].

It would be desirable to design an IL that displays high CO_2 solubility and that is stable with respect to moisture and air. It is expected that highly fluorinated ILs with a large anion size, such as tris(fluoroalkyl)trifluorophosphate based ILs, should fulfill these requirements [15]. This work investigates the solubility of CO_2 in such an IL i.e., [emim][FAP] at temperatures ranging from (283.75 to 364.13) K and pressures up to 10.40 MPa. The molecular structure of [emim][FAP] is schematically shown in Figure 3.1.

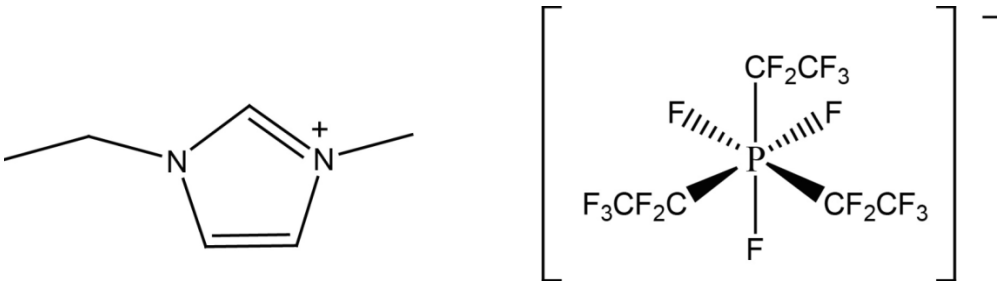

Figure 3.1: Structure of 1-ethyl-3-methylimidazolium tris(pentafluoroethyl)trifluorophosphate ([emim][FAP]).

To the best of our knowledge the CO_2 solubility in this IL has never been measured before.

3.2 Experimental

3.2.1 Materials

The CO_2 gas was supplied by Hoek Loos with a purity of 99.995%. The IL [emim][FAP] was provided by Merck Chemical Company with a purity of ≥ 99.0 % and was used as such. The water content of the IL was measured using Karl Fischer moisture analysis and was less than 200 ppm. Within the temperature range of the experiments, the IL did not show any decomposition or reaction with the CO_2.

3.2.2 Experimental set-up and procedure

The solubility of CO_2 in [emim][FAP] IL was determined by measuring bubble point pressures at different temperatures and compositions using the Cailletet equipment. The pressure was adjusted for a sample at constant composition until a (liquid + vapor)-to-(liquid) phase transition was visually observed.

The main part of the Cailletet equipment is a Pyrex glass tube, which serves as high pressure vessel and equilibrium cell. A known quantity of IL was transferred to the Pyrex tube

(Cailletet tube). Thereafter, the tube was connected to a gas rack, and the ionic liquid sample was frozen by liquid nitrogen. Subsequently, the IL is degassed under vacuum, see Figure 3.2.

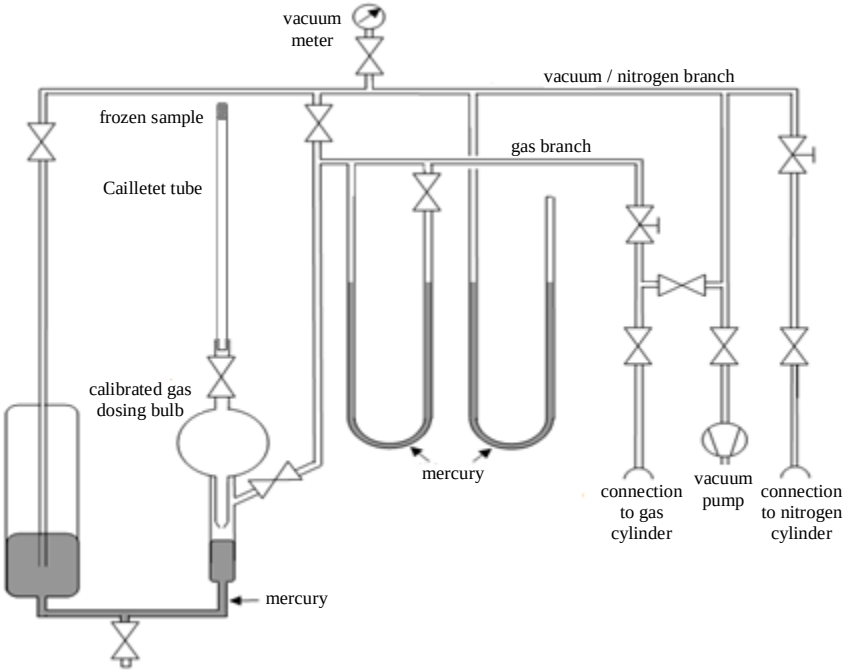

Figure 3.2: Schematic representation of the gas-rack [16].

Next, a vessel with a calibrated volume was filled with CO_2. The amount of moles of CO_2 (n) in the calibrated vessel could be calculated using the virial equation of state (Eq.1) since pressure (P), temperature (T) and volume (V_m) were known. The second viral coefficient (B) was taken from literature [17].

$$\frac{PV_m}{RT} = 1 + \frac{B}{V_m} \qquad \text{Eq.1}$$

Mercury was used to push the CO_2 into the Cailletet tube, to seal the sample and to act as pressure-transmitter fluid. After the sample of known composition was sealed into Cailletet tube with mercury, the tube was immersed in the mercury in the autoclave, see Figure 3.3.

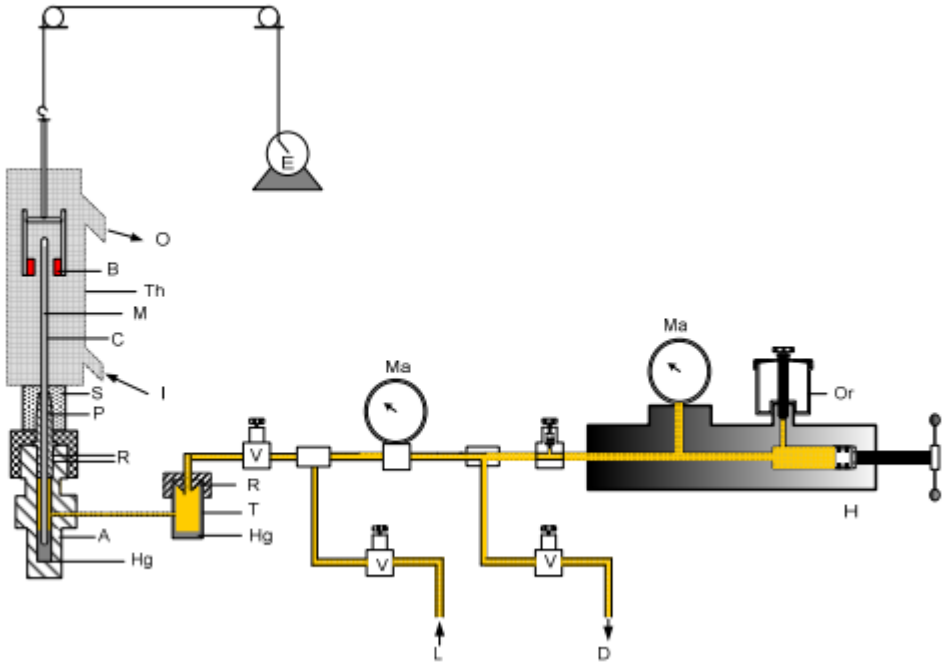

Figure 3.3: The Cailletet apparatus: A, autoclave; B, magnets; C, Cailletet tube; D, drain; E, motor; H, rotating hand pump; Hg, mercury; I, inlet thermostat liquid; L, connection to dead weight pressure gauge; M, mixture being investigated; Ma, manometers; O, outlet thermostat liquid; Or, hydraulic oil reservoir; P, closing plug; R, O-rings; S, silicone rubber stopper; T, mercury trap; Th, glass thermostat; V, valve [18].

In the equipment shown in Figure 3.3, the pressure was generated by pressing hydraulic oil into the system with a screw-type hand pump, which caused the level of the mercury column in tube to rise and to create the desired pressure in the top. A dead-weight pressure gauge was used to measure the pressure. The temperature of the sample was kept constant by circulating the heat transferring fluid through a thermostat jacket surrounding the Cailletet tube. The temperature was measured with a platinum resistance thermometer inserted in the heat jacket. The sample was kept well-mixed by moving a steel ball with two moving magnets. The Cailletet equipment allows measurement of phase equilibria within a pressure range of 0.1 to 15 MPa and temperatures ranging from 255 to 470 K, depending on the heat-transferring fluid used. In our experiment the fluid used was water; thus, the temperature range was limited from 275 to 370 K. The uncertainty of the measurements is ± 0.005 mole fraction in the composition, ± 0.01 K for the temperature measurements and ± 0.003 MPa for the pressure measurements.

3.3 Results and discussion

3.3.1 Physical properties of IL

Knowledge of the properties of the ILs is a prerequisite for choosing a suitable IL to apply in gas separation technology. Physical properties such as density, viscosity, surface tension, thermal stability, etc. are crucial for an optimum process design. For instance, the viscosity is a major factor that determines the rate of mass transport in the ILs since the viscosity of ILs has a strong inversely influence on the gas diffusion in ILs [19]. In other words, ILs with high viscosities may cause a slow mass transfer of the gases in the gas separation applications. For this reason there is a major interest to focus on a new generation of ILs exhibiting lower viscosities.

The viscosity and density of [emim][FAP] were measured at 0.1MPa in the temperature range from 293.15 to 363.15 K using an Anton Paar SVM 3000 facility. In Table 3.1 the experimental data are presented. All data were measured in triplicate. Standard deviations less than ± 0.20 mP.s in the viscosity and ± 0.1 $kg \cdot m^{-3}$ in the density were obtained, respectively. In Figure 3.4 the experimental data of the viscosity and density are depicted as a function of temperature.

Table 3.1: Experimental data of dynamic viscosity (η) and density (ρ) of [emim][FAP] at several temperatures.

T (K)	η (mP.s)	ρ ($kg \cdot m^{-3}$)
293.15	75.52	1714.2
303.15	49.06	1702.4
313.15	33.80	1690.6
323.15	24.37	1678.9
333.15	18.23	1667.2
343.15	14.11	1655.6
353.15	11.20	1644.1
363.15	9.09	1632.8

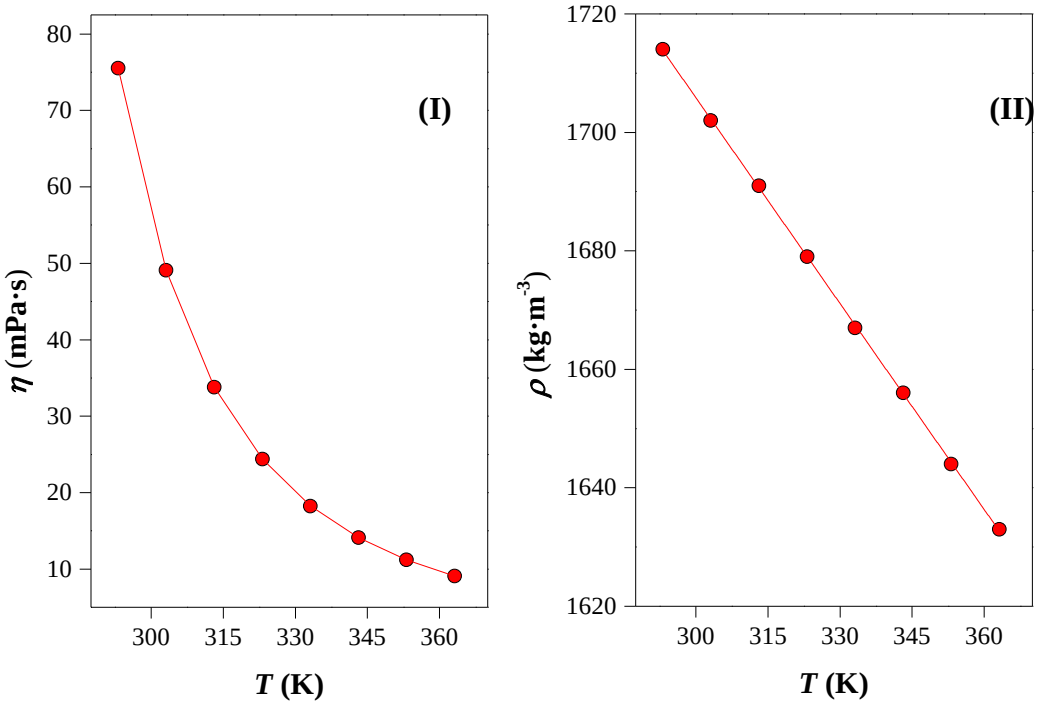

Figure 3.4: Graphic representation of the **(I)** viscosity and **(II)** density, of [emim][FAP] at 0.1MPa as a function of temperature.

It can be observed that the temperature has a more pronounced effect on the viscosity than on the density. The viscosity decreases exponentially with increasing temperature. Several theoretical models and empirical or semi-empirical expressions are available in literature relating the viscosity of liquids to pressure and / or temperature [20]. In this work, the Vogel-Tammann-Fulcher (VTF) equation was used to correlate the experimental viscosity data with temperature [20]:

$$\eta(T) = A_\eta \cdot \exp\left[\frac{B_\eta}{(T - C_\eta)}\right] \qquad \text{Eq.2}$$

where $\eta(T)$ is the viscosity in mPa·s, T is the temperature in K, and A_η, B_η and C_η are adjustable parameters. The parameters and the relative average deviation for the fitting of the viscosity with the VTF equation are listed in Table 3.2. It can be concluded that the VTF equation satisfactory fits the experimental data.

Table 3.2: Fitting parameters of the VFT equation and relative average deviation (AD) for the viscosity data.

	A_η (mPa·s)	B_η (K)	C_η (K)	AD (%)
[emim][FAP]	1.678×10^{-1}	806.8	161.1	0.1

The experimental density data (ρ) in the studied temperature (T) range was correlated using a first order polynomial:

$$\left(\rho / \mathrm{kg \cdot m^{-3}}\right) = a + b \cdot T \qquad \text{Eq.3}$$

where a and b are fitting parameters. Table 3.3 shows the values of the fitting parameters of equation (3).

Table 3.3: Fitting parameters and root mean square deviations for the liner fitting of the density dependency with temperature .

	a / kg·m^{-3}	b /kg·m^{-3} K^{-1}	R^2
[emim][FAP]	2054	− 1.159	1.0

As shown in Figure 3.5, the viscosities measured for [emim][FAP] are slightly higher than those reported for ILs based on the [Tf_2N^-] anion and lower than ILs based on ($Et[SO_4]^-$) anions [21, 22].

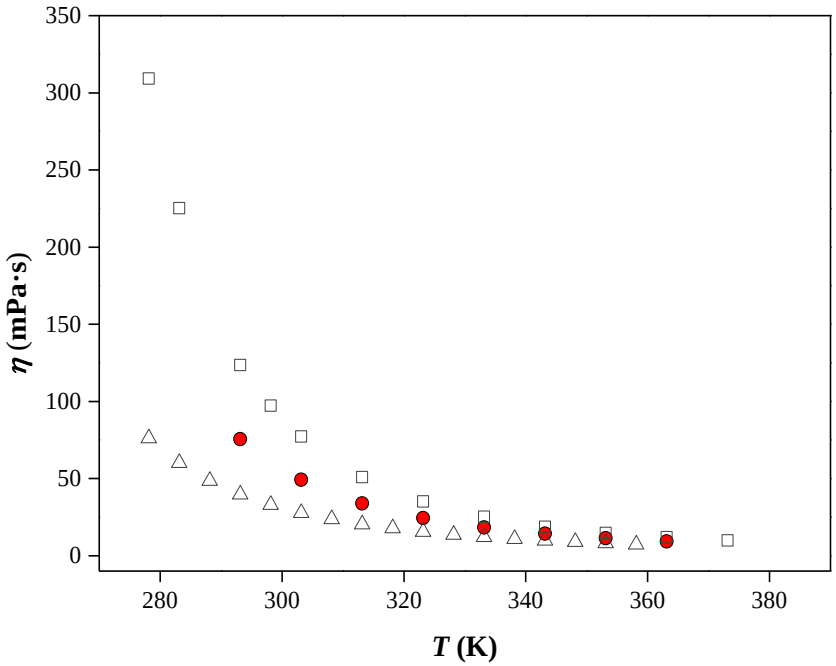

Figure 3.5: Viscosities as a function of temperature: ●, [emim][FAP]; △, [emim][Tf_2N]; □, [emim][$Et(SO_4)$].

The density decreases with increasing length of the alkyl chain present in the imidazolium cation and increases with the molecular mass of the anion in the order $[BF_4]<[PF_6]<[Tf_2N]<[FAP]$ [23].

The surface tension measurements were performed using the Kruss K11Mk4 tensiometer. It can be seen from Table 3.4 that with increasing temperature the surface tension of [emim][FAP] slightly decreases. All values were measured in triplicate with standard deviation of ± 0.070 $mN \cdot m^{-1}$.

Table 3.4: Experimental data of surface tension (σ) of [emim][FAP] at several temperatures (*T*)

T (K)	σ ($mN \cdot m^{-1}$)
295.53	35.21
312.07	34.66
319.49	34.35
331.71	33.43

The heat capacity of the IL [emim][FAP] was measured using a differential scanning calorimeter (Perkin-Elmer Pyris Diamond DSC) over the temperature range from (298.15 to 363.15) K. The experimental data obtained are reported in Table 3.5. It was observed that the heat capacity of [emim][FAP] slightly increases with increasing temperature.

Table 3.5: Experimental data of heat capacity of [emim][FAP] IL at several temperatures (*T*)

T (K)	c_p ($J \cdot K^{-1} \cdot g^{-1}$)
298.15	2.27
313.15	2.32
333.15	2.37
363.15	2.45

The thermal stability of [emim][FAP] was investigated with a Thermo Gravimetric Analyzer (TGA, Perkin Elmer model 4000) in a N_2 atmosphere and applying a heating rate of 5 $K \cdot min^{-1}$ in the temperature range of (323 – 873) K. The thermogram for [emim][FAP] is presented in Figure 3.6.

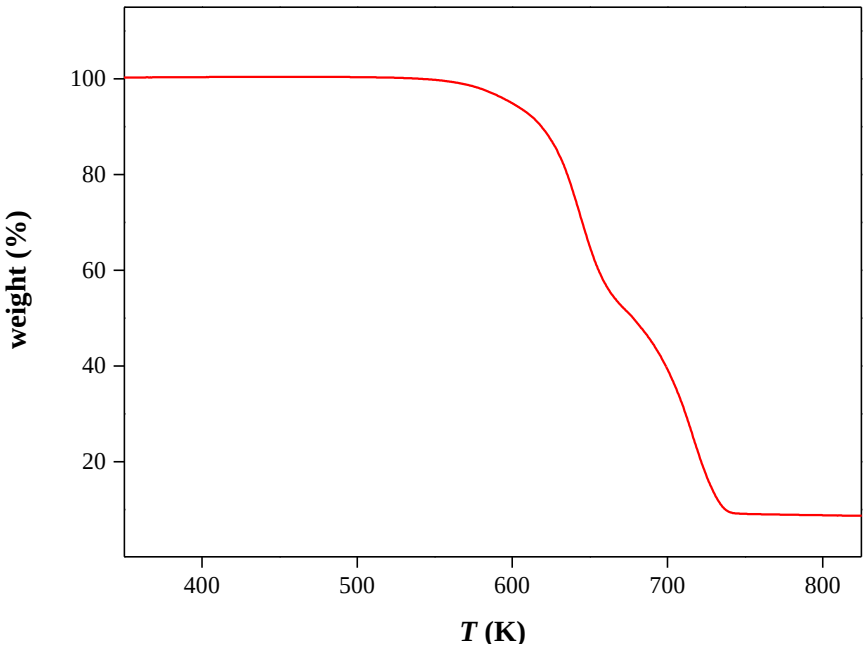

Figure 3.6 : TGA thermogram for [emim][FAP].

It can be seen from Figure 3.6 that [emim][FAP] IL starts to decompose around 623 K. To evaluate the thermal stability of the IL [emim][FAP] at isothermal conditions, the weight loss of [emim][FAP] was measured at several temperatures under N_2 atmosphere during 12 hours.

Table 3.6: Weight loss % of [emim][FAP] after 12 hours at several temperatures.

T (K)	Weight loss (%)
373.15	0.2
425.15	0.4
523.15	33.5

As can be seen from Table 3.6, the weight loss of the sample after heating at 523.15 K was 33.5 %, while the weight loss of the samples was only 0.2 %, 0.4 % after heating at 373.15 K and 425.15 K, respectively. The IL [emim][FAP] was provided by Merck Chemical Company with a purity of $\geq$ 99.0 % and the water content was less than 200 ppm. Thus, the weight loss at the lower temperatures could be caused by evaporation of the impurities. Consequently, [emim][FAP] can resist operating temperatures in the gas sweetening process up to at least 400 K.

3.3.2 Solubility of CO_2 in IL

The solubility of CO_2 in the IL [emim][FAP] was determined at temperatures ranging from 283.75 to 364.13 K and pressures up to 10.40 MPa by measuring the bubble point pressures at various compositions of CO_2 in the IL. The water content was kept below 200 ppm for all samples prepared. The results are shown in Table 3.7 and graphically presented in Figure 3.7.

Table 3.7: Experimental bubble-point pressures (P) for various concentrations of CO_2 (x_{CO2}) and temperatures (T) in the CO_2 + [emim][FAP] system.

x_{CO2} (mol %)	T (K)	P (MPa)	T (K)	P (MPa)	T (K)	P (MPa)
	313.89	0.447	344.00	0.664		
10.03	323.92	0.510	354.04	0.748		
	333.85	0.580	364.09	0.837		
	283.93	0.536	313.83	0.934	343.98	1.452
20.45	293.95	0.654	323.82	1.092	354.09	1.636
	303.89	0.787	333.97	1.270	364.08	1.839
	283.94	0.837	313.88	1.487	343.99	2.332
30.12	293.69	1.024	323.92	1.741	354.05	2.653
	303.87	1.237	333.97	2.035	364.09	2.999
	283.89	1.221	313.94	2.229	343.91	3.532
39.97	293.90	1.518	323.94	2.633	353.92	4.030
	303.93	1.884	333.97	3.078	364.13	4.569
	283.75	1.716	313.88	3.177	344.03	5.167
50.10	293.88	2.145	323.93	3.779	354.03	5.937
	303.87	2.628	333.96	4.446	364.03	6.742
	293.83	3.137	324.07	5.661	353.93	9.062
60.00	303.83	3.758	333.98	6.698	364.06	10.400
	313.95	4.553	344.00	7.833		

[a]Standard uncertainties u are $u(T) = 0.01$ K, $u(P) = 0.003$ MPa, and $u(x_{CH4}) = 0.005$

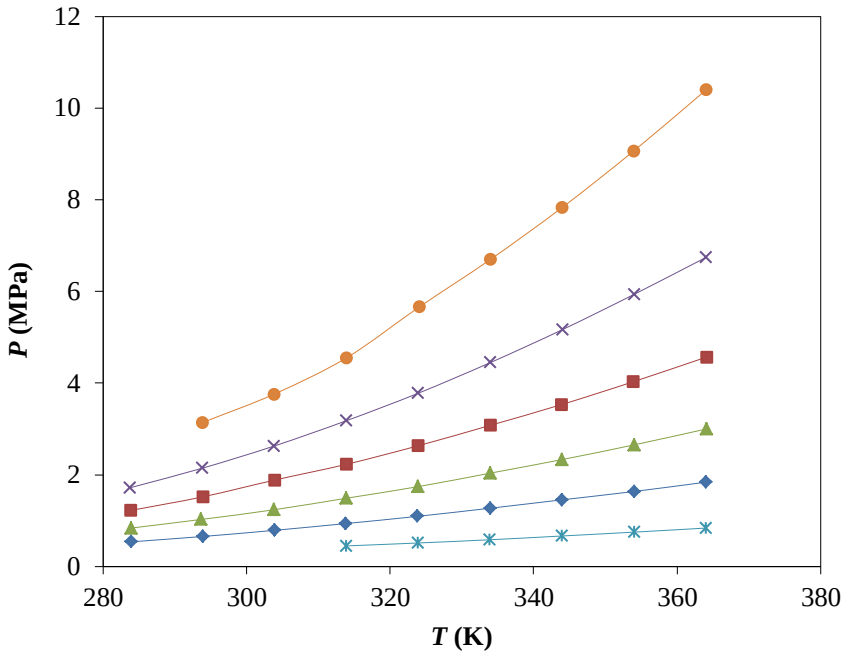

Figure 3.7: Experimentally determined isopleths of the bubble point pressures for several compositions of CO_2 in the binary system CO_2 + [emim][FAP]: ✱, 10.03 mol%; ◆, 20.45 mol%; ▲, 30.12 mol%; ■, 39.97 mol%; ✖, 50.10 mol%; ●, 60.00 mol%

From Figure 3.7 it can be concluded that the bubble point pressures increase with increasing temperature i.e, the solubility of CO_2 in the IL [emim][FAP] decreases with increasing temperature. This is the common trend for the solubility of CO_2 in ILs [5, 7, 8, 11, 24-26]. Thus, when the temperature is increased, a simultaneous increase in pressure is required to dissolve a fixed amount of CO_2 in [emim][FAP]. For example, a pressure of 2.1 MPa is required to dissolve 50 mol% of CO_2 at T = 293 K, while the required pressure is 5.08 MPa at T = 343 K.

When the mole fraction of CO_2 is increased isothermally, the bubble point pressures increase sharply. This can be better observed from Figure 3.8, where the bubble point pressure is plotted against the mole fraction of CO_2 at fixed temperature. It can be seen that the bubble point pressures increase more than linearly with increasing CO_2 concentration at given temperature, which is the typical behavior for IL + CO_2 systems [27]. This phase behavior for binary systems of CO_2 + [emim][FAP] IL systems probably belongs to type III of the van Konynenburg and Scott classification. Many researchers have reported that CO_2 + IL systems belong to type III behavior [28, 29].

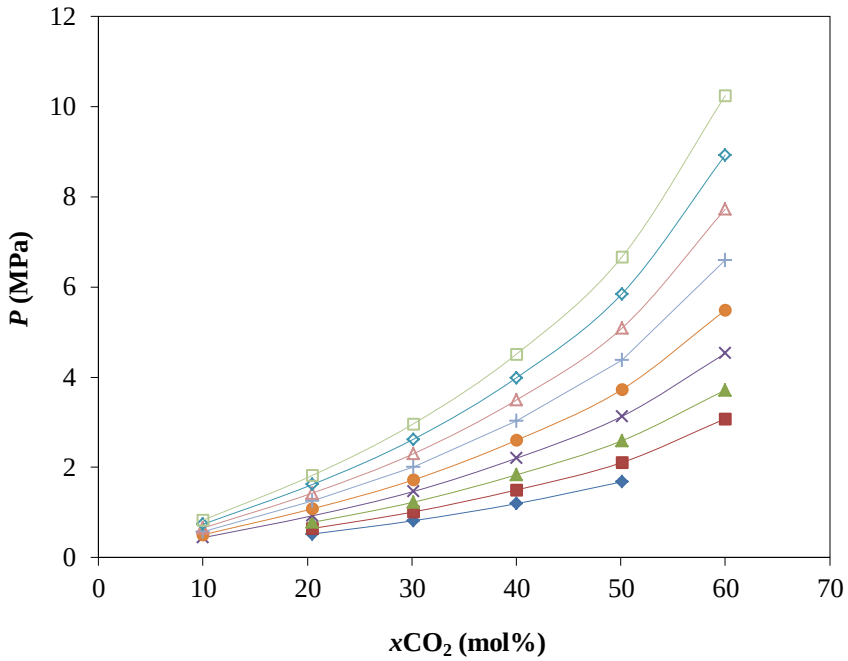

Figure 3.8: Isotherms of the bubble point pressures at several temperatures of the binary system CO_2 + [emim][FAP]: ◆, 283 K; ■, 293 K; ▲, 303 K; ×, 313 K; ●, 323 K; +, 333 K; △, 343; ◇, 353 K; □, 363 K .

The results for the solubility of CO_2 in [emim][FAP] can be expressed in terms of Henry's constants using the Krichevsky–Kasarnovsky equation (Eq. 4) [30]:

$$\ln\frac{f_2}{x_2} = \ln H_{21} + \frac{\bar{V}_2^{\infty}(P - P_1^S)}{RT} \qquad \text{Eq.4}$$

where f_2 is the fugacity of CO_2 in the gas phase, x_2 is the mole fraction of CO_2 in solvent (1), P_1^s is the saturated vapor pressure of solvent (1), H_{21} is Henry's constant of gas (2) in solvent (1) at the liquid saturation pressure, $\bar{V}_2^{\infty}$ is the partial molar volume of gas (2) at infinite dilution, R is the universal gas constant, and T is the absolute temperature. In this work, the solvent is the IL [emim][FAP], which has a negligible vapor pressure.[24] Therefore, the saturated vapor pressure P_1^s is zero, and f_2 can be substituted for the fugacity of pure CO_2 gas. Equation (1) can then be rearranged into equation (5):

$$\ln\frac{f_2}{x_2} = \ln H_{21} + \frac{\bar{V}_2^{\infty}(P)}{RT} \qquad \text{Eq. 5}$$

Therefore, when the solubility data of CO_2 in [emim][FAP] are plotted in the form of a Krichevsky–Kasarnovsky plot ($\ln(f_2/x_2)$ versus P), the intercept and slope yield $\ln H_{21}$ and $\overline{V}_2^{\infty}$ at each temperature. Table 3.8 presents the Henry's constants obtained in this work for the solubility of CO_2 in [emim][FAP]. Again, it is observed that highest solubility, indicated by lowest Henry's constants, is achieved at lowest temperatures, and that the solubility decreases with increasing temperature.

Table 3.8: Henry's constants (H) for the solubility of CO_2 in [emim][FAP] at several temperatures (T).

T (K)	H (MPa)
283	2.24
293	2.76
303	3.32
313	4.06
323	4.68
333	5.36
343	6.09
353	6.86
363	7.71

In Figure 3.9, the solubilities of CO_2 in [emim][FAP] at 333 K are compared to the solubilities of CO_2 at the same temperature in other ILs sharing the same cation.

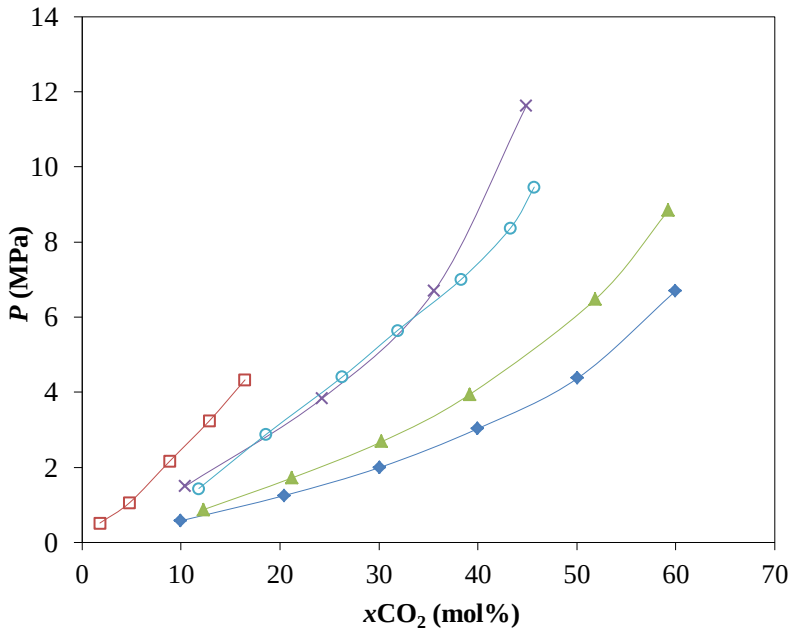

Figure 3.9: Comparison of the isotherms at 333 K for several binary systems consisting of CO_2 + 1-ethyl-3-methylimidazolium based ILs: ◆, [emim][FAP] + CO_2 [This work]; ▲, [emim][Tf_2N] + CO_2 [7]; ○, [emim][$EtSO_4$] + CO_2 [4]; ✖, [emim][PF_6] + CO_2 [31]; □, [emim][BF_4] + CO_2 [8].

It can be seen from Figure 3.9 that the solubility of CO_2 in [emim][FAP] is higher than in all other ILs with the same cation following the trend: [emim][FAP] > [emim][Tf_2N] > [emim][$EtSO_4$] = [emim][PF_6] > [emim][BF_4]. For example, at 333 K the IL [emim][FAP] is able to dissolve up to 60 mol% of CO_2 at a pressure of only 6.7 MPa, which is much lower than the required pressure in all other ILs with the same cation. This is most likely due to the presence of a large amount of fluorine atoms in the anion, which results in an increase of the CO_2 solubility in the IL [11]. The reason of this phenomena is that the fluorine atoms show a specific interaction with CO_2 [32, 33]. Moreover, the IL [emim][FAP] shows higher stability with respect to moisture and air compared to other fluorinated ILs with smaller anions, such as ILs with the [PF_6^-] or the [BF_4^-] anion [14]. Therefore, [emim][FAP] is an attractive solvent for gas separation and carbon capture processes.

Figure 3.10 presents a comparison between the most widely used solvents in the natural gas sweetening process and the IL [emim][FAP]. The CO_2 solubility increases at higher pressures in the IL [emim][FAP] and in the physical solvent (Selexol). The absorption loading of CO_2 in [emim][FAP] IL is slightly higher than in Selexol. At low pressures, the chemical aqueous solutions of amines (DEA and MDEA) show higher CO_2 loading, while the IL tends to be favored over chemical solvents at higher pressures. Aqueous solutions of amines have several drawbacks such as high solvent losses caused by evaporation, degradation, poor thermal stability and much energy for regeneration is needed as tabulated in Table 3.9, and, moreover, aqueous solutions of amines cause equipment corrosion [34-36]. Physical solvents in general suffer from a high affinity for hydrocarbons [37]. This indicates that [emim][FAP] can be a competitive solvent with the commercial solvents for CO_2 removal from natural gas as long as it shows a lower affinity for hydrocarbons.

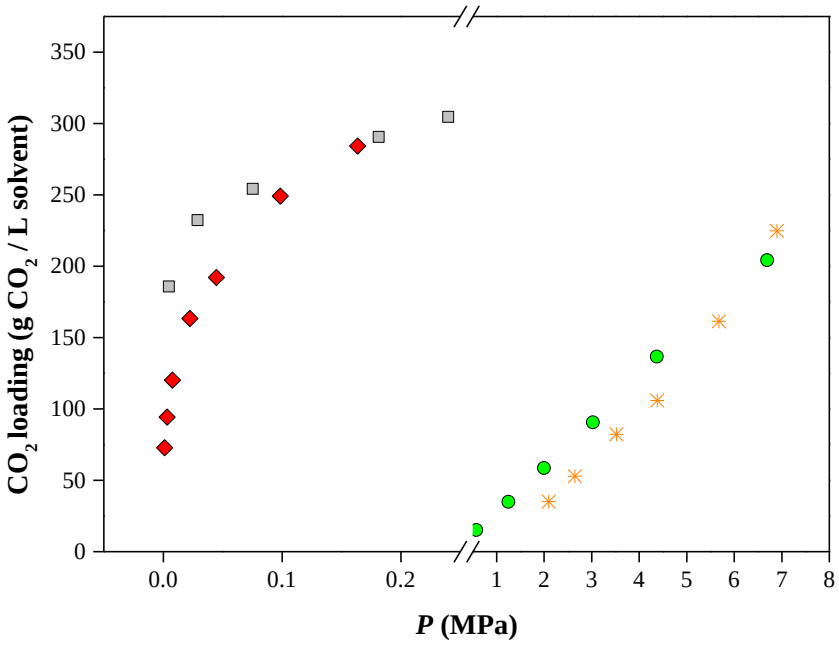

Figure 3.10: Absorption capacity of CO_2 in different solvents: ●, [emim][FAP]; ✳, Selexol.[38]; ■, DEA 30 % [39]; ◆, MDEA 30% [40] at T = 333 K.

Table 3.9: Enthalpy of solution of CO_2 in various solvents.

Solvent	$\Delta_{sol}h$ (kJ/mol)
DEA 30 wt%	-70
Selexol	-16
[emim][FAP]	-12

3.4 Conclusions

The solubility of CO_2 in the IL [emim][FAP] has been experimentally determined. It is shown that CO_2 is more soluble in this IL than in any other IL sharing the same cation. The reason is that the anion of this IL is highly fluorinated. Moreover, the anion size is large, resulting in a higher stability with respect to moisture and air, compared to other fluorinated ILs. Therefore, [emim][FAP] is a promising solvent for industrial gas separation and carbon capture processes.

3.5 References

[1] P. Scovazzo, J. Kieft, D.A. Finan, C. Koval, D. DuBois, R. Noble, Gas separations using non-hexafluorophosphate [PF_6] anion supported ionic liquid membranes, Journal of Membrane Science, 238 (2004) 57-63.

[2] E.D. Bates, R.D. Mayton, I. Ntai, J.H. Davis, CO_2 Capture by a Task-Specific Ionic Liquid, Journal of the American Chemical Society, 124 (2002) 926-927.

[3] D. Wappel, G. Gronald, R. Kalb, J. Draxler, Ionic liquids for post-combustion CO_2 absorption, International Journal of Greenhouse Gas Control, 4 (2010) 486-494.

[4] L.A. Blanchard, Z. Gu, J.F. Brennecke, High-Pressure Phase Behavior of Ionic Liquid/CO_2 Systems, Journal of Physical Chemistry *B*, 105 (2001) 2437-2444.

[5] J. Kumelan, Á. Pérez-Salado Kamps, D. Tuma, G. Maurer, Solubility of CO_2 in the ionic liquid [hmim][Tf2N], Journal of Chemical Thermodynamics, 38 (2006) 1396-1401.

[6] Y. Chen, S. Zhang, X. Yuan, Y. Zhang, X. Zhang, W. Dai, R. Mori, Solubility of CO_2 in imidazolium-based tetrafluoroborate ionic liquids, Thermochimica Acta, 441 (2006) 42-44.

[7] A.M. Schilderman, S. Raeissi, C.J. Peters, Solubility of carbon dioxide in the ionic liquid 1-ethyl-3-methylimidazolium bis(trifluoromethylsulfonyl)imide, Fluid Phase Equilibria, 260 (2007) 19-22.

[8] A.N. Soriano, B.T. Doma, M.-H. Li, Solubility of Carbon Dioxide in 1-Ethyl-3-methylimidazolium Tetrafluoroborate, Journal of Chemical & Engineering Data, 53 (2008) 2550-2555.

[9] X. Huang, C.J. Margulis, Y. Li, B.J. Berne, Why Is the Partial Molar Volume of CO_2 So Small When Dissolved in a Room Temperature Ionic Liquid? Structure and Dynamics of CO_2 Dissolved in [Bmim][PF_6], Journal of the American Chemical Society, 127 (2005) 17842-17851.

[10] C. Cadena, J.L. Anthony, J.K. Shah, T.I. Morrow, J.F. Brennecke, E.J. Maginn, Why Is CO_2 So Soluble in Imidazolium-Based Ionic Liquids?, Journal of the American Chemical Society, 126 (2004) 5300-5308.

[11] R.E. Baltus, B.H. Culbertson, S. Dai, H. Luo, D.W. DePaoli, Low-Pressure Solubility of Carbon Dioxide in Room-Temperature Ionic Liquids Measured with a Quartz Crystal Microbalance, Journal of Physical Chemistry *B*, 108 (2003) 721-727.

[12] S.N.V.K. Aki, B.R. Mellein, E.M. Saurer, J.F. Brennecke, High-Pressure Phase Behavior of Carbon Dioxide with Imidazolium-Based Ionic Liquids, Journal of Physical Chemistry *B*, 108 (2004) 20355-20365.

[13] I. Minami, M. Kita, T. Kubo, H. Nanao, S. Mori, The Tribological Properties of Ionic Liquids Composed of Trifluorotris(pentafluoroethyl) Phosphate as a Hydrophobic Anion, Tribology Letters, 30 (2008) 215-223.

[14] J. Huddleston, A. Visser, M. Reichert, H. Willauer, G. Broker, R. Rogers, Characterization and comparison of hydrophilic and hydrophobic room temperature ionic liquids incorporating the imidazolium cation, Green Chemistry, 3 (2001) 156-164.

[15] M.J. Muldoon, S.N.V.K. Aki, J.L. Anderson, J.K. Dixon, J.F. Brennecke, Improving Carbon Dioxide Solubility in Ionic Liquids, Journal of Physical Chemistry *B*, 111 (2007) 9001-9009.

[16] M.C. Kroon, Combined reactions and separations using ionic liquids and carbon dioxide, Delft University of Technology, (2006).

[17] D.R. Lide, CRC Handbook of Chemistry and Physics, 85th Edition, Taylor & Francis, (2004).

[18] T.W. De Loos, H.J. Van der Kooi, P.L. Ott, Vapor-liquid critical curve of the system ethane + 2-methylpropane, Journal of Chemical & Engineering Data, 31 (1986) 166-168.

[19] D. Morgan, L. Ferguson, P. Scovazzo, Diffusivities of Gases in Room-Temperature Ionic Liquids: Data and Correlations Obtained Using a Lag-Time Technique, Industrial & Engineering Chemistry Research, 44 (2005) 4815-4823.

[20] D.S. Viswanath, Viscosity of Liquids: Theory, Estimation, Experiment, and Data, Springer, 2007.

[21] J.G. Huddleston, A.E. Visser, W.M. Reichert, H.D. Willauer, G.A. Broker, R.D. Rogers, Characterization and comparison of hydrophilic and hydrophobic room temperature ionic liquids incorporating the imidazolium cation, Green Chemistry, 3 (2001) 156-164.

[22] H. Schmidt, M. Stephan, J. Safarov, I. Kul, J. Nocke, I.M. Abdulagatov, E. Hassel, Experimental study of the density and viscosity of 1-ethyl-3-methylimidazolium ethyl sulfate, The Journal of Chemical Thermodynamics, 47 (2012) 68-75.

[23] L.E. Barrosse-Antle, A.M. Bond, R.G. Compton, A.M. O'Mahony, E.I. Rogers, D.S. Silvester, Voltammetry in Room Temperature Ionic Liquids: Comparisons and Contrasts with Conventional Electrochemical Solvents, Chemistry – An Asian Journal, 5 (2010) 202-230.

[24] S. Raeissi, C.J. Peters, A potential ionic liquid for CO_2-separating gas membranes: selection and gas solubility studies, Green Chemistry, 11 (2009) 185-192.

[25] K. Lark-Horovitz, A.J. Vivian, Methods in Experimental Physics, Academic Press, 6 Part A, (1959) 21-186.

[26] M. Shokouhi, M. Adibi, A.H. Jalili, M. Hosseini-Jenab, A. Mehdizadeh, Solubility and Diffusion of H_2S and CO_2 in the Ionic Liquid 1-(2-Hydroxyethyl)-3-methylimidazolium Tetrafluoroborate, Journal of Chemical & Engineering Data, 55 (2009) 1663-1668.

[27] S. Raeissi, C.J. Peters, Carbon Dioxide Solubility in the Homologous 1-Alkyl-3-methylimidazolium Bis(trifluoromethylsulfonyl)imide Family, Journal of Chemical & Engineering Data, 54 (2008) 382-386.

[28] S. Raeissi, L. Florusse, C.J. Peters, Scott–van Konynenburg phase diagram of carbon dioxide + alkylimidazolium-based ionic liquids, The Journal of Supercritical Fluids, 55 (2010) 825-832.

[29] A. Shariati, K. Gutkowski, C.J. Peters, Comparison of the phase behavior of some selected binary systems with ionic liquids, AIChE Journal, 51 (2005) 1532-1540.

[30] M. Rahmati-Rostami, C. Ghotbi, M. Hosseini-Jenab, A.N. Ahmadi, A.H. Jalili, Solubility of H_2S in ionic liquids [hmim][PF6], [hmim][BF4], and [hmim][Tf2N], Journal of Chemical Thermodynmics, 41 (2009) 1052-1055.

[31] A. Shariati, C.J. Peters, High-pressure phase behavior of systems with ionic liquids: II. The binary system carbon dioxide + 1-ethyl-3-methylimidazolium hexafluorophosphate, Journal of Supercritical Fluids, 29 (2004) 43-48.

[32] S.G. Kazarian, B.J. Briscoe, T. Welton, Combining ionic liquids and supercritical fluids: ATR-IR study of CO dissolved in two ionic liquids at high pressures, Chemical Communications, (2000) 2047-2048.

[33] P. Raveendran, S.L. Wallen, Exploring CO_2-Philicity: Effects of Stepwise Fluorination, Journal of Physical Chemistry *B*, 107 (2003) 1473-1477.

[34] O.F. Dawodu, A. Meisen, Degradation of alkanolamine blends by carbon dioxide, The Canadian Journal of Chemical Engineering, 74 (1996) 960-966.

[35] S. Ahn, H.-J. Song, J.-W. Park, J. Lee, I. Lee, K.-R. Jang, Characterization of metal corrosion by aqueous amino acid salts for the capture of CO_2, Korean Journal of Chemical Engineering, 27 (2010) 1576-1580.

[36] J.K. Carson, K.N. Marsh, A.E. Mather, Enthalpy of solution of carbon dioxide in (water +n monoethanolamine, or diethanolamine, or N-methyldiethanolamine) and (water + mono ethanolamine + N-methyldiethanolamine) at T = 298.15 K, The Journal of Chemical Thermodynamics, 32 (2000) 1285-1296.

[37] D. Chinn, D. Vu, M. Driver, L. Boudreau, CO_2 removal from gas using ionic liquid absorbents, Google Patents, (2005).

[38] A.-L. Revelli, F. Mutelet, J.-N.l. Jaubert, High Carbon Dioxide Solubilities in Imidazolium-Based Ionic Liquids and in Poly(ethylene glycol) Dimethyl Ether, The Journal of Physical Chemistry *B*, 114 (2010) 12908-12913.

[39] D.-J. Seo, W.-H. Hong, Solubilities of Carbon Dioxide in Aqueous Mixtures of Diethanolamine and 2-Amino-2-methyl-1-Propanol, Journal of Chemical & Engineering Data, 41 (1996) 258-260.

[40] K.P. Shen, M.H. Li, Solubility of carbon dioxide in aqueous mixtures of monoethanolamine with methyldiethanolamine, Journal of Chemical & Engineering Data, 37 (1992) 96-100.

Chapter 4

Solubility of Methane in the Ionic Liquid [emim][FAP]

This chapter is adapted from the following publication: M. Althuluth, M.C. Kroon, C.J. Peters, Ind. Eng. Chem. Res., 51 (2012) 16709-16712.

4.1 Introduction

There is an increasing attention for global warming caused by the effects of power and industrial emissions, particularly carbon dioxide (CO_2) emissions. Removal of CO_2 from flue gases (CO_2 capture) is one of the technologies that could reduce the greenhouse gas emissions. So far, the CO_2 capture technologies have been found to be technically challenging and they are not cost effective technologies to be commercialized in a large scale [2].

Therefore, the worldwide demand for the use of natural gas as a cleaner and more efficient fuel is still increasing. Natural gas combustion leads to negligible sulfur dioxide (SO_2) emissions, low nitrous oxide (N_2O) levels, and low CO_2 emissions in comparison with oil or coal [3].

Natural gas can also contain significant amounts of CO_2. High amounts of CO_2 in natural gas streams for electricity generation reduce the efficiency of power plants, because the presence of CO_2 reduces the heating value of natural gas. Furthermore, the presence of CO_2 leads to corrosion in equipment and pipelines. The removal of CO_2 from sour gas (gas sweetening) is therefore crucial [4].

Amine absorption processes are most widely applied for the removal of acid gases (CO_2 and hydrogen sulfide, H_2S) from natural gas. These processes use a solvent, such as MEA, which reacts reversibly with the acid gases under formation of MEA carbamates. The acid gas-rich MEA solution is then sent to a stripper, where it is reheated to release the acid gas and to regenerate the absorbent. The MEA solution is then recycled to the absorber [5].
However, the MEA process is considered as an uneconomic process, because of the following disadvantages: (i) high energy requirement for regeneration, (ii) high equipment corrosion, and (iii) absorbent (amine) degradation [6-8]. Therefore, there is a strong need to replace the conventional gas separation solvents with more stable and safer ones. Recently, ionic liquids (ILs) were introduced to the market as novel environmentally benign solvents [9]. The unique properties of ILs, such as their negligible vapor pressure, their good thermal stability and their tunable properties, make them excellent candidates for replacing the conventional solvents, e.g., in organic synthesis and catalysis, electrochemistry and separation technology [10-14]. ILs can also be used in gas absorption processes e.g., as

solvents for carbon capture [15, 16]. The phase behavior of IL systems is of great importance for the design of these novel separation processes.

The solubility of CO_2 in different ILs has been widely studied by several groups [17-21]. However, papers on methane (CH_4) solubility in ILs are scarce [22-27] . Generally, ILs were found to show high CO_2 solubilities, whereas CH_4 solubilities were much lower. Therefore, ILs could be attractive absorbents for gas separations.

Previously, we found that the ionic liquid [emim][FAP] shows the highest carbon dioxide (CO_2) solubility of all ILs so far studied[1]. Therefore, it is expected that this IL shows a high selectivity for CO_2/CH_4 separation, as long as the solubility of CH_4 in this IL is sufficiently low.

In this work, we will measure the CH_4 solubility in [emim][FAP]. A comparison with the CO_2 solubility in the same IL will be made in order to evaluate the selectivity of the separation process. This value will be compared to the selectivity for gas separations using other ILs.

4.2 Experimental

4.2.1 Materials

CH_4 gas was supplied by Hoek Loos with a purity of 99.995%. The IL [emim][FAP] was provided by Merck Chemical Company with a purity of ≥ 99.0 % and was used as such. The water content of the IL was measured using Karl Fischer moisture analysis and was less than 130 ppm. Within the temperature range of the experiments, the IL did not show any decomposition or reaction with CH_4.

4.2.2 Experimental procedure

The solubility of CH_4 in [emim][FAP] was determined by measuring bubble point pressures at different temperatures and compositions using the Cailletet equipment. The pressure was adjusted for a sample at constant composition until a (liquid + vapor)-to-(liquid) phase transition was visually observed.

4.3 Results and discussion

The solubility of CH_4 in the IL [emim][FAP] was determined at temperatures ranging from 293.30 to 363.13 K and pressures up to 8.69 MPa by measuring the bubble point pressures at various compositions of CH_4 in the IL. The water content was kept below 130 ppm for all samples prepared. The results are shown in Table 4.1 and graphically presented in Figure 4.1

Table 4.1: Experimental bubble-point pressures (P) for various concentrations of CH_4 (x_{CH4}) and temperatures (T) in the CH_4 + [emim][FAP] system[a]

x_{CH4}	T (K)	P (MPa)	T (K)	P (MPa)	T (K)	P (MPa)
0.052	293.30	2.076	323.36	2.234	353.24	2.392
	303.29	2.151	333.27	2.299	363.13	2.421
	313.42	2.185	343.32	2.368		
0.105	293.53	4.510	323.52	4.955	353.44	5.270
	303.55	4.673	333.30	5.068	363.42	5.359
	313.45	4.807	343.45	5.201		
0.129	293.58	5.831	323.52	6.395	353.42	6.766
	303.54	6.024	333.47	6.533	363.39	6.860
	313.54	6.202	343.42	6.652		
0.155	303.57	7.728	333.45	8.321	363.37	8.692
	313.49	7.951	343.43	8.484		
	323.46	8.123	353.43	8.583		

[a]Standard uncertainties u are $u(T) = 0.01$ K, $u(P) = 0.003$ MPa, and $u(x_{CH4}) = 0.005$

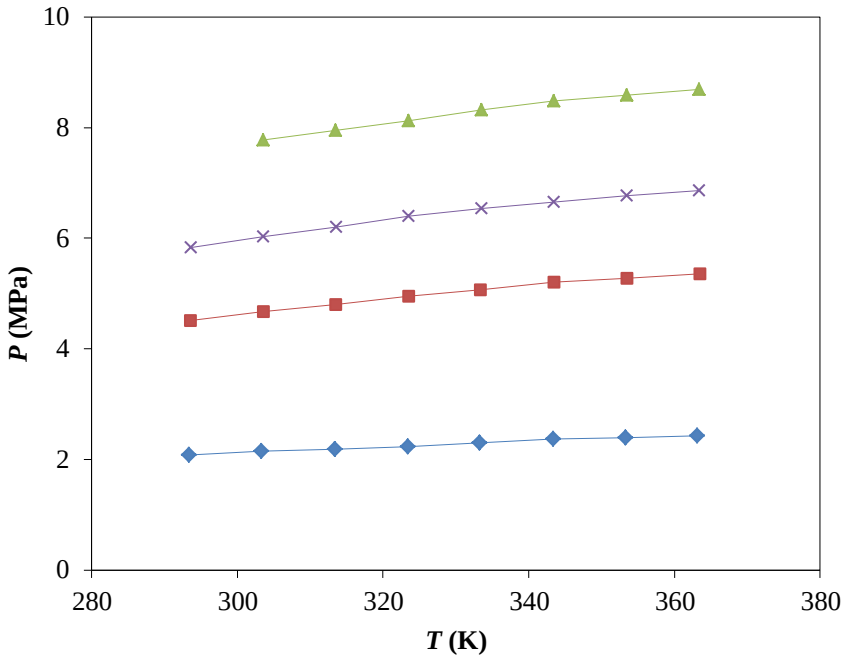

Figure 4.1: Experimentally determined isopleths of the bubble point pressures for several compositions of CH_4 in the binary system CH_4 + [emim][FAP]: ◆, 5.2 mol%; ■, 10.5 mol%; ✖, 12.9 mol%; ▲, 15.5 mol%.

From Figure 4.1 it can be concluded that the bubble point pressures of CH_4 in the IL [emim][FAP] increase linearly with temperature, indicating that the solubility decreases with increasing temperature. Moreover, higher pressures are needed to absorb larger amounts of CH_4. This can be better observed from Figure 4.2, where the bubble point pressure is plotted against the mole fraction of CH_4 at fixed temperature.

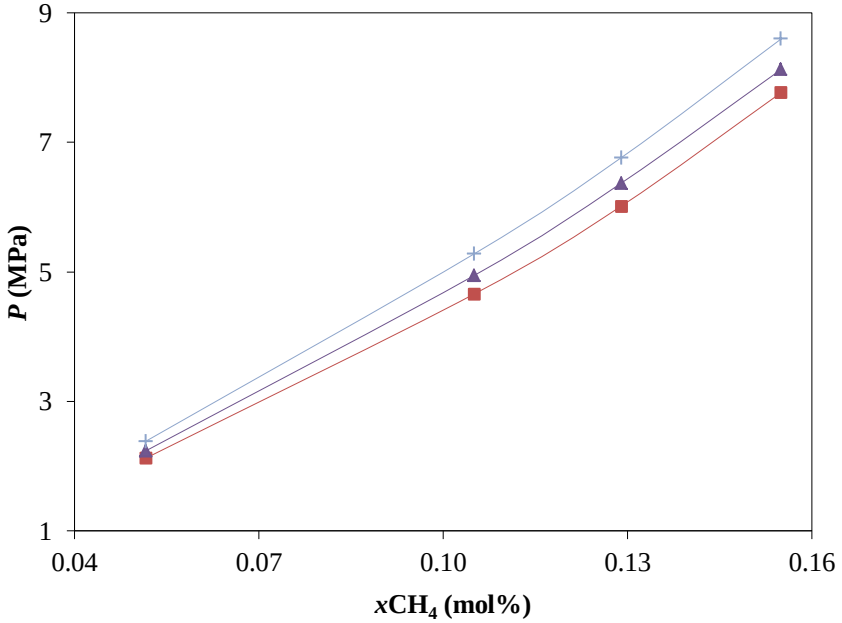

Figure 4.2: Isotherms of the bubble point pressures at several temperatures of the binary system CH_4 + [emim][FAP]: ■, 303 K; ▲, 323 K; ✚, 353 K.

Figure 4.2 shows that the bubble point pressures increase slightly more than linearly with increasing CH_4 concentration at given temperature. This is completely different from the typical behavior for IL + CO_2 systems, where the CO_2 solubility curves exhibit a concave behavior [27,28]. This difference in the shapes of solubility curves can benefit the separation process [29].

Figure 4.3 compares the solubilities of CH_4 and CO_2 in [emim][FAP] at a temperature of 333.15 K. It can be observed that the solubility of CH_4 is much lower compared to the solubility of CO_2. For example, at 333.15 K and 8.27 MPa up to 15.50 mol% of CH_4 can be dissolved in [emim][FAP], while up to 60 mol% of CO_2 can be dissolved at the same temperature and a pressure of 6.69 MPa only. These results confirm that [emim][FAP] could be used for separating CO_2 from natural gas.

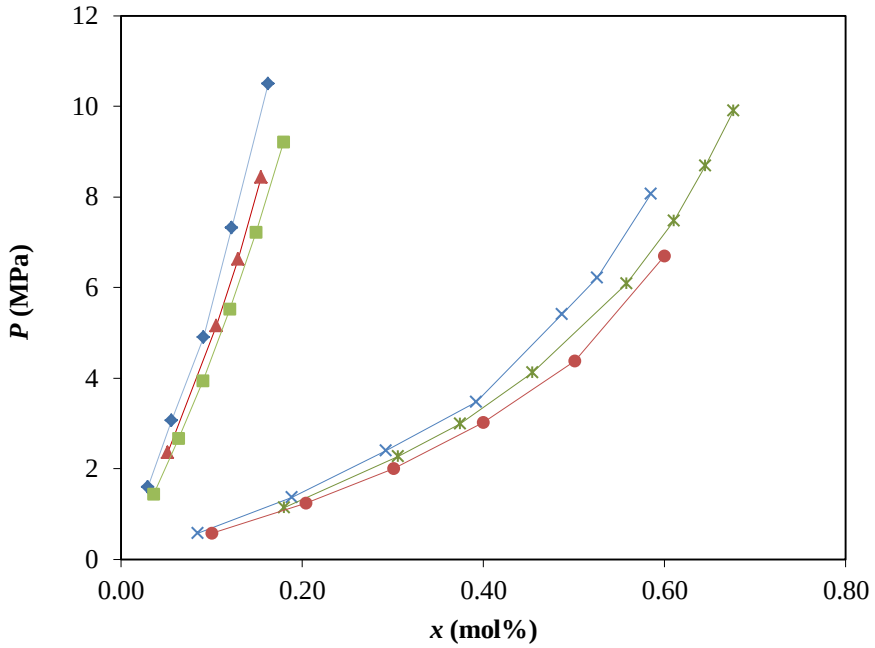

Figure 4.3: Comparison of the solubilities of CH_4 and CO_2 in various ILs at 333.15 K: ●, [emim][FAP] + CO_2 [1]; ✳, [hmim][Tf_2N] + CO_2 [18]; ×, [bmim][Tf_2N] + CO_2 [28]; ▲, [emim][FAP] + CH_4 [this work]; ■, [hmim][Tf_2N] + CH4 [27]; ◆, [bmim][Tf_2N] + CH_4 [24].

Similar behavior was observed for the CO_2 and CH_4 solubilities in other ILs e.g., [bmim][Tf_2N] [24, 28] and [hmim][Tf_2N] [18, 27], see Figure 4.3. This comparison shows that the solubility of CH_4 in the various ILs slightly decreases in the order: [hmim][Tf_2N] > [emim][FAP] > [bmim][Tf_2N]. Carvalho and Coutinho [30] reported that the solubility of CH_4 is related to polarity of IL, the CH_4 solubility decreases with the increase in the polarity

of IL. Thus, this parameter (polarity) can be used as the basis for the choice of ILs that maximize the selectivities of CO_2/CH_4.

There are also a few data available regarding the CH_4 solubility in other ILs [22, 25, 26]. However, these data are not shown in Figure 4.3, because they were measured only at low pressures. Therefore, they cannot be presented in the same graph.

Solubilities of CH_4 were also compared with other solvents proposed for the natural gas sweetening. Figure 4.4 shows the comparison of the solubility of CH_4 in different commercial solvents at 313.15 K. It was observed that [emim][FAP] absorbs CH_4 almost similar to Genosorb 1753 (mixture of polyethylene glycol dimethyl ethers) [31], but more than TEGMME [32] and MDEA 35 wt% [33]. It should be noted that [emim][FAP] is more expensive than these conventional solvents.

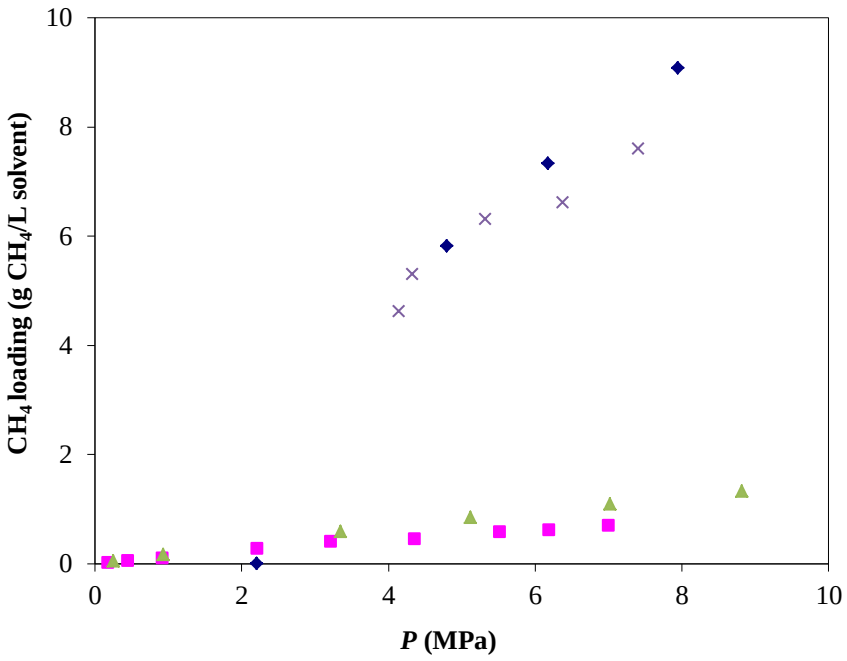

Figure 4.4**:** Comparison of the solubilities of CH_4 in [emim][FAP] and various solvents at 313.15 K: ◆, [emim][FAP] [this work]; ×, Genosorb 1753 [31]; ■, TEGMME [32]; ▲, MDEA 30 wt % [33].

The results for the solubility of CH_4 in [emim][FAP] can be expressed in terms of Henry's constants using the Krichevsky–Kasarnovsky equation (see chapter 3, eq. 5) [34]. Table 4.2 compares the Henry's constants for the solubility of CH_4 and CO_2 in the IL [emim][FAP]. The selectivity for the CO_2/CH_4 separation is calculated by dividing the Henry's constant of CH_4 by the Henry's constant of CO_2.

Table 4.2: Henry's constants (H) for the solubility of CO_2 and CH_4 in [emim][FAP] and selectivities ($S = H_{CH4}/H_{CO2}$) at various temperatures (T)

T (K)	H_{CO2} (MPa)	H_{CH4} (MPa)	$S_{CO2/CH4}$
303	3.32	38.48	11.58
313	4.05	39.48	9.74
323	4.67	40.47	8.65
333	5.35	41.46	7.74
343	6.08	42.45	6.98
353	6.86	43.44	6.33
363	7.70	44.43	5.77

Table 4.2 shows that the separation ratios of CO_2/CH_4 in [emim][FAP] range from 5.77 to 11.58 depending on the operating conditions, where the maximum separation ratio is achieved at the lowest temperatures. Separation selectivities of CO_2/CH_4 in [emim][FAP] were compared with selectivities in [bmim][Tf_2N] [24, 28] and [hmim][Tf_2N] [22]. At a temperature of 333.15 K, the separation ratios of CO_2/CH_4 are 7.74, 8.26 and 6.10 for [emim][FAP], [bmim][Tf_2N] and [hmim][Tf_2N], respectively. The selectivity in [emim][FAP] is thus similar to the CO_2/CH_4 separation ratios in other ILs.

4.4 Conclusions

The IL [emim][FAP] is a good solvent for natural gas sweetening because it combines a high CO_2 solubility with a low absorption capacity for CH_4, as indicated by the high solubility selectivities achieved (5.77 to 11.58), depending on the operating conditions. The maximum selectivity is achieved at the lowest temperatures, and is similar to the selectivities observed for other ILs.

4.5 References

[1] M. Althuluth, M.T. Mota-Martinez, M.C. Kroon, C.J. Peters, Solubility of Carbon Dioxide in the Ionic Liquid 1-Ethyl-3-methylimidazolium Tris(pentafluoroethyl) trifluorophosphate, Journal of Chemical & Engineering Data, 57 (2012) 3422-3425.

[2] M. Ramdin, T.W. de Loos, T.J.H. Vlugt, State-of-the-Art of CO_2 Capture with Ionic Liquids, Industrial & Engineering Chemistry Research, 51 (2012) 8149-8177.

[3] Natural Gas : Issues and Trends; Energy Information Administration.: Washington, D.C., DOE/EIA-0560(98), (1998).

[4] K. Simons, K. Nijmeijer, M. Wessling, Gas–liquid membrane contactors for CO_2 removal, Journal of Membrane Science, 340 (2009) 214-220.

[5] C. Stewart, M.-A. Hessami, A study of methods of carbon dioxide capture and sequestration—the sustainability of a photosynthetic bioreactor approach, Energy Conversion & Management, 46 (2005) 403-420.

[6] D.J. Fauth, E.A. Frommell, J.S. Hoffman, R.P. Reasbeck, H.W. Pennline, Eutectic salt promoted lithium zirconate: Novel high temperature sorbent for CO_2 capture, Fuel Processing Technology, 86 (2005) 1503-1521.

[7] J.T. Yeh, K.P. Resnik, K. Rygle, H.W. Pennline, Semi-batch absorption and regeneration studies for CO_2 capture by aqueous ammonia, Fuel Processing Technology, 86 (2005) 1533-1546.

[8] K.P. Resnik, J.T. Yeh, H.W. Pennline, Aqua ammonia process for simultaneous removal of CO_2, SO_2 and NO_x, International Journal of Environmental Technology and Management, 4 (2004) 89-104.

[9] P. Scovazzo, J. Kieft, D.A. Finan, C. Koval, D. DuBois, R. Noble, Gas separations using non-hexafluorophosphate [PF_6] anion supported ionic liquid membranes, Journal of Membrane Science, 238 (2004) 57-63.

[10] L. Duchet, J.C. Legeay, D. Carrié, L. Paquin, J.J. Vanden Eynde, J.P. Bazureau, Synthesis of 3,5-disubstituted 1,2,4-oxadiazoles using ionic liquid-phase organic synthesis (IoLiPOS) methodology, Tetrahedron, 66 (2010) 986-994.

[11] M.V.B. Zanoni, E.I. Rogers, C. Hardacre, R.G. Compton, The electrochemical reduction of the purines guanine and adenine at platinum electrodes in several room temperature ionic liquids, Analytica Chimica Acta 659 (2010) 115-121.

[12] N. Fontanals, S. Ronka, F. Borrull, A.W. Trochimczuk, R.M. Marcé, Supported imidazolium ionic liquid phases: A new material for solid-phase extraction, Talanta, 80 (2009) 250-256.

[13] K.R. Seddon, Ionic Liquids for Clean Technology, Journal of Chemical Technology & Biotechnology, 68 (1997) 351-356.

[14] P. Kubisa, Ionic liquids as solvents for polymerization processes—Progress and challenges, Progress in Polymer Science, 34 (2009) 1333-1347.

[15] E.D. Bates, R.D. Mayton, I. Ntai, J.H. Davis, CO_2 Capture by a Task-Specific Ionic Liquid, Journal of the American Chemical Society , 124 (2002) 926-927

[16] D. Wappel, G. Gronald, R. Kalb, J. Draxler, Ionic liquids for post-combustion CO_2 absorption, International Journal of Greenhouse Gas Control, 4 (2010) 486-494.

[17] L.A. Blanchard, Z. Gu, J.F. Brennecke, High-Pressure Phase Behavior of Ionic Liquid/CO_2 Systems, Journal of Physical Chemistry *B*, 105 (2001) 2437-2444.

[18] J. Kumełan, Á. Pérez-Salado Kamps, D. Tuma, G. Maurer, Solubility of the Single Gases Methane and Xenon in the Ionic Liquid [hmim][Tf_2N], Industrial & Engineering Chemistry Research , 46 (2007) 8236-8240.

[19] Y. Chen, S. Zhang, X. Yuan, Y. Zhang, X. Zhang, W. Dai, R. Mori, Solubility of CO_2 in imidazolium-based tetrafluoroborate ionic liquids, Thermochim. Acta, 441 (2006) 42-44.

[20] A.M. Schilderman, S. Raeissi, C.J. Peters, Solubility of carbon dioxide in the ionic liquid 1-ethyl-3-methylimidazolium bis(trifluoromethylsulfonyl)imide, Fluid Phase Equilibria, 260 (2007) 19-22.

[21] A.N. Soriano, B.T. Doma, M.-H. Li, Solubility of Carbon Dioxide in 1-Ethyl-3-methylimidazolium Tetrafluoroborate, Journal of Chemical & Engineering Data, 53 (2008) 2550-2555.

[22] A. Finotello, J.E. Bara, D. Camper, R.D. Noble, Room-Temperature Ionic Liquids: Temperature Dependence of Gas Solubility Selectivity, Industrial & Engineering Chemistry Research , 47 (2007) 3453-3459.

[23] J J. Jacquemin, P. Husson, V. Majer, M.F.C. Gomes, Low-pressure solubilities and thermodynamics of solvation of eight gases in 1-butyl-3-methylimidazolium hexafluorophosphate, Fluid Phase Equilibria, 240 (2006) 87-95.

[24] S. Raeissi, C.J. Peters, High pressure phase behaviour of methane in 1-butyl-3-methylimidazolium bis(trifluoromethylsulfonyl)imide, Fluid Phase Equilibria, 294 (2010) 67-71.

[25] J.L. Anthony, J.M. Crosthwaite, D.G. Hert, S.N.V.K. Aki, E.J. Maginn, J.F. Brennecke, Phase Equilibria of Gases and Liquids with 1-n-butyl-3-Methylimidazolium Tetrafluoroborate, in: R.D. Rogers, K.R. Seddon (Eds.) Ionic Liquids as Green Solvents, American Chemical Society, Washington, (2003) 110-120.

[26] J.L. Anthony, E.J. Maginn, J.F. Brennecke, Solubilities and Thermodynamic Properties of Gases in the Ionic Liquid 1-n-Butyl-3-methylimidazolium Hexafluorophosphate, Journal of Physical Chemistry *B*, 106 (2002) 7315-7320.

[27] J. Kumełan, Á. Pérez-Salado Kamps, D. Tuma, G. Maurer, Solubility of CO_2 in the ionic liquid [hmim][Tf_2N], Journal of Chemical thermodynamics, 38 (2006) 1396-1401.

[28] S. Raeissi, C.J. Peters, Carbon Dioxide Solubility in the Homologous 1-Alkyl-3-methylimidazolium Bis(trifluoromethylsulfonyl)imide Family, Journal of Chemical & Engineering Data, 54 (2008) 382-386.

[29] S. Raeissi, C.J. Peters, A potential ionic liquid for CO_2-separating gas membranes: selection and gas solubility studies, Green Chemsitry, 11 (2009) 185-192.

[30] P.J. Carvalho, J.A.P. Coutinho, The polarity effect upon the methane solubility in ionic liquids: a contribution for the design of ionic liquids for enhanced CO_2/CH_4 and H_2S/CH_4 selectivities, Energy & Environmental Science, 4 (2011) 4614-4619.

[31] A.V. Rayer, A. Henni, P. Tontiwachwuthikul, High-Pressure Solubility of Methane (CH_4) and Ethane (C_2H_6) in Mixed Polyethylene Glycol Dimethyl Ethers (Genosorb 1753) and Its Selectivity in Natural Gas Sweetening Operations, Journal of Chemical & Engineering Data, 57 (2012) 764-775.

[32] A. Henni, A.E. Mather, The solubility of methane in triethylene glycol monomethyl ether, Fluid Phase Equilibria, 108 (1995) 213-218.

[33] F.-Y. Jou, J.J. Carroll, A.E. Mather, F.D. Otto, Solubility of Methane and Ethane in Aqueous Solutions of Methyldiethanolamine, Journal of Chemical & Engineering Data, 43 (1998) 781-784.

[34] M. Rahmati-Rostami, C. Ghotbi, M. Hosseini-Jenab, A.N. Ahmadi, A.H. Jalili, Solubility of H_2S in ionic liquids [hmim][PF6], [hmim][BF4], and [hmim][Tf_2N], Journal of Chemical thermodynamics, 41 (2009) 1052-1055.

Chapter 5

Solubility of Light Hydrocarbons in the Ionic Liquid [emim][FAP]

This chapter is adapted from the following publication: M. Althuluth, M.T. Mota-Martinez, A. Berrouk, M.C. Kroon, C.J. Peters, The Journal of Supercrit. Fluids, 90 (2014) 65-72.

5.1 Introduction

The separation of carbon dioxide (CO_2) from methane (CH_4) is an important process in many industrial areas such as natural gas processing and biogas purification [1].

The CO_2 content in natural gas can vary from 4 to 50 %. Before natural gas can be transported in pipelines to end-users, it has to be treated to protect the pipelines against corrosion. Moreover, CO_2 has no heating value and must therefore be removed. Besides CO_2, natural gas also contains significant amounts of ethane (C_2H_6), some propane (C_3H_8), butane (C_4H_{10}), and other higher hydrocarbons. In addition, the gas contains undesirable impurities, such as water, nitrogen, and hydrogen sulphide [2].

In natural gas treating the loss of small hydrocarbons to the CO_2-rich stream is a concern. It is desirable to maintain these compounds in the CH_4-rich stream, because of their economic value. As the higher-molecular-weight hydrocarbons may form condensates, leading to the production of liquid slugs, these hydrocarbons have to be removed from the CH_4-rich stream. Moreover, the presence of higher-molecular-weight hydrocarbons decreases the methane number. Because of their economic value, the lower hydrocarbons can be recovered as a separate liquid phase and used as a liquefied gas for various industrial and commercial applications [3].

There are many methods available for the removal of acid gases from gas streams. The most commonly used technology is based on chemical and physical absorption [4]. Physical solvents are in favour over chemical solvents when the concentration of acid gases is very high due to the lower regeneration costs. Physical solvents are also preferred when the natural gas is available at high pressure, because physical absorption is strongly pressure dependent. However, if the concentration of small hydrocarbons is high, a physical solvent may not be the best option due to higher co-absorption of these hydrocarbons. The best solvent should have a high capacity for acid gases and a low capacity for hydrocarbons [5].

Recently, ionic liquids (ILs) have been proposed as selective absorbents for CO_2 capture [6], as they were found to show high CO_2 solubilities in ILs and, therefore, a high loading capacity for acid gases [7-17]. The high-pressure solubility in ILs of lower hydrocarbons such

as CH_4, C_2H_6, C_3H_8 and C_4H_{10} in ILs has been much less investigated [18-22]. For that reason, this study focuses on the absorptive capacity of ILs for these hydrocarbons.

In previous work [23] we found that the IL [emim][FAP] shows a very high absorptive capacity for CO_2 [13] and a good selectivity for the CO_2/CH_4 mixture [23]. In this work, the solubilities of the small hydrocarbons C_2H_6, C_3H_8 and C_4H_{10} in the same IL will be experimentally determined, and compared to the CO_2 and CH_4 solubilities in [emim][FAP].

5.2 Experimental

5.2.1 Materials

The IL [emim][FAP] was provided by Merck Chemical Company with a purity of ≥ 99.0 %. Prior to the experiments, the IL was dried under vacuum at a temperature of 350 K. The water content of the IL was measured using Karl Fischer moisture analysis (Metrohm 756 KF Coulometer), and was found to be less than 100 ppm. The gases (C_2H_6, C_3H_8 and C_4H_{10}) were purchased from Hoek Loos with a purity of 99.95% and used as received.

5.2.2 Experimental procedure

The phase behavior of the binary systems [emim][FAP] + hydrocarbon was determined at different temperatures and compositions using a so-called Cailletet equipment [24]. At a certain temperature, the pressure was adjusted until a phase transition was visually observed. The following phase transitions were observed in this study: (i) liquid + vapour to liquid (LV→L), (ii) liquid$_1$ + liquid$_2$ to liquid (L_1L_2→L), (iii) liquid$_1$ + liquid$_2$ + vapor to liquid$_1$ + liquid$_2$ (L_1L_2V→L_1L_2) and (iv) liquid$_1$ + liquid$_2$ + vapor to liquid$_1$ + supercritical fluid (SCF) (L_1L_2V→L_1+L_2=V), see Figure 5.1.

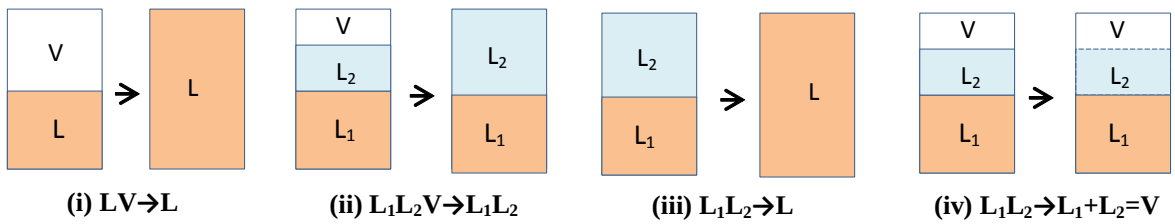

Figure 5.1: A schematic represents phase transitions observed in our experiments: L = liquid phase; L_1 = ionic liquid rich phase; L_2 = hydrocarbon-rich liquid phase; V = vapor phase.

The critical endpoint (L_1+L_2=V) was determined by changing pressure and temperature slowly with small increments and maintaining the volume of liquid and vapor phase equal until the meniscus between both phases (L_2 and V) disappeared. The Cailletet equipment allows measurement of phase equilibria within a pressure range of 0.1 to 15 MPa and temperatures ranging from 275 to 370 K, because water was used as a heat-transferring fluid.

5.3 Results and discussion

Knowledge of the phase behavior of ILs and small hydrocarbons is important for gas separation using ILs as absorbents. In this work, the phase behavior of binary mixtures consisting of the IL [emim]FAP] and a small hydrocarbon (C_2H_6, C_3H_8 or C_4H_{10}) is investigated. The LV→L (bubble points), the L_1L_2→L (cloud points) and the L_1L_2V→L_1L_2 (three-phase line) or L_1L_2V→L_1+L_2=V (critical endpoint) data for the three investigated binary systems are listed in Tables A5.1-A5.3 (appendix A), respectively.

5.3.1 Phase equilibria of the [emim][FAP] + C_2H_6 system

The different phase transitions in the IL + C_2H_6 system are graphically depicted in Figure 5.2. First of all, it can be noticed that LV→L transitions only can be found at C_2H_6 concentrations lower than 27.5 mol%. Under these circumstances, the bubble point pressure increases with increasing gas concentration in the IL at a given temperature.

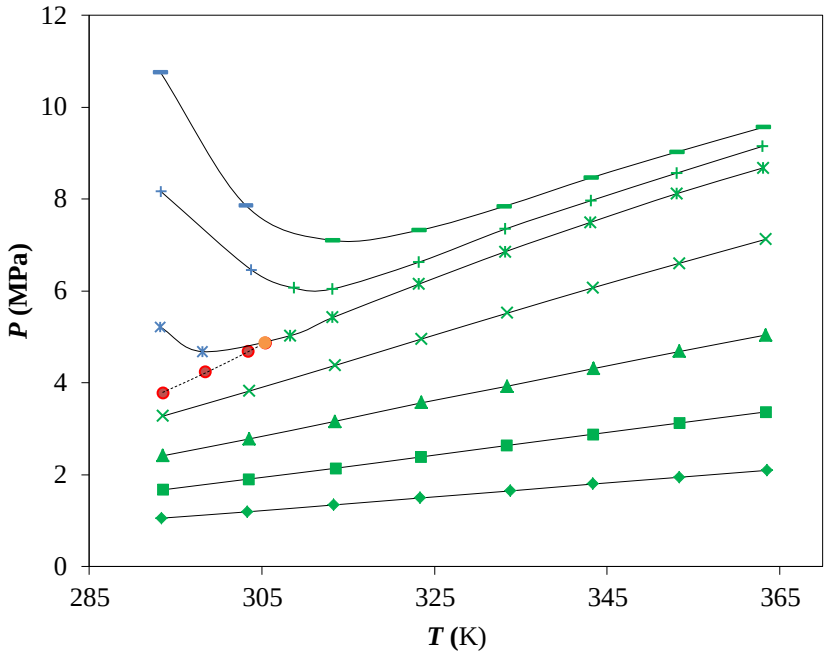

Figure 5.2: Experimentally determined isopleths for several compositions of C_2H_6 in the binary system C_2H_6 + [emim][FAP]: ◆, 10.0 mol%; ■, 15.0 mol%; ▲, 20.1 mol%; ×, 25.0 mol%; ∗, 27.5 mol%; +, 28.0 mol%; –, 28.5 mol%; ●, 30.0 mol%. Other legends: LV→L (**green**); L_1L_2→L (**blue**); L_1L_2V→ L_1L_2 (**red**); UCEP (**orange**); dashed lines represent P^{sat} of pure C_2H_6[25].

When the gas concentration is increased to 27.5 mol% or higher, at low temperatures, a second liquid phase appeared. At that moment, the phase transition observed is of the type L_1L_2V→L_1L_2. Thus, three phases coexist at equilibrium: the IL-rich phase is in equilibrium with a C_2H_6- liquid phase and C_2H_6-vapor phase. The three-phase line ends in the upper critical end point (UCEP), where L_2 is critical with V in the presence of L_1 (T_c = 305.4±0.1 K and P_c = 4.863±0.003 MPa). This UCEP nearly coincides with the critical point of pure C_2H_6 (T_c = 305.3 and P_c = 4.872) [26]. Also, the three-phase line almost coincides with the vapor pressure line of pure C_2H_6. This indicates that the second liquid phase is almost pure C_2H_6. Shiflet and Yokozeki [9] confirmed that the second liquid phase is nearly pure for binary systems consisting of refrigerants and ILs.

A two-phase region (L_1 + L_2) can be found above the three-phase line at temperatures below the UCEP. Thus, a L_1L_2→L transition (cloud point) was observed at higher pressures (above the pressure of the three-phase line). The cloud point shifts significantly to higher pressures, even when the C_2H_6 concentration is only slightly increased. This can be better observed from the *P-x* plot in Figure 5.3, where the bubble and cloud point pressures are plotted against the mole fraction of ethane at fixed temperature.

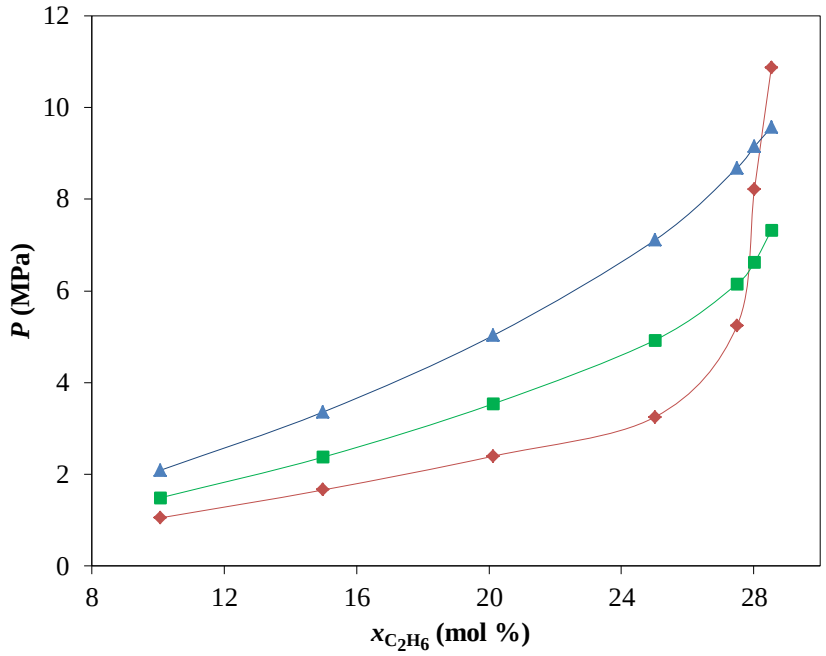

Figure 5.3: Isotherms of the binary system C_2H_6 + [emim][FAP]: ◆, 293 K; ■, 323 K; ▲, 363 K.

At T = 293 K, which is below the temperature of the UCEP, it can be concluded that bubble points are present at low pressures (C_2H_6 is more soluble as a gas in the IL phase), while at higher pressures only cloud points are observed (C_2H_6 is hardly soluble as a liquid in the IL phase). This explains the significant increase of the slope of the isothermal curve.

At supercritical conditions of C_2H_6, i.e. at temperatures above the UCEP, the pressure almost linearly increases with lower values of the mole fraction of C_2H_6 in the mixture. Therefore, the isotherms at temperatures above the temperature of the UCEP, the isotherms at 323 K and 363 K in Figure 5.3 do not show the extremely sharp increase of the slope in the *P*-*x* diagram.

The solubility of C_2H_6 in [emim][FAP] was compared to that of other ILs with the same anion [27]. It was found that the solubility of C_2H_6 in ILs follows the order: [hmim][FAP] ≈ [bmim][FAP] > [emim][FAP].

5.3.2 Phase equilibria of the [emim][FAP] + C_3H_8 system

Figure 5.4 shows the different phase transitions in the binary system [emim][FAP] + C_3H_8. From this figure it can be observed that LV→L transitions are present over the full temperature range at C_3H_8 concentrations up to 20 mol%. At higher concentrations, a second liquid phase is formed. Similar to the [emim][FAP] + C_2H_6 binary system, the pressure of the three-phase line ($L_1L_2V \rightarrow L_1L_2$) in the [emim][FAP] + C_3H_8 system also was found to be nearly coinciding with the vapor pressure curve of pure C_3H_8, which confirms that the second

liquid phase is nearly pure C_3H_8. The UCEP temperature was not determined, because this temperature was above the limits of the experimental set up.

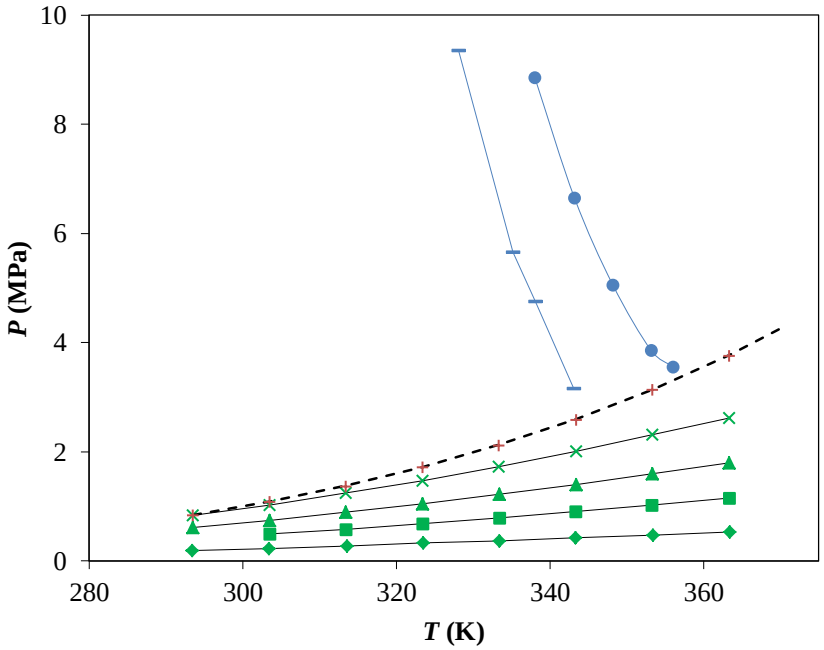

Figure 5.4: Experimentally determined isopleths for several compositions of C_3H_8 in the binary system C_3H_8 + [emim][FAP]: ◆, 4.90 mol%; ■, 10.1 mol%; ▲, 14.90 mol%; ×, 20.0 mol%; –, 24.5 mol%; ●, 25.0 mol%; +, 30.1 mol%. Other legends: LV→L (**green**); L_1L_2→L (**blue**); L_1L_2V→ L_1L_2 (**red**); dashed lines represent P^{sat} of pure C_3H_8[25].

At higher concentrations of C_3H_8 in the mixture, a L_1L_2→L transition was found at high pressures. Under these circumstances, the solubility of liquid C_3H_8 in the IL was observed to be higher at higher temperatures. This is contrary to the solubility of gaseous C_3H_8, which is higher at lower temperatures. For example, a pressure of 5.06 MPa is required to dissolve 25 mol% of C_3H_8 at T = 348.2 K, while the required pressure is only 3.86 MPa at T = 353.2 K. Figure 5.5 shows the *P*-*x*-diagram of the binary [emim][FAP] + C_3H_8 system. The isotherms are almost linear at low pressures (bubble points), but show a sudden sharp increase in pressure at higher concentrations of C_3H_8 (cloud points). Finally, it can be noticed that the UCEP is not reached, because all isotherms show the non-linear trend with pressure that only occurs below the critical point of C_3H_8.

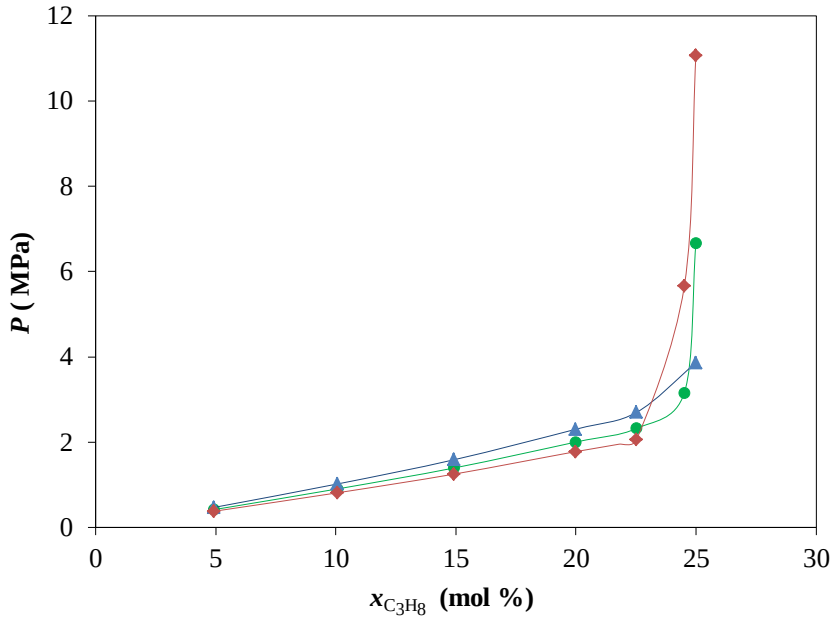

Figure 5.5: Isotherms of the binary system C_3H_8 + [emim][FAP]: ◆, 335 K; ●, 343 K; ▲, 353 K

5.3.3 Phase equilibria of the [emim][FAP] + C_4H_{10} system

The phase behavior of the binary mixture, [emim][FAP] + C_4H_{10} is presented in Figure 5.6. The results show a similar almost linear trend for the LV→L transitions, as was also observed for the bubble points of C_2H_6 and C_3H_8 in the same IL.

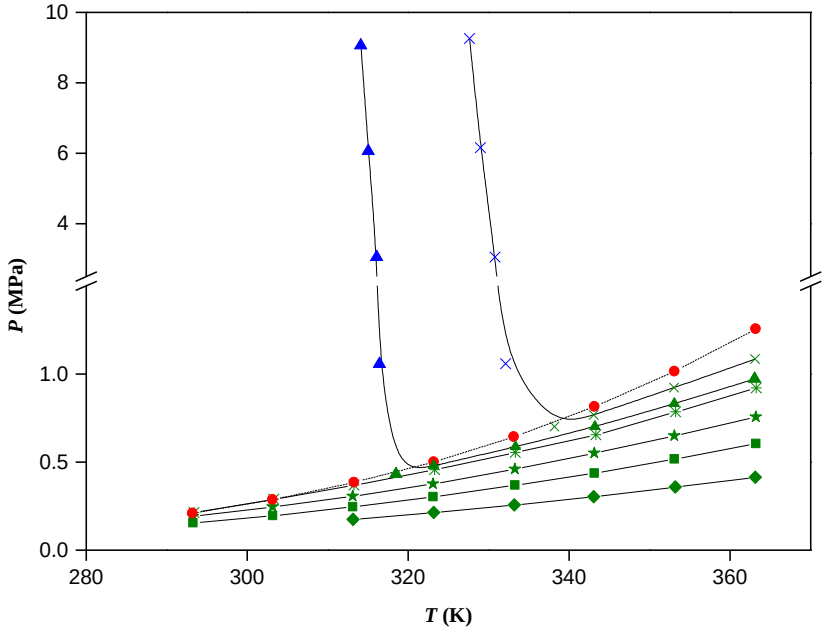

Figure 5.6: Experimentally determined isopleths for several compositions of C_4H_{10} in the binary system C_4H_{10} + [emim][FAP]: ◆, 7.0 mol%; ■, 10.0 mol%; ★, 12.6%; ✳, 15.0 mol%; ▲, 16.0 mol%; ×, 17.5 mol%; ●, 24.9 mol%. Other legends: LV→L (**green**); L_1L_2→L (**blue**); L_1L_2V→ L_1L_2 (**red**); dashed line represent, P^{sat} of pure C_4H_{10} [25].

Also, similar to the [emim][FAP] + C_2H_6 and C_3H_8 systems, a second liquid phase was formed at higher concentrations of C_4H_{10}, where, within the experimental accuracy (±0.003 MPa), the pressure of the three-phase line ($L_1L_2V \rightarrow L_1L_2$) nearly coincides with the vapour pressure curve of pure C_4H_{10}, see Figure 5.6. However, $L_1L_2V \rightarrow L_1L_2$ transitions occur at C_4H_{10} concentrations of around 15.0 mol% or higher, while $L_1L_2V \rightarrow L_1L_2$ transitions were present in the [emim][FAP] + C_3H_8 system at concentrations of 22.5 mol% or higher. For comparison, in the [emim][FAP] + C_2H_6 system $L_1L_2V \rightarrow L_1L_2$ transitions occurred at concentrations of 27.5% or higher, which indicates that longer hydrocarbons may show liquid-liquid immiscibility at lower concentrations.

Figure 5.6 shows that the slope of the $L_1L_2 \rightarrow L$ transitions in the [emim][FAP] + C_4H_{10} system is much steeper than that of the $L_1L_2 \rightarrow L$ transitions in the C_2H_6 + IL and C_3H_8 + IL systems. Therefore, it was hard to detect the cloud point by keeping the temperature constant and varying the pressure. Instead, for these measurements the pressure was kept constant, while the temperature was slowly increased with an increment of 0.1 K until the last droplet of the second liquid phase has disappeared. Figure 5.7 shows the bubble point and cloud point pressures for two selected temperatures, where the difference between the two types of phase transitions is clearly shown by the sharp bending. For both isotherms, the system is below its UCEP at all conditions measured.

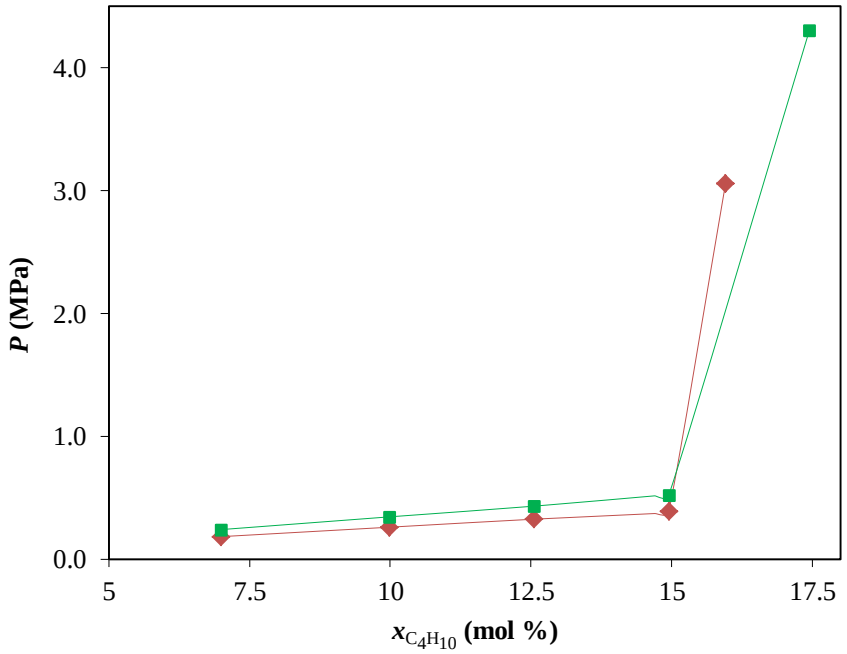

Figure 5.7: Isotherms of the binary system C_4H_{10} + [emim][FAP]: ◆, 316 K; ■, 330 K

5.3.4 Comparison of the [emim][FAP] + CO_2 vs. the [emim][FAP] + hydrocarbon

Figure 5.8 compares the solubilities of CO_2, CH_4, C_2H_6, C_3H_8 and C_4H_{10} in [emim][FAP] at a temperature of 330 K. It can be noticed that C_4H_{10} shows a higher solubility in [emim][FAP] than C_3H_8, C_2H_6 and CO_2, but the maximum achievable molar fraction is lowest because of the existence of a liquid-liquid immiscibility region at higher concentrations. On the other hand, it can be observed that the solubility of CH_4 is much lower compared to the solubility of the other gases.

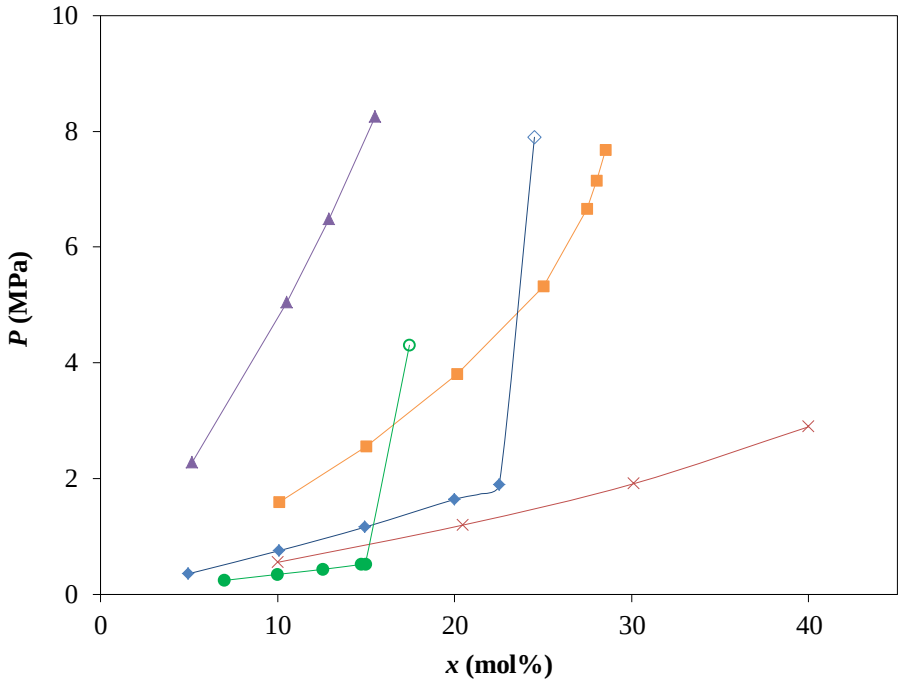

Figure 5.8:. Comparison of the solubilities of CO_2, CH_4, C_2H_6, C_3H_8 and C_4H_{10} in emim[FAP] at 330 K: ▲, [emim][FAP] + CH_4[23]; ■, [emim][FAP] + C_2H_6; ◆, [emim][FAP] + C_3H_8; ×, [emim][FAP] + CO_2 [13]; ●, [emim][FAP] + C_4H_{10}. Solid symbols represent (LV→L); open symbols represent (L_1L_2→L).

Henry coefficients at different temperatures can be calculated from the experimental solubility data using the Krichevsky-Kasarnovsky equation (see chapter 3, eq. 5) [13]. Table 5.4 presents the calculated results.

Table 5.4: Henry's Law constants for CO_2, CH_4, C_2H_6, C_3H_8 and C_4H_{10} in [emim][FAP].

T (K)	HCH_4 (MPa)[23]	HC_2H_6 (MPa)	HC_3H_8 (MPa)	HC_4H_{10} (MPa)	HCO_2 (MPa)[13]
303	38.45	10.54	4.60	2.04	3.32
313	39.36	11.76	5.40	2.51	4.06
323	40.39	13.02	6.29	3.06	4.68
333	41.43	14.30	7.21	3.67	5.36
343	42.39	15.60	8.14	4.33	6.09
353	43.17	16.89	9.09	5.03	6.86
363	43.66	18.17	10.21	5.78	7.71

In Figure 5.9 the Henry coefficients of CH_4, C_2H_6, C_3H_8 and C_4H_{10} in [emim][FAP] are presented.

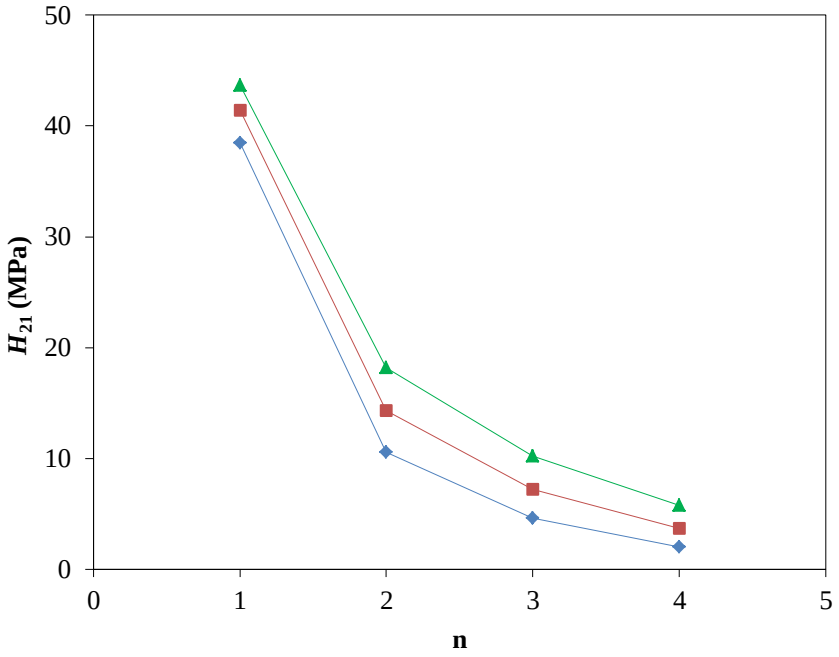

Figure 5.9: Effect of the hydrocarbon chain length on its solubility in [emim][FAP] at several temperatures: ◆, 303 K; ■, 333 K; ▲, 363 K.

It can be clearly observed that the hydrocarbon solubility increases in [emim][FAP] as the hydrocarbon chain becomes longer. The same behavior was observed for the solubility of the hydrocarbons in [bmim][Tf_2N] [18]. This observation could be attributed to an increase in dispersive forces between the alkyl chain of the IL and the longer chain of the hydrocarbons [28].

Table 5.5 reports the selectivity of CO_2 over hydrocarbons in the IL [emim][FAP] as a function of temperature. The separation ratio between CO_2 and hydrocarbons decreases as the hydrocarbon chain becomes longer. Thus, the selectivity increases in the order: $S_{CO2/C4H10}$ <

$S_{CO_2/C_3H_8} < S_{CO_2/C_2H_6} < S_{CO_2/CH_4}$. The maximum selectivities are achieved at the lowest temperatures. Therefore, the CO_2 removal from natural gas streams is recommended to be performed at lower temperatures in order to achieve the best separation.

Table 5.5: Selectivities ($S_{CO_2/HC} = H_{HC}/H_{CO_2}$) of CO_2 over hydrocarbons (HC) at various temperatures (T).

T (K)	S_{CO_2/CH_4}	S_{CO_2/C_2H_6}	S_{CO_2/C_3H_8}	$S_{CO_2/C_4H_{10}}$
303	11.58	3.17	1.39	0.61
313	9.69	2.90	1.33	0.62
323	8.63	2.78	1.34	0.65
333	7.73	2.67	1.35	0.69
343	6.96	2.56	1.34	0.71
353	6.29	2.46	1.33	0.73
363	5.66	2.36	1.32	0.75

Separation selectivities of CO_2/HC in [emim][FAP] were compared with selectivities in another IL ([hmim][Tf_2N]) [12, 29] and also in a "physical solvent" (Genosorb 1753) [30]. For example, at a temperature of 333 K, the separation ratios of CO_2/C_2H_6 are 2.67, 2.20 and 1.82 for [emim][FAP], [hmim][Tf_2N] and Genosorb1753, respectively. Thus, the selectivity for CO_2 separation from C_2H_6 in [emim][FAP] is higher than that in other ILs and physical solvents. Furthermore, [emim][FAP] shows a lower affinity for higher hydrocarbons [30, 31]. Therefore, hydrocarbon losses to the CO_2 stream are relatively limited. This confirms that the IL [emim][FAP] is a promising solvent for gas sweetening that can compete with commercial physical solvents.

The selectivities presented in this work are "ideal selectivities", where the selectivity is calculated by dividing the Henry constants of pure hydrocarbon by the Henry constant of pure CO_2. In reality, natural gas contains CH_4 in the presence of CO_2, C_2H_6, C_3H_8, C_4H_8, and many other compounds. Therefore, the presence of CO_2 or any other compound could affect the CH_4 solubility and vice versa [32], i.e., the solubilities of the individual components in mixed gases could be different than the solubilities of pure gases as reported in this work. This also means that the selectivities might be affected. For example, the CO_2 interaction with the anion of the IL could increase the dispersion forces causing an enhancement of the solubility of other gases in the IL compared to the solubility of the pure gas [32],[33]. Consequently, it is of major interest to investigate the phase behavior of a mixture of gases in [emim][FAP] in future studies.

5.3.5 Enthalpy of solution

The energy requirement for regeneration plays an important role in selecting a suitable CO_2 removal solvent. Therefore, enthalpies of solution ($\Delta_{sol}h$) at infinite dilution were calculated for all gases tested in this work using the following equation (Eq. 1) derived from the Van't Hoff equation [34]:

$$\Delta_{sol}h^{\infty} = R\left[\frac{\partial \ln P}{\partial\left(\frac{1}{T}\right)}\right]_x \qquad \text{Eq.1}$$

where P is the equilibrium pressure of the solute at a fixed concentration x, R is the universal gas constant, and T is the absolute temperature. Figure 5.10 shows the plot of ln(P) versus 1/T, where Δh_{abs} is obtained from the slope.

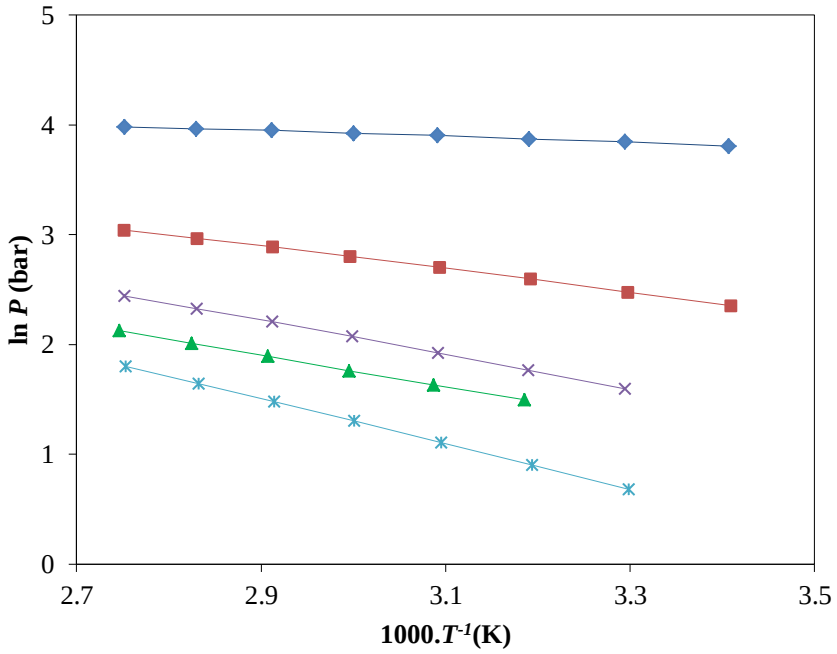

Figure 5.10: Plot of ln(P) versus 1/T for various gases at 10 mol% in [emim][FAP]: ✳, C_4H_{10}; ▲, CO_2[13]; ×, C_3H_8; ■, C_2H_6; ◆ CH_4[23].

Table 5.6 presents the $\Delta_{sol}h^{\infty}$ values for all gases in [emim][FAP]. It can be observed that the solution enthalpy increases with increasing chain length of the hydrocarbon. Thus, C_4H_{10} shows the highest $\Delta_{sol}h^{\infty}$ (-17.27 kJ⁄mol) due to a stronger interaction between the gas and the IL. This is consistent with its highest solubility.

Table 5.6: Enthalpies of solution for CO_2, CH_4, C_{2H6}, C_3H_8 and C_4H_{10} in [emim][FAP].

Gas	$\Delta_{sol} h^{\infty}$ (kJ/mol)	Ref.
CO_2	-11.89	[13]
CH_4	-2.20	[23]
C_2H_6	-8.69	
C_3H_8	-13.00	
C_4H_{10}	-17.27	

Since all hydrocarbons are physically absorbed in the IL, the enthalpies of solution are relatively low. This is considered to be an advantage, because lower amounts of energy are needed for removing the gases from the absorbent [35]. Thus, the regeneration of the IL simply can be done by reducing the system pressure [33].

5.4 Conclusions

At low concentrations, the solubility of small hydrocarbons in [emim][FAP] increases with increasing hydrocarbon chain length: $CH_4 < C_2H_6 < C_3H_8 < C_4H_{10}$. Further, it was found that an increase in hydrocarbon chain length decreases the maximum achievable solubility, because of the occurrence of liquid-liquid immiscibility at higher concentrations of the hydrocarbon. The UCEP of C_2H_6 in the IL was found to be nearly equal to the critical point of pure C_2H_6. Enthalpies of solution were found to be low, resulting in lower energy costs for regeneration. The enthalpies of absorption increased with increasing chain length of the hydrocarbons. Maximum selectivities for CO_2 removal from small hydrocarbons are achieved at lower temperatures, and found to be higher than selectivities in other ILs and physical solvents. This confirms that the IL [emim][FAP] is a promising candidate absorbent that can compete with commercial physical solvents for gas sweetening processes.

Appendix A

Table A5.1: Experimental bubble, cloud-point pressures (P) and the three phase line (L_1L_2V) for various concentrations of ethane ($x C_2H_6$) and temperatures (T) in the C_2H_6 + [emim][FAP] system[a].

***x*= 10.1 %**			***x*= 15.0 %**			***x*= 20.0 %**		
T(K)	P (MPa)	Phase Transition	T(K)	P (MPa)	Phase Transition	T(K)	P (MPa)	Phase Transition
293.33	1.054	LV →L	293.47	1.670	LV →L	293.53	2.413	LV →L
303.28	1.193	LV →L	303.45	1.906	LV →L	303.49	2.778	LV →L
313.33	1.343	LV →L	313.50	2.141	LV →L	313.42	3.160	LV →L
323.29	1.493	LV →L	323.36	2.386	LV →L	323.50	3.566	LV →L
333.78	1.648	LV →L	333.36	2.636	LV →L	333.40	3.926	LV →L
343.37	1.798	LV →L	343.33	2.881	LV →L	343.46	4.311	LV →L
353.36	1.945	LV →L	353.39	3.126	LV →L	353.37	4.681	LV →L
363.52	2.096	LV →L	363.34	3.367	LV →L	363.36	5.041	LV →L

***x*= 25.0 %**			***x*= 27.5 %**			**x=28.0%**		
T(K)	P (MPa)	Phase Transition	T(K)	P (MPa)	Phase Transition	T(K)	P (MPa)	Phase Transition
293.50	3.275	LV →L	293.22	5.216	L_1L_2 →L	293.29	8.164	L_1L_2 →L
303.51	3.821	LV →L	298.11	4.680	L_1L_2 →L	303.75	6.462	L_1L_2 →L
313.43	4.376	LV →L	308.24	5.025	LV →L	308.74	6.062	LV→L
323.44	4.952	LV →L	313.19	5.421	LV →L	313.13	6.043	LV →L
333.42	5.517	LV →L	323.15	6.146	LV →L	323.14	6.623	LV →L
343.32	6.067	LV →L	333.16	6.852	LV →L	333.15	7.344	LV →L
353.37	6.602	LV →L	343.05	7.492	LV →L	343.12	7.965	LV →L
363.34	7.122	LV →L	353.05	8.117	LV →L	353.08	8.565	LV →L
						362.98	9.146	LV →L

***x*= 28.5 %**			***x*= 30.0%**		
T(K)	P (MPa)	Phase Transition	T(K)	P (MPa)	Phase Transition
293.23	10.761	L_1L_2 →L	293.51	3.775	L_1L_2V → L_1L_2
303.14	7.860	L_1L_2 →L	298.42	4.240	L_1L_2V → L_1L_2
313.15	7.101	LV →L	303.40	4.686	L_1L_2V → L_1L_2
323.17	7.320	LV →L	305.35	4.863	L_1L_2V → L1+ L_2=V
333.07	7.841	LV →L			
343.09	8.461	LV →L			
353.03	9.022	LV →L			
363.10	9.562	LV →L			

[a]Standard uncertainties u are $u(T)$ = 0.01 K, $u(P)$ = 0.003 MPa, and $u(x_{C_2H_6})$ = 0.005

Table A5.2: Experimental bubble, cloud-point pressures (P) and the three phase line (L_1L_2V) for various concentrations of propane (xC_3H_8) and temperatures (T) in the C_3H_8 + [emim][FAP] system[a].

x= 4.9 %			**x= 10.1 %**			**x= 14.9 %**		
T(K)	P (MPa)	Phase Transition	T(K)	P (MPa)	Phase Transition	T(K)	P (MPa)	Phase Transition
293.46	0.193	LV → L	-	-	-	293.50	0.609	LV → L
303.48	0.232	LV → L	303.52	0.494	LV → L	303.51	0.745	LV → L
313.58	0.276	LV → L	313.47	0.584	LV → L	313.43	0.896	LV → L
323.53	0.327	LV → L	323.44	0.684	LV → L	323.44	1.051	LV → L
333.44	0.368	LV → L	333.46	0.794	LV → L	333.47	1.226	LV → L
343.4	0.423	LV → L	343.39	0.910	LV → L	343.44	1.401	LV → L
353.48	0.472	LV → L	353.33	1.025	LV → L	353.36	1.596	LV → L
363.46	0.530	LV → L	363.37	1.151	LV → L	363.38	1.796	LV → L
x= 20.0%			**x = 22.5%**			**x= 24.5 %**		
T(K)	P (MPa)	Phase Transition	T(K)	P (MPa)	Phase Transition	T(K)	P (MPa)	Phase Transition
293.55	0.839	LV → L	293.42	0.850	$L_1L_2V \rightarrow L_1L_2$	326.23	11.561	$L_1L_2 \rightarrow L$
303.52	1.023	LV → L	303.71	1.100	$L_1L_2V \rightarrow L_1L_2$	328.15	9.358	$L_1L_2 \rightarrow L$
313.48	1.243	LV → L	313.38	1.385	$L_1L_2V \rightarrow L_1L_2$	335.17	5.656	$L_1L_2 \rightarrow L$
323.45	1.473	LV → L	323.42	1.695	LV → L	338.09	4.756	$L_1L_2 \rightarrow L$
333.39	1.733	LV → L	333.36	2.000	LV → L	343.09	3.155	$L_1L_2 \rightarrow L$
343.42	2.014	LV → L	343.37	2.336	LV → L	-	-	
353.4	2.314	LV → L	353.33	2.711	LV → L	-	-	
363.38	2.615	LV → L	-	-	-	-	-	
x= 25.0 %			**x= 30.1 %**					
T(K)	P (MPa)	Phase Transition	T(K)	P (MPa)	Phase Transition			
335.07	11.064	$L_1L_2 \rightarrow L$	293.49	0.841	$L_1L_2V \rightarrow L_1L_2$			
338.04	8.863	$L_1L_2 \rightarrow L$	303.53	1.081	$L_1L_2V \rightarrow L_1L_2$			
343.19	6.660	$L_1L_2 \rightarrow L$	313.46	1.370	$L_1L_2V \rightarrow L_1L_2$			
348.20	5.059	$L_1L_2 \rightarrow L$	323.45	1.715	$L_1L_2V \rightarrow L_1L_2$			
353.19	3.859	$L_1L_2 \rightarrow L$	333.41	2.116	$L_1L_2V \rightarrow L_1L_2$			
356.06	3.560	$L_1L_2 \rightarrow L$	343.46	2.586	$L_1L_2V \rightarrow L_1L_2$			
			353.41	3.132	$L_1L_2V \rightarrow L_1L_2$			
			363.4	3.758	$L_1L_2V \rightarrow L_1L_2$			

[a]Standard uncertainties u are $u(T)$ = 0.01 K, $u(P)$ = 0.003 MPa, and $u(x_{C_3H_8})$ = 0.005

Table A5.3: Experimental bubble, cloud-point pressures (P) and the three phase line (L_1L_2V) for various concentrations of propane (xC_4H_{10}) and temperatures (T) in the C_4H_{10} + [emim][FAP] system[a].

***x*= 7.0 %**			***x*= 10.0 %**			***x*= 12.6 %**		
T(K)	P (MPa)	Phase Transition	T(K)	P (MPa)	Phase Transition	T(K)	P (MPa)	Phase Transition
313.13	0.175	LV → L	293.28	0.154	LV → L	293.28	0.192	LV → L
323.16	0.214	LV → L	303.17	0.197	LV → L	303.17	0.246	LV → L
333.16	0.258	LV → L	313.12	0.246	LV → L	313.12	0.307	LV → L
343.06	0.304	LV → L	323.10	0.303	LV → L	323.10	0.377	LV → L
353.18	0.358	LV → L	333.24	0.369	LV → L	333.24	0.460	LV → L
363.12	0.414	LV → L	343.14	0.438	LV → L	343.14	0.551	LV → L
		LV → L	353.07	0.517	LV → L	353.07	0.649	LV → L
		LV → L	363.19	0.605	LV → L	363.19	0.757	LV → L

***x*= 15.0%**			***x* = 16.0%**			***x*= 17.5%**		
T(K)	P (MPa)	Phase Transition	T(K)	P (MPa)	Phase Transition	T(K)	P (MPa)	Phase Transition
293.39	0.215	$L_1L_2V \rightarrow L_1L_2$	314.11	9.060	$L_1L_2 \rightarrow L$	327.62	9.263	$L_1L_2 \rightarrow L$
303.30	0.290	$L_1L_2V \rightarrow L_1L_2$	315.02	6.059	$L_1L_2 \rightarrow L$	328.97	6.161	$L_1L_2 \rightarrow L$
313.28	0.369	LV → L	316.09	3.058	$L_1L_2 \rightarrow L$	330.78	3.060	$L_1L_2 \rightarrow L$
323.30	0.456	LV → L	316.45	1.057	$L_1L_2 \rightarrow L$	332.10	1.059	$L_1L_2 \rightarrow L$
333.30	0.555	LV → L	318.47	0.432	LV → L	338.18	0.701	LV → L
343.30	0.655	LV → L	323.16	0.480	LV → L	343.06	0.767	LV → L
353.23	0.785	LV → L	333.33	0.587	LV → L	353.03	0.923	LV → L
363.23	0.920	LV → L	343.18	0.702	LV → L	363.07	1.085	LV → L
			353.06	0.832	LV → L			
			363.06	0.973	LV → L			

***x*= 24.9 %**		
T(K)	P (MPa)	Phase Transition
293.20	0.211	$L_1L_2V \rightarrow L_1L_2$
303.11	0.287	$L_1L_2V \rightarrow L_1L_2$
313.28	0.385	$L_1L_2V \rightarrow L_1L_2$
323.17	0.502	$L_1L_2V \rightarrow L_1L_2$
333.12	0.644	$L_1L_2V \rightarrow L_1L_2$
343.13	0.815	$L_1L_2V \rightarrow L_1L_2$
353.07	1.015	$L_1L_2V \rightarrow L_1L_2$
363.17	1.257	$L_1L_2V \rightarrow L_1L_2$

[a]Standard uncertainties u are $u(T)$ = 0.01 K, $u(P)$ = 0.003 MPa, and $u(x_{C_4H_{10}})$ = 0.005

5.5 References

[1] S. Atchariyawut, R. Jiraratananon, R. Wang, Separation of CO_2 from CH_4 by using gas–liquid membrane contacting process, Journal of Membrane Science, 304 (2007) 163-172.

[2] R.W. Baker, K. Lokhandwala, Natural Gas Processing with Membranes: An Overview, Industrial & Engineering Chemistry Research, 47 (2008) 2109-2121.

[3] M. Arruebo, J. Coronas, M. Menéndez, J. Santamaría, Separation of hydrocarbons from natural gas using silicalite membranes, Separation and Purification Technology, 25 (2001) 275-286.

[4] G. Aldana, R. Arai, D. G. Elliot, An Evaluation of Sources of CO_2 for EOR in Venezuela, in: Proceedings of the Sixty-Third Annual Gas Processors Association Convention, New Orleans, Louisiana, (1984).

[5] N. Korens, D. R. Simbeck, D. J. Wilhelm, Process Screening Analysis of Alternative Gas Treating and Sulfur Removal for Gasification, in, Prepared for U.S. Department of Energy by SFA Pacific, Inc., Revised Final Report, (2002).

[6] E.D. Bates, R.D. Mayton, I. Ntai, J.H. Davis, CO_2 Capture by a Task-Specific Ionic Liquid, Journal of the American Chemical Society, 124 (2002) 926-927.

[7] L.A. Blanchard, Z. Gu, J.F. Brennecke, High-Pressure Phase Behavior of Ionic Liquid/CO_2 Systems, The Journal of Physical Chemistry B, 105 (2001) 2437-2444.

[8] J. Kumełan, Á. Pérez-Salado Kamps, D. Tuma, G. Maurer, Solubility of CO_2 in the ionic liquid [hmim][Tf2N], The Journal of Chemical Thermodynamics, 38 (2006) 1396-1401.

[9] Y. Chen, S. Zhang, X. Yuan, Y. Zhang, X. Zhang, W. Dai, R. Mori, Solubility of CO_2 in imidazolium-based tetrafluoroborate ionic liquids, Thermochimica Acta, 441 (2006) 42-44.

[10] A.M. Schilderman, S. Raeissi, C.J. Peters, Solubility of carbon dioxide in the ionic liquid 1-ethyl-3-methylimidazolium bis(trifluoromethylsulfonyl)imide, Fluid Phase Equilibria, 260 (2007) 19-22.

[11] A.N. Soriano, B.T. Doma, M.-H. Li, Solubility of Carbon Dioxide in 1-Ethyl-3-methylimidazolium Tetrafluoroborate, Journal of Chemical & Engineering Data, 53 (2008) 2550-2555.

[12] A. Finotello, J.E. Bara, D. Camper, R.D. Noble, Room-Temperature Ionic Liquids: Temperature Dependence of Gas Solubility Selectivity, Industrial & Engineering Chemistry Research, 47 (2007) 3453-3459.

[13] M. Althuluth, M.T. Mota-Martinez, M.C. Kroon, C.J. Peters, Solubility of Carbon Dioxide in the Ionic Liquid 1-Ethyl-3-methylimidazolium Tris(pentafluoroethyl) trifluoro phosphate, Journal of Chemical & Engineering Data, 57 (2012) 3422-3425.

[14] A. Shariati, C.J. Peters, High-pressure phase behavior of systems with ionic liquids: Part III. The binary system carbon dioxide + 1-hexyl-3-methylimidazolium hexafluorophosphate, The Journal of Supercritical Fluids, 30 (2004) 139-144.

[15] A. Shariati, C.J. Peters, High-pressure phase behavior of systems with ionic liquids: II. The binary system carbon dioxide+1-ethyl-3-methylimidazolium hexafluorophosphate, The Journal of Supercritical Fluids, 29 (2004) 43-48.

[16] K.I. Gutkowski, A. Shariati, C.J. Peters, High-pressure phase behavior of the binary ionic liquid system 1-octyl-3-methylimidazolium tetrafluoroborate + carbon dioxide, The Journal of Supercritical Fluids, 39 (2006) 187-191.

[17] P.J. Carvalho, V.H. Álvarez, J.J.B. Machado, J. Pauly, J.-L. Daridon, I.M. Marrucho, M. Aznar, J.A.P. Coutinho, High pressure phase behavior of carbon dioxide in 1-alkyl-3-methylimidazolium bis(trifluoromethylsulfonyl)imide ionic liquids, The Journal of Supercritical Fluids, 48 (2009) 99-107.

[18] S. Raeissi, C.J. Peters, High pressure phase behaviour of methane in 1-butyl-3-methylimidazolium bis(trifluoromethylsulfonyl)imide, Fluid Phase Equilibria, 294 (2010) 67-71.

[19] J.L. Anthony, E.J. Maginn, J.F. Brennecke, Solubilities and Thermodynamic Properties of Gases in the Ionic Liquid 1-n-Butyl-3-methylimidazolium Hexafluorophosphate, The Journal of Physical Chemistry B, 106 (2002) 7315-7320.

[20] J.L. Anderson, J.K. Dixon, J.F. Brennecke, Solubility of CO_2, CH_4, C_2H_6, C_2H_4, O_2, and N2 in 1-Hexyl-3-methylpyridinium Bis(trifluoromethylsulfonyl)imide: Comparison to Other Ionic Liquids, Accounts of Chemical Research, 40 (2007) 1208-1216.

[21] G. Hong, J. Jacquemin, M. Deetlefs, C. Hardacre, P. Husson, M.F. Costa Gomes, Solubility of carbon dioxide and ethane in three ionic liquids based on the bis{(trifluoromethyl)sulfonyl}imide anion, Fluid Phase Equilibria, 257 (2007) 27-34.

[22] B.-C. Lee, S.L. Outcalt, Solubilities of Gases in the Ionic Liquid 1-n-Butyl-3-methylimidazolium Bis(trifluoromethylsulfonyl)imide, Journal of Chemical & Engineering Data, 51 (2006) 892-897.

[23] M. Althuluth, M.C. Kroon, C.J. Peters, Solubility of Methane in the Ionic Liquid 1-Ethyl-3-methylimidazoliumTris(pentafluoroethyl)trifluorophosphate, Industrial & Engineering Chemistry Research, 51 (2012) 16709-16712.

[24] T.W. De Loos, H.J. Van der Kooi, P.L. Ott, Vapor-liquid critical curve of the system ethane + 2-methylpropane, Journal of Chemical & Engineering Data, 31 (1986) 166-168.

[25] B.E. Poling, J.M. Prausnitz, J.P. O'Connell, The Properties of Gases and Liquids, fifth ed., McGraw-Hill, New York, (2001).

[26] J.M. Smith, H. Van Ness, M.M. Abbott, Introduction to Chemical Engineering Thermodynamics, Seventh ed., McGraw-Hill Education, (2005).

[27] J.M. Smith, H.C. Van Ness, M.M. Abbott, Introduction to chemical engineering thermodynamics, McGraw-Hill, (2005).

[28] A.R. Ferreira, M.G. Freire, J.C. Ribeiro, F.M. Lopes, J.o.G. Crespo, J.o.A.P. Coutinho, An Overview of the Liquid−Liquid Equilibria of (Ionic Liquid + Hydrocarbon) Binary Systems and Their Modeling by the Conductor-like Screening Model for Real Solvents, Industrial & Engineering Chemistry Research, 50 (2011) 5279-5294.

[29] L.J. Florusse, S. Raeissi, C.J. Peters, High-Pressure Phase Behavior of Ethane with 1-Hexyl-3-methylimidazolium Bis(trifluoromethylsulfonyl)imide, Journal of Chemical & Engineering Data, 53 (2008) 1283-1285.

[30] A.V. Rayer, A. Henni, P. Tontiwachwuthikul, High-Pressure Solubility of Methane (CH_4) and Ethane (C_2H_6) in Mixed Polyethylene Glycol Dimethyl Ethers (Genosorb 1753) and Its Selectivity in Natural Gas Sweetening Operations, Journal of Chemical & Engineering Data, 57 (2012) 764-775.

[31] S.F. Sciamanna, S. Lynn, Solubility of hydrogen sulfide, sulfur dioxide, carbon dioxide, propane, and n-butane in poly(glycol ethers), Industrial & Engineering Chemistry Research, 27 (1988) 492-499.

[32] D.G. Hert, J.L. Anderson, S.N.V.K. Aki, J.F. Brennecke, Enhancement of oxygen and methane solubility in 1-hexyl-3-methylimidazolium bis(trifluoromethylsulfonyl) imide using carbon dioxide, Chemical Communications, (2005) 2603-2605.

[33] A. Muhammad, A. Shafeeq, Z. ul Hasan Rizvi, A. Ijaz, M.I.A. Mutalib, Experimental solubility of CO_2 and CH_4 in imidazolium based ionic liquid; [C6mim][BF4] at high pressures, in: Chemical, Biological and Environmental Engineering (ICBEE), 2nd International Conference, (2010), 39-42.

[34] J.H. Hildebrand, R.L. Scott, Regular solutions, Prentice-Hall, (1962).

[35] D. Chinn, D. Vu, M. Driver, L. Boudreau, CO_2 removal from gas using ionic liquid absorbents, Google Patents, (2005).

Chapter 6

Modeling Solubilities of Gases in the Ionic Liquid [emim][FAP]

This chapter is adapted from the following publication: M. Althuluth, A. S. Berrouk, M. C. Kroon and C. J. Peters, Ind. Eng. Chem. Res. 53 (2014) 11818-11821

6.1 Introduction

The use of an ionic liquid (IL) in gas separation seems to be promising, especially for carbon capture. Many researchers have experimentally proven that carbon dioxide (CO_2) is higher soluble in ILs compared to other gases [1-3].

Accurate knowledge of the phase equilibria of mixtures consisting of gases and ILs is very important in designing absorption systems. However, experimental measurements of phase equilibria of mixtures with ILs are expensive and time-consuming. Therefore, it is recommended to have thermodynamic models for estimating gas solubilities in ILs. Models are used for correlation of existing data and to predict phase equilibria in regions where experimental data are not available. Equations of state (EoS) are widely used to describe the properties of pure fluids or their mixtures. In the last few years, this kind of models has been widely applied to model phase equilibria of IL mixtures. For example, Shiflett and Yokozeki used an EoS to model the solubility of CO_2 in [bmim][PF_6] [4]. Shin *et al.* modeled the high-pressure solubility of CO_2 in ILs belonging to the homologous 1-alkyl-3-methylimidazolium bis(trifluoromethylsulfonyl) amide [$C_n$mim][Tf_2N] series [5], Also Alvarez and Aznar used an EoS to model the vapor-liquid equilibrium (VLE) of binary systems composed of a IL + supercritical CO_2 or fluoroform (CHF_3) [6].

In this work, we will use the Peng-Robinson EoS (PR-EoS) to model the gas solubility of CO_2, methane (CH_4), ethane (C_2H_6), propane (C_3H_8) and butane (C_4H_{10}) in [emim][FAP] for the first time over wide ranges of pressure, temperature and composition. We found this IL to be a very promising solvent for gas sweetening, because this IL is low viscous, the solubility of CO_2 in this IL is very high and the solubilities of small hydrocarbons are much lower [3, 7, 8]. The PR-EoS was selected to model our experimental data, since it is a simple approach for modeling phase equilibria of mixtures and because this model is commonly used in many process simulators e.g., Hysys, Aspen, Promax, etc. Furthermore, the application of the PR-EoS to the VLE of systems of ILs and CO_2 has been reported by a number of sources [4-6]. However, little attention was given to the VLE of ILs and other gases, such as small hydrocarbons including CH_4, C_2H_6, C_3H_8 and C_4H_{10}.

The thermodynamic model

The PR-EoS was developed in 1976 by Peng and Robinson [9] and can be expressed as:

$$P = \frac{RT}{V_m - b} - \frac{a}{V_m\left(V_m + b\right) + b\left(V_m - b\right)} \quad \text{Eq.1}$$

where P is the pressure, V_m the molar volume, T the temperature, a the attractive interaction parameter, b the parameter that accounts for the co-volume and R the universal gas constant. For a mixture, the a and b parameters are obtained from quadratic mixing rules:

$$a = \sum\sum x_i x_j a_{ij} \quad \text{Eq.2}$$

and

$$b = \sum\sum x_i x_j b_{ij} \quad \text{Eq.3}$$

with:

$$a_{ij} = \sqrt{a_i a_j}\left(1 - k_{ij}\right) \quad \text{Eq.4}$$

and

$$b_{ij} = \frac{b_i + b_j}{2}\left(1 - l_{ij}\right) \quad \text{Eq.5}$$

In Eqs. (4) and (5), k_{ij} and l_{ij} are adjustable parameters, the so-called binary interaction parameters. The pure component parameters a_i and b_i are determined by the following equations:

$$a_i = 0.457235\frac{R^2 T_{ci}^2}{P_{ci}}\alpha_i \quad \text{Eq.6}$$

$$b_i = 0.077796\frac{RT_{ci}}{P_{ci}} \quad \text{Eq.7}$$

$$\alpha_i = \left[1 + m_i\left(1 - \sqrt{T/T_{ci}}\right)\right]^2 \quad \text{Eq.8}$$

$$m_i = 0.37464 + 1.54226\omega_i - 0.26992\omega^2{}_i \quad \text{Eq.9}$$

where T_c is the critical temperature, P_c is the critical pressure, α is a temperature dependent parameter and ω the acentric factor. For most ILs, the critical properties and the acentric factors are impossible to determine experimentally, because they decompose before the

temperature reaches the critical point. For this reason, Valderrama *et al.* have used a modified Lydersen-Joback-Reid group contribution method to determine the critical properties, normal boiling point temperatures and acentric factors of several ILs [10]. This method only requires knowledge of the structure of the ILs and its molecular weight.

6.2 Results and Discussion

To model the VLE of a mixture (gas + IL) by using the PR-EoS, critical properties and the acentric factors for both the gases and the IL are required. The critical properties of the gases were taken from the literature [11], while the critical properties for the IL were estimated by using the modified group contribution method of Lydersen-Joback-Reid [10]. To estimate the critical properties of the IL, the [emim][FAP] was separated into various functional groups as presented in Table 6.1, and the estimated critical properties are reported in Table 6.2.

Table 6.1: Functional groups considered in the modified Lyderson-Joback-Reid Method for [emim][FAP].

Without rings		With rings	
$-CH_3$	2	=CH-	3
$-CH_2-$	1	>N-	1
>C<	6	$[>N=]^+$	1
-F	18		
$[P]^-$	1		

Table 6.2: Critical properties and acentric factors used as input in PR-EoS.

Ionic liquid	M/g·mol^{-1}	T_c/K	P_c/MPa	ω
[emim][FAP]	566.10	760.5	1.005	0.874
CO_2	44.01	304.2	7.383	0.224
CH_4	16.04	190.6	4.599	0.012
C_2H_6	30.07	305.3	4.872	0.100
C_3H_8	44.09	369.8	4.248	0.152
C_4H_{10}	58.12	425.1	3.796	0.200

The experimental solubility data of CO_2, CH_4, C_2H_6, C_3H_8 or C_4H_{10} in [emim][FAP], as obtained previously [3, 7, 8], were modeled with the PR-EoS and the quadratic mixing rules. The binary interaction parameters were optimized using the Nelder-Mead simplex method by minimizing the objective function *F*, as defined as the absolute average deviation (*AAD*) between experimental data and calculated results [12], all calculations were performed using a MATLAB code which is written by Angel Martin [12].

$$F = \frac{1}{N}\sum_{i=1}^{N}\left|\frac{P_i^{exp} - P_i^{cal}}{P_i^{exp}}\right| \times 100 \qquad \text{Eq.10}$$

In Eq. [10], *N* is the number of experimental data points, $P^{\exp}$ and P^{cal}, the experimental and calculated bubble point pressures, respectively. The root-mean-square deviation is also included for better judgment the proposed model.

$$RMSD = \sqrt{\frac{1}{N}\sum_{i=1}^{N}\left|\frac{P_i^{exp} - P_i^{cal}}{P_i^{exp}}\right|^2} \times 100 \qquad \text{Eq.11}$$

6.2.1 The system CO_2 + [emim][FAP]

The solubility data of the mixture CO_2 + [emim][FAP] were first correlated with the PR-EoS and quadratic mixing rules with only one temperature dependent binary interaction parameter. It was found that the absolute average deviation (*AAD* %) was higher than 10% for all isotherms. This means that using only one binary parameter k_{12}, even temperature dependent, it is impossible to correlate all data points accurately.

The results were significantly improved by using two binary interaction parameters k_{12} and l_{12}. The geometric mean rule employed in the cross energy parameter is based on the London theory for dispersion forces (Eq.4) [13]. The binary interaction parameter k_{12} is necessary for correcting the geometric rule in case of strong solvating systems, e.g. in our case due to polar forces (dipole moment of the ion pair and quadrupolar moment of the carbon dioxide) and is temperature-dependent. The binary interaction parameter l_{12} is needed to correct for the volume of mixing [14]. The l_{12} was fixed (temperature-independent).

In that case, the model correlates the experimental data accurately over the entire range of measurements as depicted in Figure 6.1.

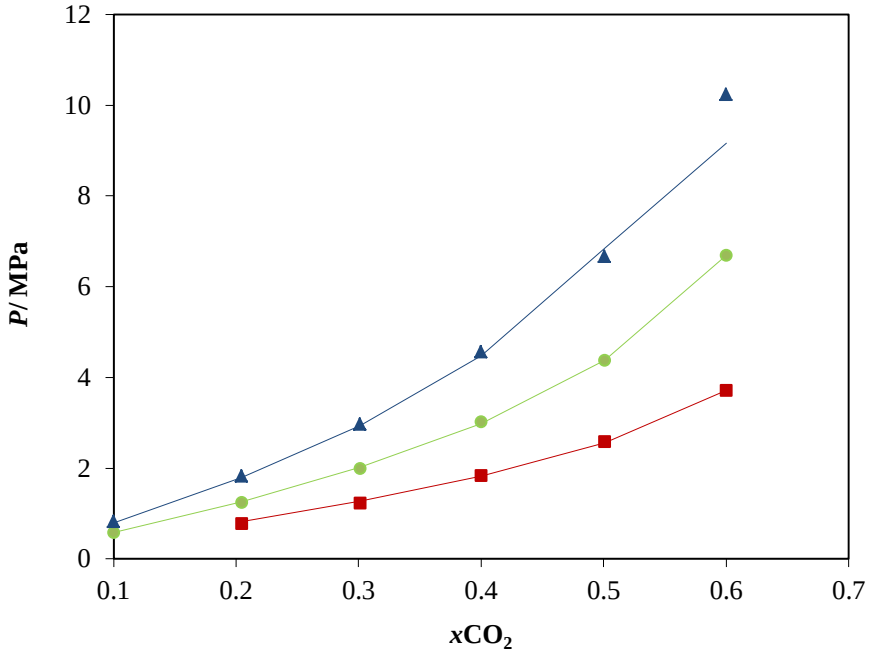

Figure 6.1: VLE of the binary mixture CO_2 + [emim][FAP] at three selected temperatures: ■, 303 K; ●, 333 K; ▲, 363 K. The symbols represent experimental data; lines represent correlation results.

Table 6.3: Binary interaction parameters and deviation values for the mixture of CO_2 + [emim][FAP].

T (K)	$k_{12} \times 10^{-1}$	l_{12}	AAD %	Max error %	RMSD %
293-363	-0. 38- (-0.45)	0.64	2.17	3.35	2.40

Table 6.3 reports all optimized parameters of Eqs. 1, 4 and 5 and the deviations in calculated bubble point pressures for the mixture of CO_2 + [emim][FAP]. From Table 6.3, it can be seen that the total *AAD* is less than 3%. Figure 6.2 shows the temperature dependency of the adjustable parameter in Eq. 12, which is in agreement with findings reported in literature [15-17].

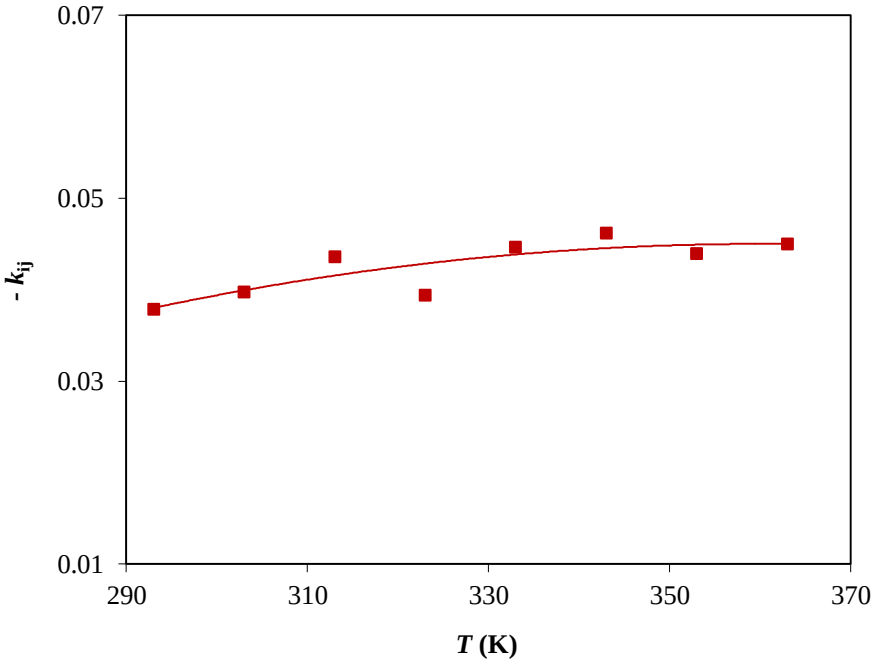

Figure 6.2: Dependence of binary interaction parameter on the temperature for the binary mixture of CO_2 + [emim][FAP].

The relationship between the k_{12} and T for the CO_2 + [emim][FAP] system correlated as follows:

$$k_{12} = -1.535\times10^{-6}T^2 + 1.107\times10^{-3}T - 1.545\times10^{-1} \qquad \text{Eq.12}$$

Above equation allows to calculate the binary interaction parameters k_{12} for the system CO_2 + [emim][FAP] IL at any temperature.

6.2.2 The binary systems hydrocarbon + [emim][FAP]

For the binary mixtures of hydrocarbon and [emim][FAP], calculations with only one temperature dependent binary interaction parameter (k_{12}) were performed and compared with experiment. Experimental data and calculated results at three selected temperatures are shown in Figure 6.3.

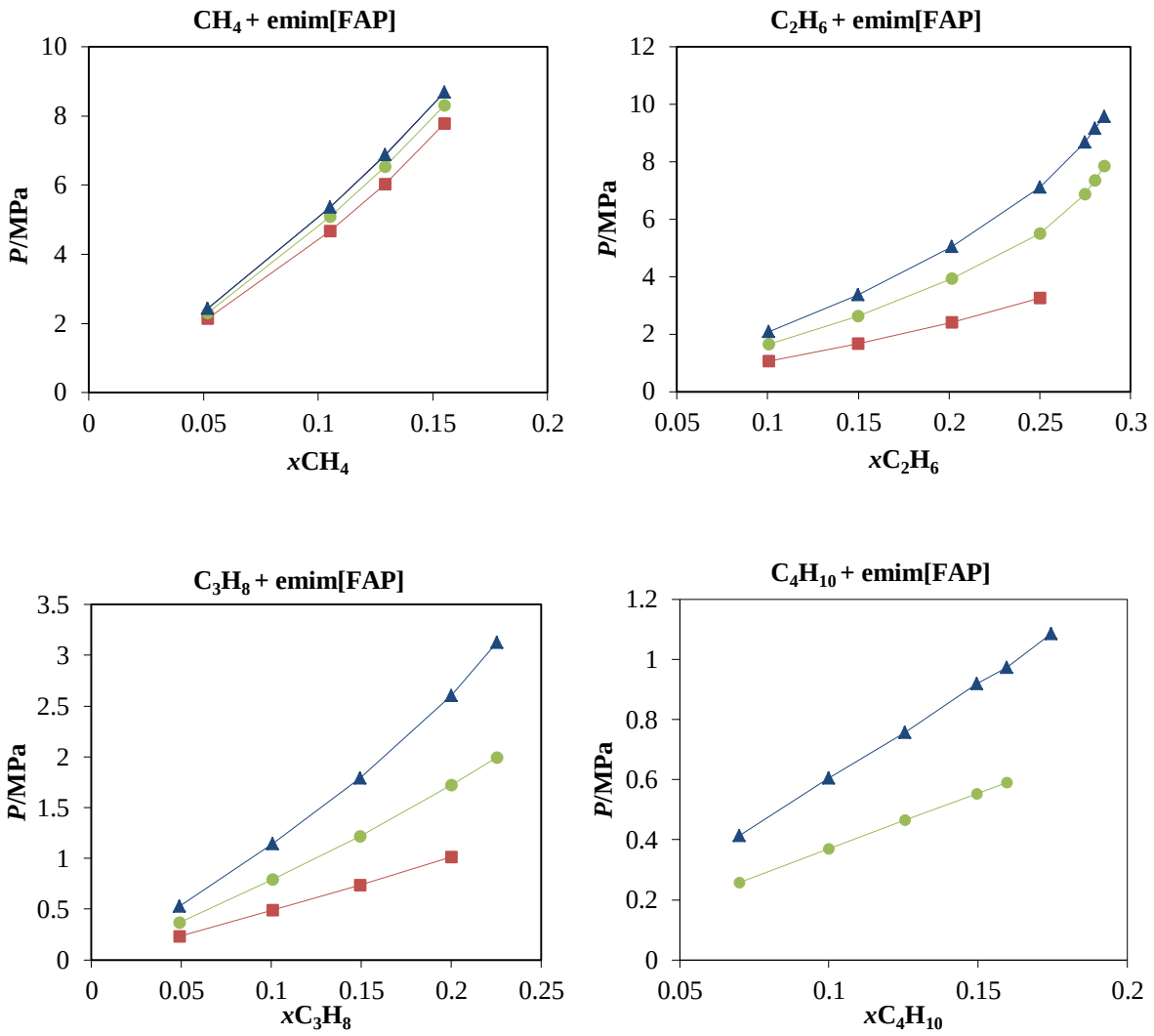

Figure 6.3: VLE of binary mixtures hydrocarbon + [emim][FAP] at three selected temperatures: ■, 303 K; ●, 333 K; ▲, 363 K. The symbols represent experimental data; the lines represent correlation results.

This figure shows that the model correlates the experimental data accurately even at higher concentrations with an *AAD* less than 1% for all systems. The optimized parameters and deviations in calculated bubble point pressures are reported in Table 6.4.

Table 6. 4: Binary interaction parameters and deviation values for the mixtures of hydrocarbon + [emim][FAP].

System	T (K)	k_{12}	AAD %	Max error %	RMSD %
CH_4+ [emim][FAP]	303-363	0.34-0.40	0.34	0.89	0.49
C_2H_6 + [emim][FAP]	293-363	0.25-0.31	0.39	0.84	0.52
C_3H_8 + [emim][FAP]	303-363	0.24-0.29	0.34	0.88	0.48
C_4H_{10} + [emim][FAP]	323-363	0.24-0.27	0.47	0.98	0.59

As can be seen in Figure 6.4, with increasing temperature the binary parameter (k_{12}) increases linearly. This confirms that it is not possible to correlate the solubility data accurately over the entire temperature range using a temperature independent parameter.

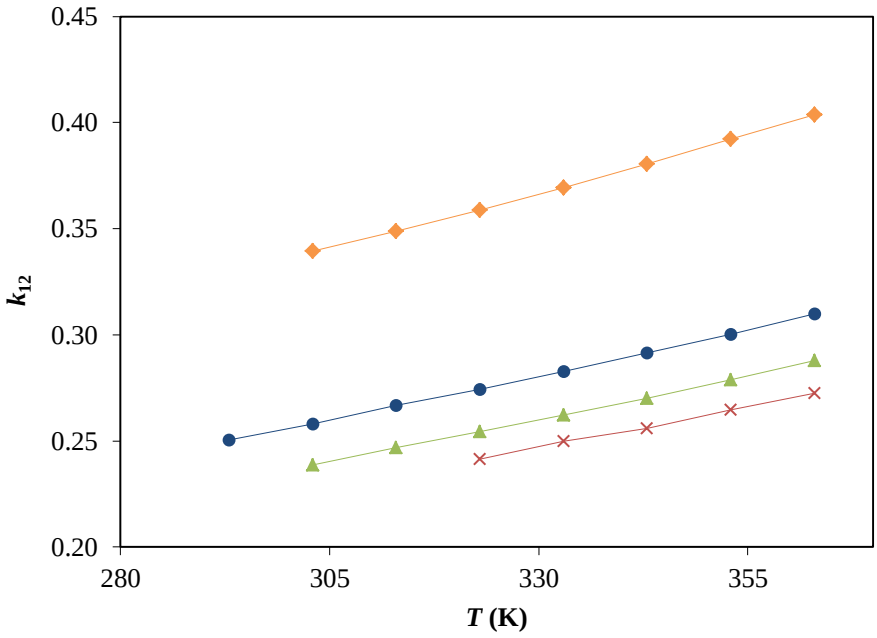

Figure 6.4: Dependence of the binary interaction parameter om temperature: ×; C_4H_{10} + [emim][FAP]; ▲, C_3H_8 + [emim][FAP]; ●, C_2H_6 + [emim][FAP]; ◆, CH_4 + [emim][FAP].

Further, it was found that the value of the binary interaction parameter k_{12} is much higher in the CH_4 + IL system than in the other systems (C_2H_6 + IL, C_3H_8 + IL and C_4H_{10} + IL), because the asymmetry between the IL and the hydrocarbon decreases with increasing alkyl chain of the hydrocarbon.

For all hydrocarbons + IL systems investigated in this study, the relationship between k_{12} and T can be correlated with:

$$k_{12} = a + bT \qquad \text{Eq.13}$$

The constants a and b are listed in Table 6.5.

Table 6.5: Binary interaction parameters of various systems as a function of the temperature.

System	Temperature range (K)	k_{12}	
		a	b
CH_4+ [emim][FAP]	303-363	1.075E-3	1.252E-2
C_2H_6 + [emim][FAP]	293-363	8.452E-4	2.104E-3
C_3H_8 + [emim][FAP]	303-363	8.103E-4	-7.044E-3
C_4H_{10} + [emim][FAP]	323-363	7.67E-4	-6.257E-3

6.3 Conclusions

The PR-EoS, combined with quadratic mixing rules, correlates the experimental solubility data accurately over a wide temperature range (293K- 363K) and pressures up to 11 MPa. This research established that the experimental data of all binary mixtures hydrocarbon + [emim][FAP] could be accurately correlated by using only one binary interaction parameter with an *AAD* less than 1%, while, on the other hand the solubility data of the binary mixture CO_2 + [emim][FAP] required two binary interaction parameters to yield *AAD* of less than 3%. Without a temperature dependency of the binary parameters the correlation is poor. Another finding of this study was that for the binary systems hydrocarbon + [emim][FAP], the value of the binary parameters decreases with increasing alkyl chain length of the hydrocarbon.

6.4 References

[1] J.L. Anderson, J.K. Dixon, J.F. Brennecke, Solubility of CO_2, CH_4, C_2H_6, C_2H_4, O_2, and N_2 in 1-Hexyl-3-methylpyridinium Bis(trifluoromethylsulfonyl)imide: Comparison to Other Ionic Liquids, Accounts of Chemical Research, 40 (2007) 1208-1216.

[2] G. Hong, J. Jacquemin, M. Deetlefs, C. Hardacre, P. Husson, M.F. Costa Gomes, Solubility of carbon dioxide and ethane in three ionic liquids based on the bis{(trifluoromethyl)sulfonyl}imide anion, Fluid Phase Equilibria, 257 (2007) 27-34.

[3] M. Althuluth, M.C. Kroon, C.J. Peters, Solubility of Methane in the Ionic Liquid 1-Ethyl-3-methylimidazolium Tris(pentafluoroethyl)trifluorophosphate, Industrial & Engineering Chemistry Research, 51 (2012) 16709-16712.

[4] M.B. Shiflett, A. Yokozeki, Solubilities and Diffusivities of Carbon Dioxide in Ionic Liquids: [bmim][PF6] and [bmim][BF4], Industrial & Engineering Chemistry Research, 44 (2005) 4453-4464.

[5] E.-K. Shin, B.-C. Lee, J.S. Lim, High-pressure solubilities of carbon dioxide in ionic liquids: 1-Alkyl-3-methylimidazolium bis(trifluoromethylsulfonyl)imide, The Journal of Supercritical Fluids, 45 (2008) 282-292.

[6] V.H. Álvarez, M. Aznar, Thermodynamic modeling of vapor–liquid equilibrium of binary systems ionic liquid + supercritical {CO_2 or CHF_3} and ionic liquid + hydrocarbons using Peng–Robinson equation of state, Journal of the Chinese Institute of Chemical Engineers, 39 (2008) 353-360.

[7] M. Althuluth, M.T. Mota-Martinez, A. Berrouk, M.C. Kroon, C.J. Peters, Removal of small hydrocarbons (ethane, propane, butane) from natural gas streams using the ionic liquid 1-ethyl-3 -methylimidazolium tris(pentafluoroethyl)trifluorophosphate, The Journal of Supercritical Fluids, 90 (2014) 65-72.

[8] M. Althuluth, M.T. Mota-Martinez, M.C. Kroon, C.J. Peters, Solubility of Carbon Dioxide in the Ionic Liquid 1-Ethyl-3-methylimidazolium Tris(pentafluoroethyl) trifluorophosphate, Journal of Chemical & Engineering Data, 57 (2012) 3422-3425.

[9] D.-Y. Peng, D.B. Robinson, A New Two-Constant Equation of State, Industrial & Engineering Chemistry Fundamentals, 15 (1976) 59-64.

[10] J.O. Valderrama, R.E. Rojas, Critical Properties of Ionic Liquids. Revisited, Industrial & Engineering Chemistry Research, 48 (2009) 6890-6900.

[11] J. M. Smith, H. Van Ness, M. M. Abbott, Introduction to Chemical Engineering Thermodynamics. Seventh ed.; McGraw-Hill Education (2005).

[12] Á. Martín, M.D. Bermejo, F.A. Mato, M.J. Cocero, Teaching advanced equations of state in applied thermodynamics courses using open source programs, Education for Chemical Engineers, 6 (2011) 114-121.

[13] G. M. Kontogeorgis, G. K. Folas, Thermodynamic Models for Industrial Applications: From Classical and Advanced Mixing Rules to Association Theories. Wiley (2009).

[14] P.H. Salim, M.A. Trebble, A modified Trebble—Bishnoi equation of state: thermodynamic consistency revisited, Fluid Phase Equilibria, 65 (1991) 59-71.

[15] J.-H. Yim, H.N. Song, K.-P. Yoo, J.S. Lim, Measurement of CO_2 Solubility in Ionic Liquids: [BMP][Tf_2N] and [BMP][$MeSO_4$] by Measuring Bubble-Point Pressure, Journal of Chemical & Engineering Data, 56 (2011) 1197-1203.

[16] J.O. Valderrama, F. Urbina, C.A. Faúndez, Gas–liquid equilibrium modeling of mixtures containing supercritical carbon dioxide and an ionic liquid, The Journal of Supercritical Fluids, 64 (2012) 32-38.

[17] T. Wang, C. Peng, H. Liu, Y. Hu, Description of the pVT behavior of ionic liquids and the solubility of gases in ionic liquids using an equation of state, Fluid Phase Equilibria, 250 (2006) 150-157.

Chapter 7

Solubility of Heavy Hydrocarbons in the Ionic Liquid [emim][FAP]

This chapter is adapted from the following publication: M. Althuluth, N. R. Rodriguez, C.J. Peters, M.C. Kroon. Submitted to J. Fluid Phase Equilib.

7.1 Introduction

Natural gas mostly consists of methane (CH_4), but it also includes significant quantities of other volatile hydrocarbons including ethane (C_2H_6), propane (C_3H_8), butane (C_4H_{10}), and pentane (C_5H_{12}), as well as traces of heavier aliphatic hydrocarbons (hexane (C_6H_{14}) and heptane (C_7H_{16})) and aromatic hydrocarbons (benzene, toluene, ethylbenzene and xylene, collectively called BTEX). Moreover, natural gas can contain acid components, such as carbon dioxide (CO_2) and hydrogen sulfide (H_2S) [1].

The volatile hydrocarbons and the heavier aliphatic hydrocarbons may stay in the natural gas stream, because they have heating value and can be liquefied. However, the acid compounds have to be removed from the natural gas stream, because they can be corrosive and have low heating value. This is normally done by amine absorption [2]. The aromatic hydrocarbons (BTEX) are also undesired in the natural gas stream, because they can cause plugging problems in downstream processing at sufficiently high concentrations. Reason is that they will be frozen before the other hydrocarbons liquefy in the (cryogenic) liquid extraction units. Moreover, they can cause catalyst coking in the sulfur recovery plant [3].

Currently, the removal of BTEX from natural gas streams by amine absorption is limited, because BTEX emissions that occur during the desorption process should be minimized. BTEX are listed by the environmental protection agency (EPA) as hazardous air pollutants. The EPA sets a standard of 25 tons per year for the total amount of aromatic compounds emitted in any plant [4]. Thus, the amount of BTEX components emitted from natural gas processing facilities has become an environmental concern.

It would be desirable to develop a new method whereby the acid compounds and the BTEX compounds can be successfully removed from the natural gas stream without any problems with emissions, while the volatile and heavier aliphatic hydrocarbons will stay in the natural gas stream. Ionic liquids (ILs) are a new class of potentially interesting absorbents that can overcome the limitations of current processing. Reason is that they show interesting solubility behavior and have a very low vapor pressure, so that they do not evaporate or lead to emissions into the atmosphere [5].

Previously we found that the IL 1-ethyl-3-methylimidazolium tris(pentafluoroethyl)trifluoro-phosphate ([emim][FAP]) shows a very high CO_2 solubility and a low affinity for small

hydrocarbons (CH_4, C_2H_6, C_3H_8, C_4H_{10}), resulting in good CO_2/hydrocarbon selectivities [6-8]. Further, this IL is low-viscous, so that absorption kinetics are fast enough. These factors make the IL [emim][FAP] an attractive solvent for natural gas separation processes. However, the absorption behavior of the heavier aliphatic hydrocarbons and BTEX in this IL has never been studied. This information is of utmost importance, because of the severe problems that BTEX can cause in the sulfur recovery unit, during liquefying, and as emissions. Thus, the investigation of the solubility of heavy hydrocarbons (aliphatic and BTEX) in the IL [emim]FAP] is crucial. In this work, these solubilities will be measured at temperatures between 293.15 and 333.15 K at atmospheric pressure. The large difference in measured solubility between the aliphatic and aromatic hydrocarbons will also be exploited for their separation using the IL as extracting agent. Ternary data for IL + aliphatic + aromatic systems will be measured and correlated with the NRTL model.

7.2 Experimental

7.2.1 Materials

All the chemicals that were used in this study are listed in Table 7.1 and they were used as such. The water content of the IL [emim][FAP] was measured prior to every experiment using Karl Fischer moisture analysis (795 KFT Titrino Metrohm Karl Fischer) and found to be less than 200 ppm in all cases.

Table 7.1: Chemicals used.

Name	Source	Purity
[emim][FAP]	Merck	≥ 99.0%
Benzene	Sigma Aldrich	99.8%
Toluene	Sigma Aldrich	99.8%
Ethylbenzene	Fluka	≥ 99.0%
o-xylene	Sigma Aldrich	≥ 99.0%
Hexane	Sigma Aldrich	≥ 99.0%
Heptane	Fluka	99.0%

7.2.2 Experimental set-up and procedure

The experiments were performed in jacketed liquid-liquid equilibrium (LLE) cells. The jackets were connected to a thermostat bath to maintain a constant temperature inside the equilibrium cells with an uncertainty in temperature of ± 0.1 K, (Figure 7.1).

Figure 7.1: Liquid-Liquid equilibrium cell.

Mixtures with a composition within the immiscibility region were prepared and placed in the equilibrium cells and kept at the desired temperature. In order to ensure thermodynamic equilibrium and to obtain complete phase separation, the mixtures were stirred for at least 3 h at 1000 rpm and left overnight to settle. For the binary mixtures, only samples from the IL-rich phase were taken after settling. For the ternary systems, both samples from the bottom (IL-rich phase) and top phase (hydrocarbon rich-phase) were taken. The samples were diluted with acetone in order to decrease the viscosity to ensure a constant injection volume in a gas chromatograph (GC) and in order to solubilize the sample to avoid phase splitting. The diluted samples were analysed using a Varian 430 GC (Figure 7.2).

Figure 7.2: Gas Chromatograph.

The GC method is described in Table 7.2. The samples were measured at least three times and the relative standard deviation was found to be less than 2%. Only the concentration of

the organics in the samples were measured. Since the solubility of ILs in the organic phase is generally very limited [9], the solubility of [emim][FAP] in the hydrocarbon-rich phase was not measured, but assumed to be zero. The IL composition in the other phase was calculated by a mass balance.

Table 7.2: GC column specifications and conditions employed for analysis of the liquid phases in the studied systems.

System Analyzed / GC conditions	**Binary**	**Ternary**
Detector Type	Flame ionization detector (FID)	Flame ionization detector (FID)
Detector Temperature	473 K	473 K
Injector Temperature	548 K	548 K
Carrier Gas	Helium	Helium
Flow Rate	2.0 mL/min	2.0 mL/min
Column Type	CP Sil 5 CB	CP A7 41
Column Dimensions	(30m×0.25mm×0.25μm)	(30m×0.25mm×1.2μm)

7.3 Results and discussion

7.3.1 Binary LLE experiments

The solubilities of the aliphatic compounds hexane and heptane and the aromatic compounds benzene, toluene, ethylbenzene and *o*-xylene in the IL [emim][FAP] were measured at 3 different temperatures (293.15, 313.15 and 333.15 K) and atmospheric pressure. The result of these binary LLE experiments are presented in Table 7.3.

Table 7.3: Equilibrium compositions in the binary mixtures of [emim][FAP] (1) + hydrocarbon compound (2)

[emim][FAP] (1) + Benzene (2)		**[emim][FAP] (1) + Toluene (2)**	
T/K	x_2	T/K	x_2
293.15	0.929	293.15	0.786
313.15	0.917	313.15	0.795
333.15	0.910	333.15	0.816
[emim][FAP] (1) + Ethylbenzene (2)		**[emim][FAP] (1) + *o*-xylene (2)**	
T/K	x_2	T/K	x_2
293.15	0.660	293.15	0.727
313.15	0.653	313.15	0.733
333.15	0.645	333.15	0.755
[emim][FAP] (1) + Hexane (2)		**[emim][FAP] (1) + Heptane (2)**	
T/K	x_2	T/K	x_2
293.15	0.056	293.15	0.030
313.15	0.078	313.15	0.039
333.15	0.078	333.15	0.043

Figure 7.3 graphically displays the LLE results of the binary mixtures of [emim][FAP] + hydrocarbon compound in *T-x* diagrams.

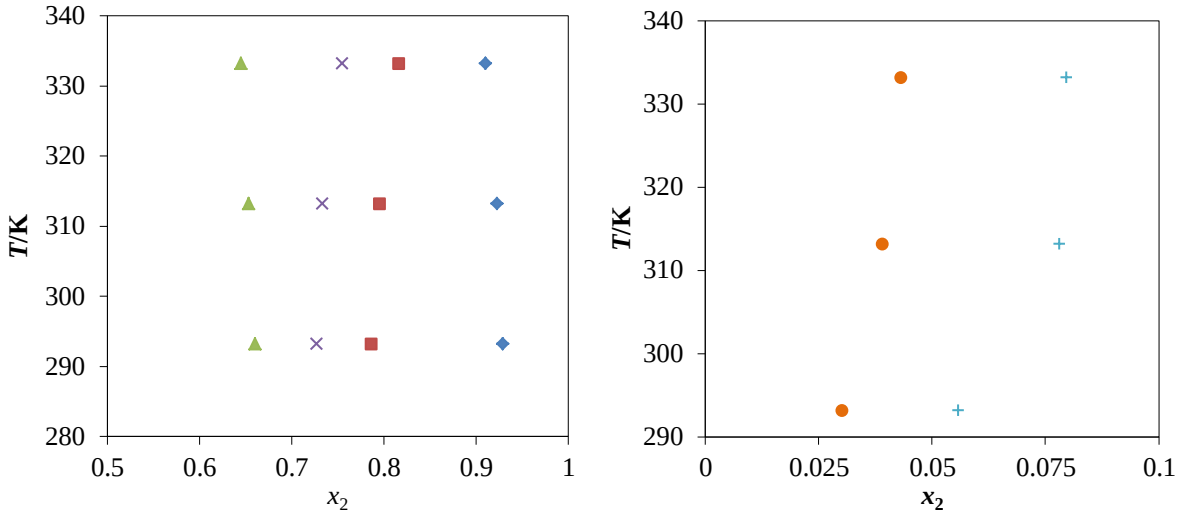

Figure 7.3: LLE diagrams for binary mixture of [emim][FAP] (1) + hydrocarbon compound (2): ◆, benzene; ■, toluene; ×, *o*-xylene; ▲, ethylbenzene; +, hexane; ●, heptane .

It can be noticed from Figure 7.3 that the solubility of the aromatic compounds in the IL [emim][FAP] is much higher than the solubility of the aliphatic compounds. This large difference in solubility can be related to the π-π interactions between the rings of the aromatic compound and the IL [10, 11], which do not take place between the aliphatic compound and the IL. Benzene shows the highest solubility in [emim][FAP]. The solubilities of toluene, *o*-xylene and ethylbenzene are lower than that of benzene, because the presence of methyl and ethyl groups on the benzene ring increases steric hindrance and reduces their packing efficiency in the IL phase. This trend is consistent with other binary IL + aromatic hydrocarbon systems [12]. Moreover, the solubility of the aliphatic compound hexane is slightly higher than that of heptane. This can be explained by the larger size of heptane, which makes it more difficult to fit into the free volume of the IL [10], even though the dispersive forces between the alkyl chain of the IL and longer chain hydrocarbon are expected to be larger [10]. Thus, solubilities in [emim][FAP] decrease in the following order: benzene > toluene > *o*-xylene > ethylbenzene >> hexane > heptane.

The influence of the temperature on the solubility of aromatics and aliphatic hydrocarbons in the IL [emim][FAP] was limited. The same behavior was observed for the solubility of aromatics in other ILs [12, 13]. All the systems examined here will most likely show upper critical solution temperature (UCST) behavior [14-16].

The solubilities of BTEX compounds in the IL [emim][FAP] were compared to the BTEX solubilities in the IL 1-ethyl-3-methylimidazolium hexafluorphoshate ([emim][PF_6]), which shares the same cation. It was found that solubility of BTEX compounds in [emim][FAP] is higher compared to their solubilities in [emim][PF_6] at the same range of temperatures [17], most likely because of the larger free volume of [emim][FAP]. Furthermore, the solubility of BTEX compounds in [emim][FAP] is much higher compared to their solubilities in aqueous amines solutions [3]. This is desirable, because the BTEX compounds will be removed from the natural gas together with the acid gases, so that plugging problems in the natural gas liquefying units that can be caused by BTEX will be minimized. However, full recovery of the BTEX compounds from the acid gas stream (without any emissions) is required in order to protect the catalyst bed in the sulfur recovery unit from coking that could be caused by BTEX components.

7.3.2 Ternary LLE experiments

The large difference in measured solubility between the aliphatic and aromatic hydrocarbons could also be exploited for their separation using the IL [emim][FAP] as extracting agent. Therefore, ternary LLE experiments of the systems (hexane + benzene + [emim][FAP]) and (heptane + toluene + [emim][FAP]) have been performed. The measured compositions at equilibrium in both liquid phases (hydrocarbon rich-phase and IL rich-phase) are reported in Table 7.4. It can be noted that the mole fraction of IL ($x_3 = 1 - x_1 - x_2$) in the hydrocarbon-rich phase is zero. The measured ternary diagrams are also plotted in Figure 7.4.

Table 7.4**:** Experimental LLE data (in mole fraction) for the systems aliphatic hydrocarbon (1) + aromatic hydrocarbon (2) + [emim][FAP] (3) at T = 293.15 K and p = 0.1MPa. Distribution coefficient (β) and selectivity (S) values are also included.

Hydrocarbon rich-phase		**Ionic liquid rich-phase**		β	S
x^{I}_1	x^{I}_2	x^{II}_1	x^{II}_2		
Heptane (1) + Toluene (2) + [emim][FAP] (3)					
0.902	0.098	0.050	0.130	1.33	23.72
0.834	0.166	0.049	0.204	1.23	21.09
0.693	0.307	0.049	0.347	1.13	16.06
0.558	0.442	0.049	0.446	1.01	11.49
0.418	0.583	0.047	0.521	0.89	7.94
0.325	0.675	0.046	0.573	0.85	6.00
0.247	0.753	0.043	0.612	0.81	4.68
0.165	0.835	0.037	0.651	0.78	3.51
Hexane (1)+ Benzene (2) + [emim][FAP] (3)					
0.900	0.100	0.101	0.206	2.06	18.37
0.839	0.161	0.106	0.285	1.77	14.04
0.701	0.299	0.105	0.440	1.47	9.82
0.579	0.421	0.101	0.522	1.24	7.12
0.446	0.554	0.097	0.585	1.06	4.84
0.349	0.651	0.095	0.624	0.96	3.53
0.264	0.736	0.078	0.650	0.88	2.97

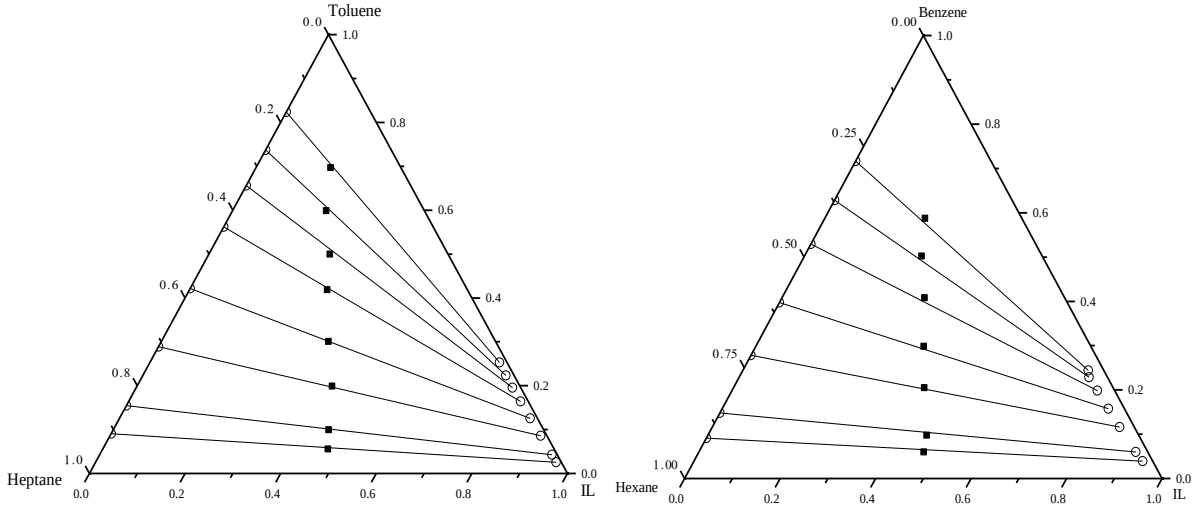

Figure 7.4: Ternary phase diagrams for the systems: heptane + toluene + [emim][FAP] and hexane + benzene + [emim][FAP] at T = 298 K and p = 0.1 MPa. Solid squares represent initial compositions, open symbols represent final composition of the phases, and lines represent the tie lines.

Figure 7.4 clearly shows the large difference in solubility between the aliphatic and aromatic compounds in the IL [emim][FAP]. The distribution coefficients (β) for the aromatic

compounds in both phases can be obtained from the ternary diagrams as the ratio of the mole fractions in IL phase and the hydrocarbon phase. For example, in the ternary system consisting of heptane + toluene + [emim][FAP], the toluene distribution coefficient can be defined as:

$$\beta_{Tol} = \frac{x_2^{II}}{x_2^{I}} \qquad \text{Eq.1}$$

where x_2^{I} is the mole fraction of toluene in the hydrocarbons-rich phase and x_2^{II} is the mole fraction of toluene in the IL-rich phase. The same equation can be applied for the benzene distribution in the system consisting of hexane + benzene + [emim][FAP].

The distribution coefficients obtained for toluene and benzene at different compositions are tabulated in Table 7.4, and graphically shown in Figure 7.5. It can be observed that the aromatics distribution coefficients (β_{Tol} and β_{Benz}) decrease with increasing concentration of the aromatic compound in the hydrocarbon-rich phase. It has been reported that the aromatic solutes and the ILs cations organize in a sandwich structure, where the aromatic solute and IL cation interact through π-π interactions. With increasing aromatics concentration the distance between aromatics solutes and IL cations increases, reducing the strength of their interaction and thus the distribution coefficient is decreased [18]. This behaviour is similar to that of other ternary IL + aliphatic + aromatic mixtures [19, 20]. The absolute value of the distribution coefficients of the aromatics in [emim][FAP] (β_{Tol} = 1.33 at x^{I}_2 < 0.1) is slightly higher than the corresponding value in other ILs, such as 2-methyl-N-ethylpyridinium bistrifluoromethylsulfonyl-imide ([2empy][Tf_2N]) (β_{Tol} = 0.85 at x^{I}_2 < 0.1) [19], probably because of the higher aromatics solubility in [emim][FAP] compared to [2empy][Tf_2N] due to the larger free volume. Therefore, the solvent-to-feed ratio needed is slightly lower.

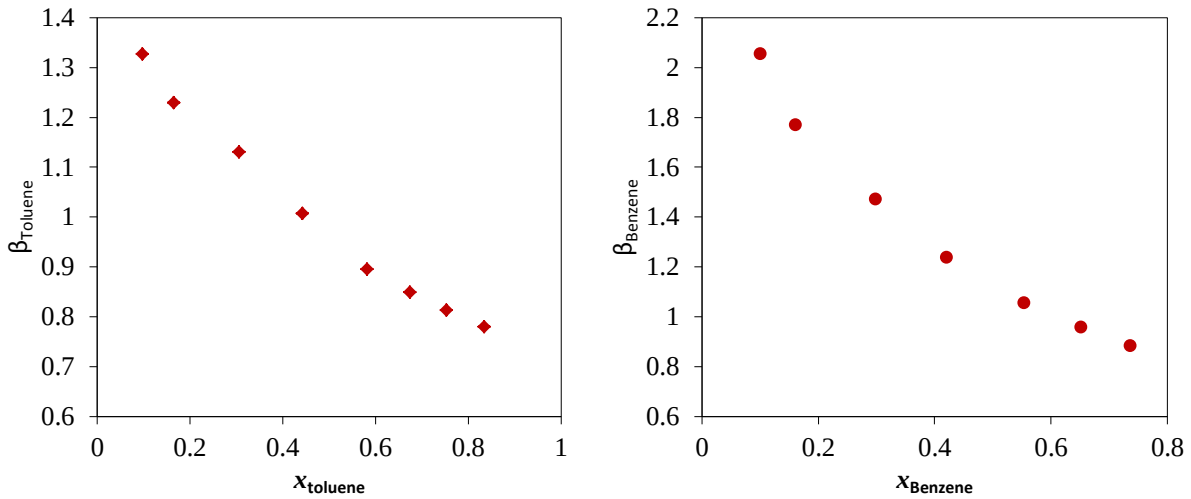

Figure 7.5**:** Experimental distribution coefficient as function of the concentration of aromatic in the hydrocarbon rich-phase for the systems: ◆, heptane + toluene + [emim][FAP]; ●, hexane + benzene + [emim][FAP] and at T= 298 K and p = 0.1 MPa.

The selectivity is defined as the ratio of the distribution coefficients of aromatic and aliphatic in both phases. For example, in the ternary system consisting of heptane + toluene + [emim][FAP], the selectivity is presented as follows:

$$S = \frac{x_2^{II} / x_2^{I}}{x_1^{II} / x_1^{I}} \qquad \text{Eq.2}$$

where x_1^{I} and x_2^{I} are the mole fractions of heptane and toluene, respectively, in the hydrocarbon-rich phase, and x_1^{II} and x_2^{II} are the mole fractions of heptane and toluene, respectively, in the IL-rich phase. The selectivities of toluene/heptane and benzene/hexane can be found in Table 7.4. They are also graphically depicted in Figure 7.6.

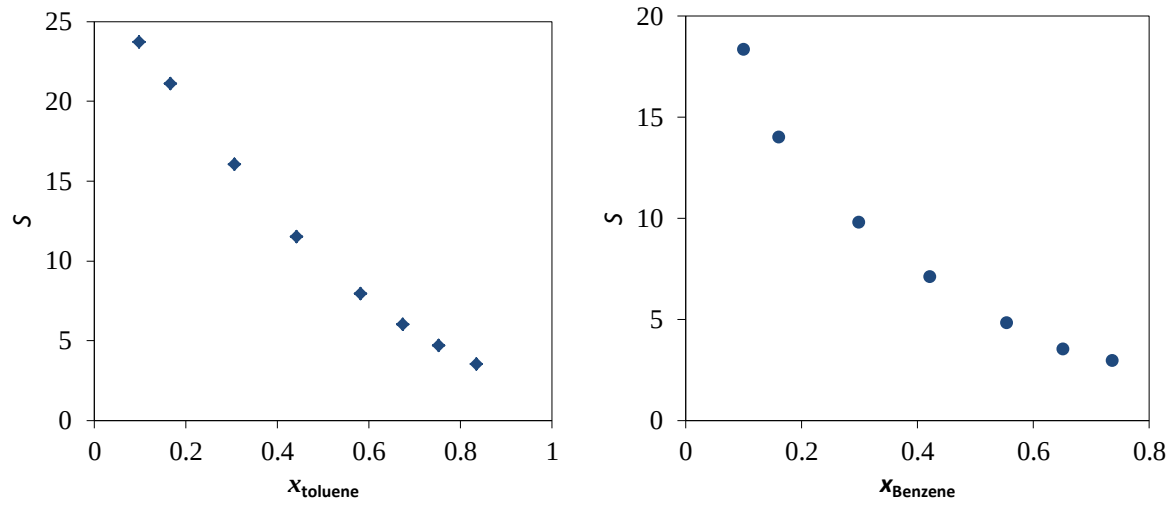

Figure 7.6: Experimental selectivity as function of the concentration of aromatic in the hydrocarbon rich-phase for the systems: ◆, heptane + toluene + [emim][FAP]; ●, hexane + benzene + [emim][FAP] at T= 298 K. and p = 0.1 MPa.

It can be seen from Figure 7.6 that the selectivities decrease as the content of aromatics increases in the hydrocarbon-rich phase. The values of the experimental selectivity were found to be comparable with other ILs [19, 20]. The high selectivity values at low aromatic concentration indicate that the IL [emim][FAP] has a much higher affinity to absorb aromatics than aliphatic hydrocarbons. Further, at high aromatics content in the hydrocarbon rich-phase, the selectivity is reduced but still higher than than 1. Thus, even if the natural gas contains significant quantities of aromatics, this IL will be able to remove the aromatics selectively from natural gas to a level that could prevent plugging in the natural gas liquefaction (NGL) units [2].

7.3.3 Modelling ternary systems

The experimental ternary LLE data have been correlated using the non-random two liquid (NRTL) model. Using the NRTL model, the activity coefficients can be calculated via:

$$\ln \gamma_i = \left(\frac{\sum_{j=1}^{n} \tau_{ji} x_j G_{ij}}{\sum_{k=1}^{n} x_k G_{ki}} \right) + \sum_{j=1}^{n} \left(\frac{x_j G_{ij}}{\sum_{k=1}^{n} x_k G_{kj}} \right) \left(\tau_{ij} - \frac{\sum_{m=1}^{n} \tau_{mi} x_m G_{mi}}{\sum_{k=1}^{n} x_k G_{kj}} \right) \qquad \text{Eq.3}$$

where:

$$G_{ij} = \exp\left(-\alpha_{ij} \tau_{ij}\right) \qquad \text{Eq.4}$$

$$\tau_{ij} = \frac{g_{ij} - g_{jj}}{RT} = \frac{\Delta g_{ij}}{RT} \qquad \text{Eq.5}$$

$$\tau_{ji} = \frac{g_{ji} - g_{ii}}{RT} = \frac{\Delta g_{ji}}{RT} \qquad \text{Eq.6}$$

and

$$\alpha_{ij} = \alpha_{ji} \qquad \text{Eq.7}$$

The NRTL parameters τ_{ij} and G_{ij} can thus be calculated via the model parameters of the NRTL equation ($\alpha_{ij}, g_{ij}, g_{jj}, g_{ji}$), where g_{ij} is an energy parameter that characterizes the interaction of species *i* and *j*, *R* is the gas constant, *T* the absolute temperature, *x* the mole fraction and α_{ij} is a parameter related to the non-randomness in the mixture. The NRTL model was fitted to experimental data by minimizing the following objective function (OF):

$$OF = \sum_{i=1}^{m}\sum_{j=1}^{n}\left(\frac{\left(\frac{1}{\beta_{ij}}\right)^{cal} - \left(\frac{1}{\beta_{ij}}\right)^{exp}}{\left(\frac{1}{\beta_{ij}}\right)^{exp}}\right)^2 \qquad \text{Eq.8}$$

where *m* is the number of experiments, *n* is the number of components in the mixture, and $(1/\beta)^{\exp}$ and $(1/\beta)^{cal}$ are the experimental and calculated solute distribution ratio, respectively.

In order to evaluate the quality of the correlation, two different deviations are presented: the root-mean-square deviation of the composition (σx) and the mean error of the solute distribution ratio ($\Delta\beta$). They were calculated as follows:

$$\sigma x = 100\sqrt{\left(\frac{\sum_i^m \sum_j^{n-1}\left(x_{ij}^{I,exp} - x_{ij}^{I,calc}\right)^2 + \left(x_{ij}^{II,exp} - x_{ij}^{II,calc}\right)^2}{2mn}\right)} \qquad \text{Eq.9}$$

$$\Delta\beta = 100\sqrt{\left(\frac{1}{m}\sum_{k=1}^{m}\left(\frac{\beta_k^{\exp} - \beta_k^{calc}}{\beta_k^{\exp}}\right)^2\right)} \qquad \text{Eq.10}$$

The regressed parameters and deviations are presented in Table 7.5. All calculations were performed with HyproTech DISTIL v5.

Table 7.5: NRTL parameters and deviations for LLE data of the ternary systems.

ij	Δg_{ij} (kJ.mol^{-1})	Δg_{ji} (kJ.mol^{-1})	α_{ij}	σx (%)	$\Delta\beta$ (%)
Hexane (1) + benzene (2) + [emim][FAP] (3)					
1-2	3.778	-1.651	0.2	0.527	0.051
1-3	23.702	3.074			
2-3	65.574	0.471			
Heptane (1) + toluene (2) + [emim][FAP] (3)					
1-2	-4.340	10.686	0.15	0.317	0.132
1-3	168.277	8.056			
2-3	6.397	5.022			

Figure 7.7 presents the experimental data together with the calculated data for both systems. It can be noticed that the LLE experimental data could be correlated well using the NRTL thermodynamic model.

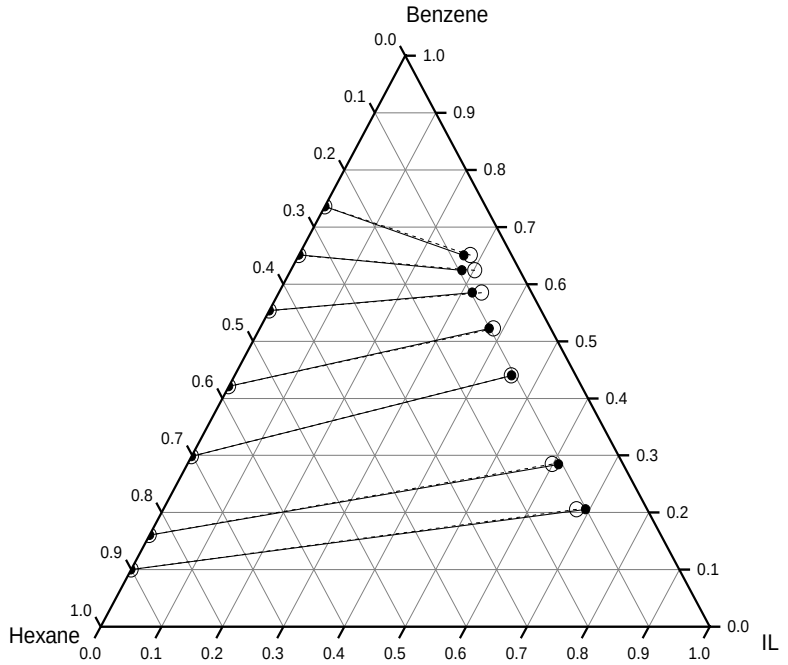

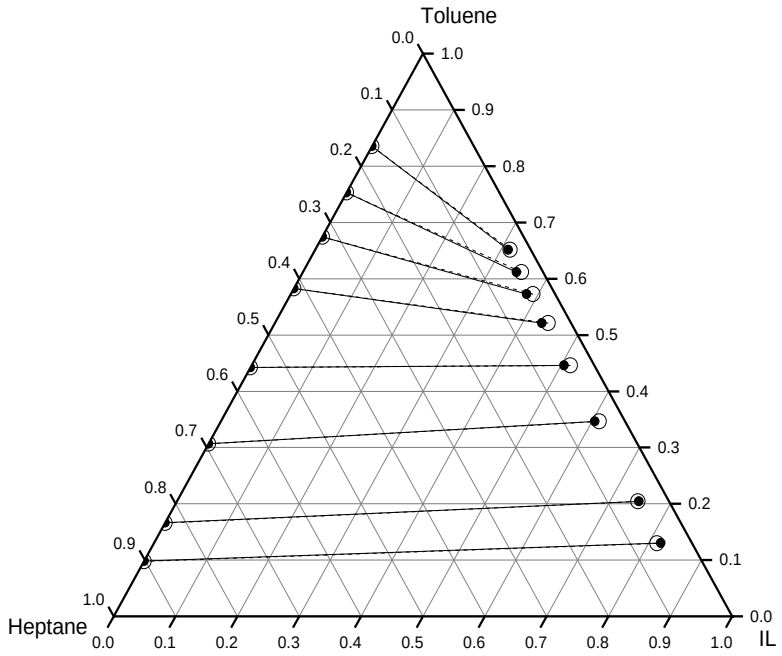

Figure 7.7: Ternary LLE data for the systems heptane (1) + toluene (2) + [emim][FAP] (3) (above) and hexane (1) + benzene (2) + [emim][FAP] (3) (below) at 293.15 K and p =0.1 MPa. Filled points and solid lines represent experimental tie-lines; open symbols and dashed lines represent calculated results using the NRTL.

7.4 Conclusions

The solubilities of the aromatic hydrocarbons benzene, toluene, ethylbenzene and *o*-xylene in the IL [emim][FAP] are much higher than the aliphatic hydrocarbons hexane and heptane. The temperature does not have a significant influence on these solubilities. Thus, when [emim][FAP] is used as gas sweetening solvent, the aromatics will be absorbed in the IL (together with CO_2), while the aliphatics will stay in the natural gas stream. The large difference in solubility between the aromatic and aliphatic compounds in [emim][FAP] can be exploited for their separation. Ternary liquid-liquid equilibrium data for the systems hexane + benzene + [emim][FAP] and heptane + toluene + [emim][FAP] have been measured. Both the distribution coefficients and selectivities decrease with increasing aromatics concentration. However, the selectivity always remains much higher than 1. Thus, even if the natural gas contains significant quantities of aromatics, this IL will be able to remove the aromatics selectively from natural gas to a level that could prevent plugging in the natural gas liquefaction (NGL) units.

7.5 References

[1] S. Mokhatab, W.A. Poe, Chapter 1 - Natural Gas Fundamentals, in: S. Mokhatab, W.A. Poe (Eds.) Handbook of Natural Gas Transmission and Processing (Second Edition), Gulf Professional Publishing, Boston, (2012) 1-42.

[2] A.J. Kidnay, W.R. Parrish, D.G. McCartney, Fundamentals of Natural Gas Processing, Second ed., CRC PressINC, (2011).

[3] A. Valtz, M. Hegarty, D. Richon, Experimental determination of the solubility of aromatic compounds in aqueous solutions of various amines, Fluid Phase Equilibria, 210 (2003) 257-276.

[4] J. Collie, M. Hlavinka, A. Ashworth, An Analysis of BTEX emissions from Amine Sweetening and Glycol Dehydration Facilities, in: Laurance Reid Gas Conditioning Conference Proceedings, Oklahoma, (1998).

[5] E.D. Bates, R.D. Mayton, I. Ntai, J.H. Davis, CO_2 Capture by a Task-Specific Ionic Liquid, Journal of the American Chemical Society, 124 (2002) 926-927.

[6] M. Althuluth, M.C. Kroon, C.J. Peters, Solubility of Methane in the Ionic Liquid 1-Ethyl-3-methylimidazolium Tris(pentafluoroethyl)trifluorophosphate, Industrial & Engineering Chemistry Research, 51 (2012) 16709-16712.

[7] M. Althuluth, M.T. Mota-Martinez, M.C. Kroon, C.J. Peters, Solubility of Carbon Dioxide in the Ionic Liquid 1-Ethyl-3-methylimidazolium Tris(pentafluoroethyl) trifluoro phosphate, Journal of Chemical & Engineering Data, 57 (2012) 3422-3425.

[8] M. Althuluth, M.T. Mota-Martinez, A. Berrouk, M.C. Kroon, C.J. Peters, Removal of small hydrocarbons (ethane, propane, butane) from natural gas streams using the ionic liquid 1-ethyl-3 -methylimidazolium tris(pentafluoroethyl)trifluorophosphate, The Journal of Supercritical Fluids, 90 (2014) 65-72.

[9] M.B. Shiflett, A. Yokozeki, Liquid−Liquid Equilibria in Binary Mixtures Containing Fluorinated Benzenes and Ionic Liquid 1-Ethyl-3-methylimidazolium Bis(trifluoromethyl sulfonyl)imide, Journal of Chemical & Engineering Data, 53 (2008) 2683-2691.

[10] A.R. Ferreira, M.G. Freire, J.C. Ribeiro, F.M. Lopes, J.o.G. Crespo, J.o.A.P. Coutinho, An Overview of the Liquid−Liquid Equilibria of (Ionic Liquid + Hydrocarbon) Binary Systems and Their Modeling by the Conductor-like Screening Model for Real Solvents, Industrial & Engineering Chemistry Research, 50 (2011) 5279-5294.

[11] U. Domanska, A. Pobudkowska, F. Eckert, Liquid-liquid equilibria in the binary systems (1,3-dimethylimidazolium, or 1-butyl-3-methylimidazolium methylsulfate + hydrocarbons), Green Chemistry, 8 (2006) 268-276.

[12] E.J. González, P.F. Requejo, Á. Domínguez, E.A. Macedo, Phase equilibria of binary mixtures (ionic liquid + aromatic hydrocarbon): Effect of the structure of the components on the solubility, Fluid Phase Equilibria, 360 (2013) 416-422.

[13] J.P. Gutierrez, W. Meindersma, A.B. de Haan, Binary and ternary (liquid-liquid) equilibrium for {methylcyclohexane (1) + toluene (2) + 1-hexyl-3-methylimidazolium tetra cyanoborate (3)/1-butyl-3-methylimidazolium tetracyanoborate (3)}, The Journal of Chemical Thermodynamics, 43 (2011) 1672-1677.

[14] U. Domańska, Thermophysical properties and thermodynamic phase behavior of ionic liquids, Thermochimica Acta, 448 (2006) 19-30.

[15] U. Domańska, A. Marciniak, Phase behaviour of 1-hexyloxymethyl-3-methyl-imidazolium and 1,3-dihexyloxymethyl-imidazolium based ionic liquids with alcohols, water, ketones and hydrocarbons: The effect of cation and anion on solubility, Fluid Phase Equilibria, 260 (2007) 9-18.

[16] U. Domańska, A. Marciniak, Liquid phase behaviour of 1-hexyloxymethyl-3-methyl-imidazolium-based ionic liquids with hydrocarbons: The influence of anion, The Journal of Chemical Thermodynamics, 37 (2005) 577-585.

[17] U. Domańska, A. Marciniak, Solubility of 1-Alkyl-3-methylimidazolium Hexafluoro phosphate in Hydrocarbons, Journal of Chemical & Engineering Data, 48 (2003) 451-456.

[18] A.R. Hansmeier, M. Jongmans, G. Wytze Meindersma, A.B. de Haan, LLE data for the ionic liquid 3-methyl-N-butyl pyridinium dicyanamide with several aromatic and aliphatic hydrocarbons, The Journal of Chemical Thermodynamics, 42 (2010) 484-490.

[19] J.n. García, S. García, J.S. Torrecilla, F. Rodríguez, Solvent Extraction of Toluene from Heptane with the Ionic Liquids N-Ethylpyridinium Bis(trifluoromethylsulfonyl)imide and z-Methyl-N-ethylpyridinium Bis(trifluoromethylsulfonyl)imide (z = 2, 3, or 4) at T = 313.2 K, Journal of Chemical & Engineering Data, 55 (2010) 4937-4942.

[20] A. Arce, M.J. Earle, H. Rodríguez, K.R. Seddon, Separation of Benzene and Hexane by Solvent Extraction with 1-Alkyl-3-methylimidazolium Bis{(trifluoromethyl)sulfonyl}amide Ionic Liquids: Effect of the Alkyl-Substituent Length, The Journal of Physical Chemistry B, 111 (2007) 4732-4736.

Chapter 8

Natural Gas Purification Using Supported Ionic Liquid Membrane

This chapter is adapted from the following publication: M. Althuluth, J.P. Overbeek, H.J. Wees, L.F. Zubeir, W.G. Haije, A. Berrouk, C.J. Peters, M.C. Kroon, J. of Membr. Sci., (2014). Under review.

8.1 Introduction

Knowledge on the solubilities and diffusivities of gases in ionic liquids (ILs) is important for the design of absorption processes, such as the gas sweetening process. The solubilities of carbon dioxide (CO_2), methane (CH_4), ethane (C_2H_6) and propane (C_3H_8) in several ILs have been studied intensively [1-5]. From these solubility studies, it can be concluded that ILs are promising absorbents for the removal of CO_2 from natural gas streams [6-8]. Especially interesting for CO_2 capture is the IL 1-ethyl-3-methylimidazolium tris(pentafluoroethyl) trifluorophosphate ([emim][FAP]), because of its high solubility for CO_2 compared to the much lower solubilities of CH_4, C_2H_6 and C_3H_8.

On the contrary, the transport of gases in ILs has been much less investigated. Only limited experimental data are available in literature [9-12]. It was found that diffusion coefficients of CO_2 in most ILs near ambient temperature are in the order of 1×10^{-6} cm^2/s, which is slower than CO_2 diffusion in traditional solvents [13]. Diffusion coefficients of small hydrocarbons in ILs were even lower [11].

Recently, new ILs were discovered that can absorb CO_2 much quicker [14-16]. For example, it took only 4 min for polymerized-ILs to reach their 90% absorption capacities and about 30 min to reach their full capacities [14]. Moreover, CO_2 absorption in protic ILs could be almost completed within 5 min [15]. In mixed IL + aqueous amine solutions 90% of the absorption capacity was reached within 15 min, and the chemisorption was completed after 25 min [16]. However, it takes about 3 h to reach equilibrium for most other ILs absorbing CO_2 physically [17].

The properties of ILs, specifically the viscosity, have an effect on the gas absorption rate. Morgan et al. [18] reported that the diffusivity of gases relates inversely to the viscosity of ILs. Thus, ILs with a high viscosity lead to low absorption and desorption rates in comparison to conventional chemical absorbents (e.g., aqueous amine solutions) and physical absorbents (e.g., Selexol). Moreover, ILs generally are more expensive than conventional solvents. Therefore, it can be difficult to apply ILs in conventional absorption columns.

For this reason, researchers have given much attention to create new cost-effective technologies using small amount of low-viscous ILs. One technology that has attracted interest is the use of supported ionic liquid membranes (SILMs) for gas sweetening. SILMs are produced by impregnating a porous membrane with a small amount of IL. This process may be economically competitive with the chemical or physical CO_2 absorption process. The main challenge for liquid membranes is that the liquid phase can evaporate over time [19]. The very low volatility of the IL is beneficial for its incorporation in a SILM, but probably not enough to completely get rid of the evaporation problem [17].

In this work, the permeabilities of pure CO_2, CH_4, C_2H_6 and C_3H_8 through a SILM consisting γ-alumina impregnated with the IL [emim][FAP] will be measured. These measurements will be used to calculate the permselectivity and diffusivity. Also, diffusivities will be measured and correlated using a suitable model [18]. Furthermore, mixed gas permeability and permselectivity for the binary mixture of CO_2/CH_4 (50/50%, v/v) will be measured and compared to the calculated ideal permselectivity. Finally, the influence of the presence of water on the permselectivity will be investigated.

8.2 Experimental

8.2.1 Preparation of SILM

The IL [emim][FAP] was provided by Merck Chemical Company with a purity of ≥ 99.0% and was used as such. The [emim][FAP] was impregnated in the top two γ-alumina layers of a tubular porous asymmetric membrane support. The support consists of a coarse α-alumina commercial support on which two less coarse α-alumina layers and two γ-alumina layers are applied by ECN (Energy research Center of the Netherlands) using the dip coating technique. The γ-alumina layers have an average pore size of ~4 nm and maximum pore size of ~14 nm. The thickness of both impregnated γ-alumina layers together is ~2.64 μm (Figure 8.1).

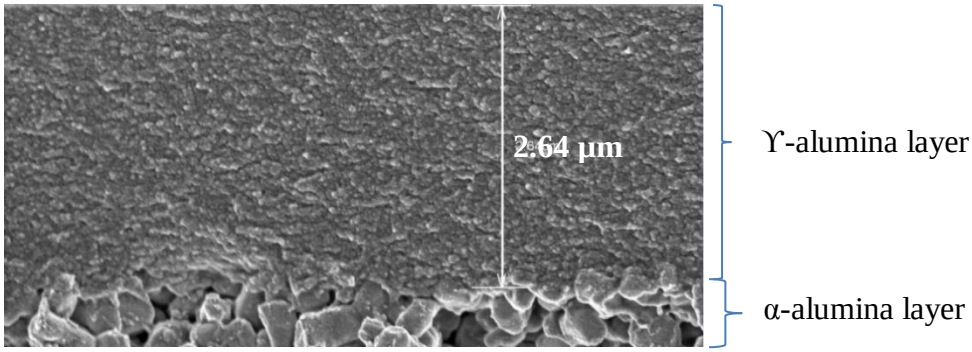

Figure 8.1: Asymmetric membrane with the γ-alumina layer at the top with an average pore size of ~4 nm.

The impregnation of the IL was done using a sponge filled with IL. The sponge was placed inside a coating vessel. This coating vessel moves with a speed of 15 mm/s along the membrane to impregnate it with the IL. The picture of the impregnation set-up is shown in Figure 8.2.

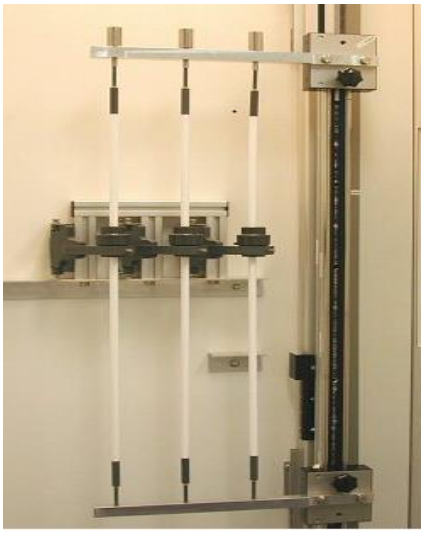

Figure 8.2: Experimental set-up used to impregnate the membrane with the IL [emim][FAP]

The impregnated SILM was analyzed using Scanning Electron Microscopy (SEM), type Hitachi 3700. Figure 8.3 shows the presence of fluorine atoms, originating from the IL [emim][FAP], as light blue spots in the SILM. From Figure 8.3 it can be concluded that the γ-alumina layers are fully impregnated with the IL and that some traces of the IL are also present in the top part of the intermediate less course α-alumina layers of the support.

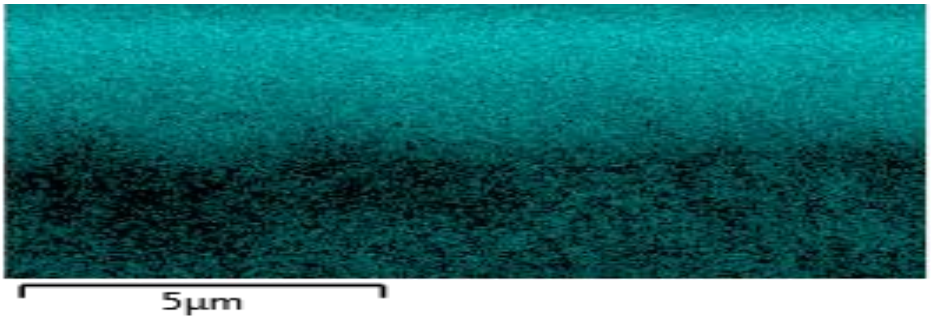

Figure 8.3: SEM picture showing the fluorine atoms (from [emim][FAP]) as light blue spots in the γ-alumina layer and the top of the support layer of the SILM.

8.2.2 Gas permeation set-up

Single gas permeabilities of He (quality test), CO_2, CH_4, C_2H_6 and C_3H_8 through the SILM have been determined using a gas permeation set-up, which is shown in Figure 8.4.

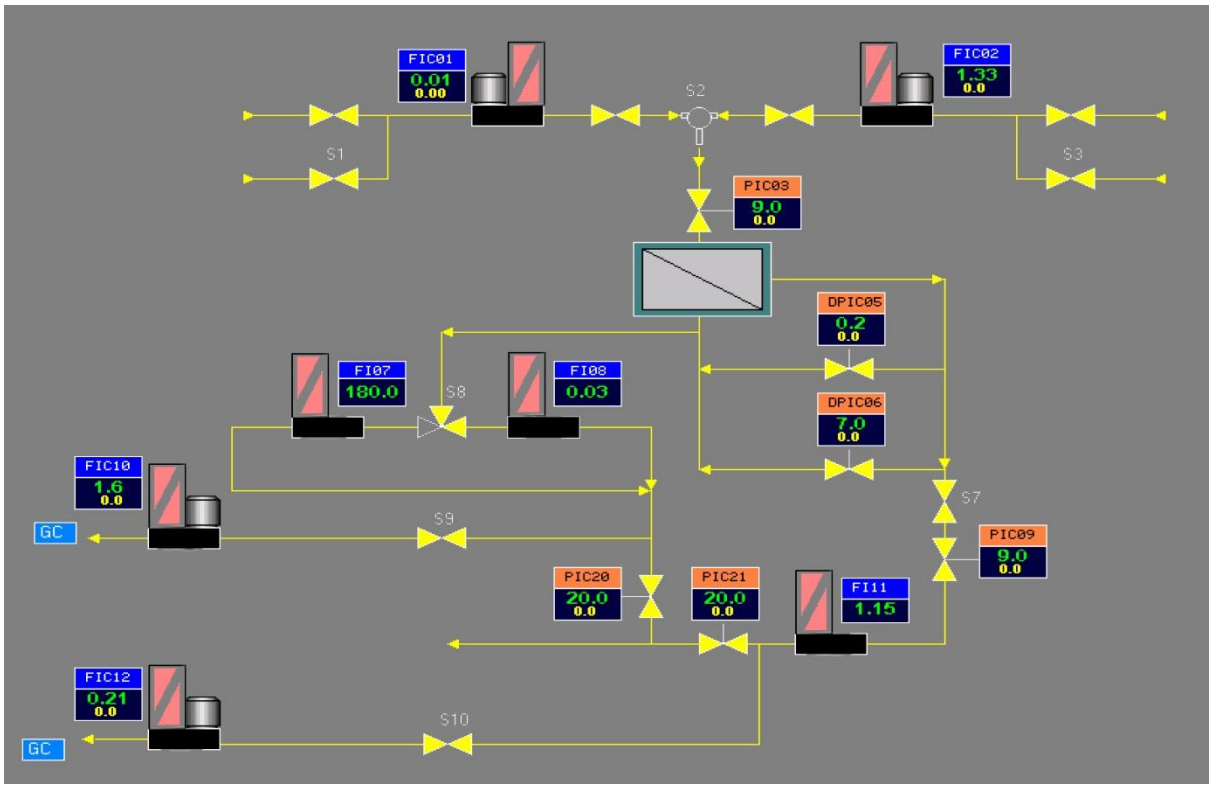

Figure 8.4: Schematic illustration of the gas permeation set-up: Pressure Indicators (PI); Pressure Indicator Controller (PIC); Flow Indicator (FI); Flow Indicator Controller (FIC); Differential Pressure Indicating Controller (DPIC).

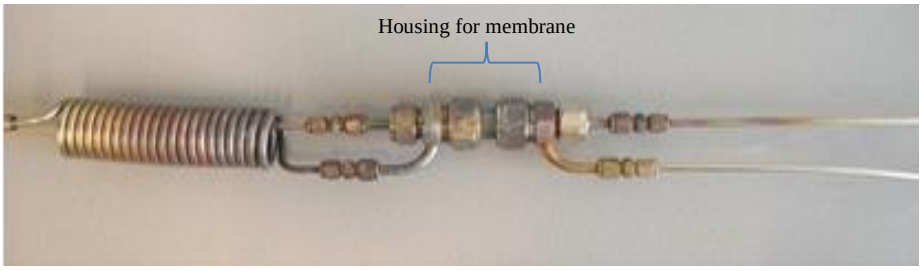

Figure 8.5: Module with 10 cm housing for tubular membranes.

The membrane was placed inside a module in which tubular membranes of 10 cm length can be housed using graphite sealings (Figure 8.5). This module was fixed horizontally inside an oven to control the experimental temperature value at 313 K; the trans-membrane pressure was set at 0.7 MPa. The stability of the membrane under these conditions was first established. The maximum capillary pressure p of a SILM can be calculated using the Young–Laplace Eq.(1):

$$\Delta p = \frac{4\sigma cos\theta}{d} \qquad \text{Eq.1}$$

where σ is the surface tension of the IL (34.6 mN/m at T=313 K), θ is the contact angle (θ = 0, because complete wetting is assumed), and d is the pore diameter of γ-alumina layer (4 nm). Then, the maximum pressure that can be used in the SILM is 34 MPa. Even though the real maximum pressure could be lower than the calculated pressure (because the pore size distribution of γ-alumina layer is non-uniform), it is still much higher than the transmembrane pressure used in this study (0.7 MPa). Therefore, the IL will not be pushed out of the pores. The stability of SILM was confirmed by constant gas permeance over time.

Prior to any permeation experiment, the graphite ring for sealing the membrane in the module and the membrane itself were checked for gas leaks by placing a fresh SILM with graphite seal in the system and pressurizing it to 0.3 MPa using a He gas flow. The permeate flow through the SILM was monitored. A constant low permeate flow value (5-15 mL/min) was an indication that the system was completely sealed (no leaks). Then, the measurements were conducted automatically by providing set pressures and temperatures. Flow indicator controllers (FIC01) and (FIC02) were used to measure and control the feed flow. Flow indicators (FI07) and (FI08) were used to measure the permeate flow. The retentate flow was

measured by flow indicator (FI011). Pressure indicator controller (PIC09) was used to set a feed/retentate pressure to the system. The pressure difference between the feed and permeate was controlled by differential pressure indicating controllers (DPIC05) or (DPIC06), depending on the pressure difference required. The results (flows, pressures and time) were stored in a database.

The permeance P ($mol \cdot m^{-2} \cdot s^{-1} \cdot Pa^{-1}$) of the gas permeating through the membrane can be defined as:

$$P = \frac{J}{\Delta p\, A} \qquad \text{Eq.2}$$

where J is the gas flow through the membrane ($mol \cdot s^{-1}$), Δp is the trans-membrane pressure (pressure difference between feed and permeate stream (Pa)), and A is the exposed area of the membrane (m^2).

The same set-up can be used for the measurement of mixed gas permeabilities, but in this case it needs to be connected with gas chromatograph (GC) to analyze the permeate and/or retentate composition (Figure 8.4). The mixed-gas permeance was calculated using the following equation:

$$P_i = \frac{J_i}{(p_{i,f} - p_{i,p})\, A} \qquad \text{Eq.3}$$

where J_i is the gas flow of component i through the membrane ($mol \cdot s^{-1}$), and $p_{i,p}$ and $p_{i,f}$ are the partial pressures of component i in the permeate and feed stream (Pa), respectively.

8.2.3 Permporometry set-up

The influence of humidity on the gas permeability through the SILM was investigated using the permporometry equipment. A schematic of this set-up can be found in Figure 8.6.

The permporometry set-up allows measurement of the influence of water on the permeance of helium (He) through the membrane. First, the dry membrane was fed with dry He gas to

obtain the initial gas permeance, while the feed/retentate pressure was adjusted to 0.2 MPa using a back pressure controller (PIC02). The permeate pressure was kept at atmospheric pressure. The pressure difference was continuously recorded by pressure transducers (PDI04) or (PDI05). The system was allowed to equilibrate until a steady-state flow of He was reached.

Subsequently, a small amount of water (H_2O) was added to the feed. The He was mixed with the H_2O in the controlled evaporator mixer (CEM). The CEM temperature was set at 363 K. The tubes going from and to the membrane module were kept at 343 K to prevent condensation of the H_2O. Thereafter, the He + H_2O mixture was fed through the membrane. The permeate and retentate streams containing He and H_2O vapor were directed to the cold traps (S-5) and (S-4) to remove H_2O vapor from the stream prior to measuring the flow rate of He. The flow of He through the SILM was continuously monitored by the flow indicators (FI04), (FI05) or (FI06). Once a steady-state flow of He was reached, a measurement point was taken. The experiment was continued by switching between humid to dry feed gas (and vice versa) over time.

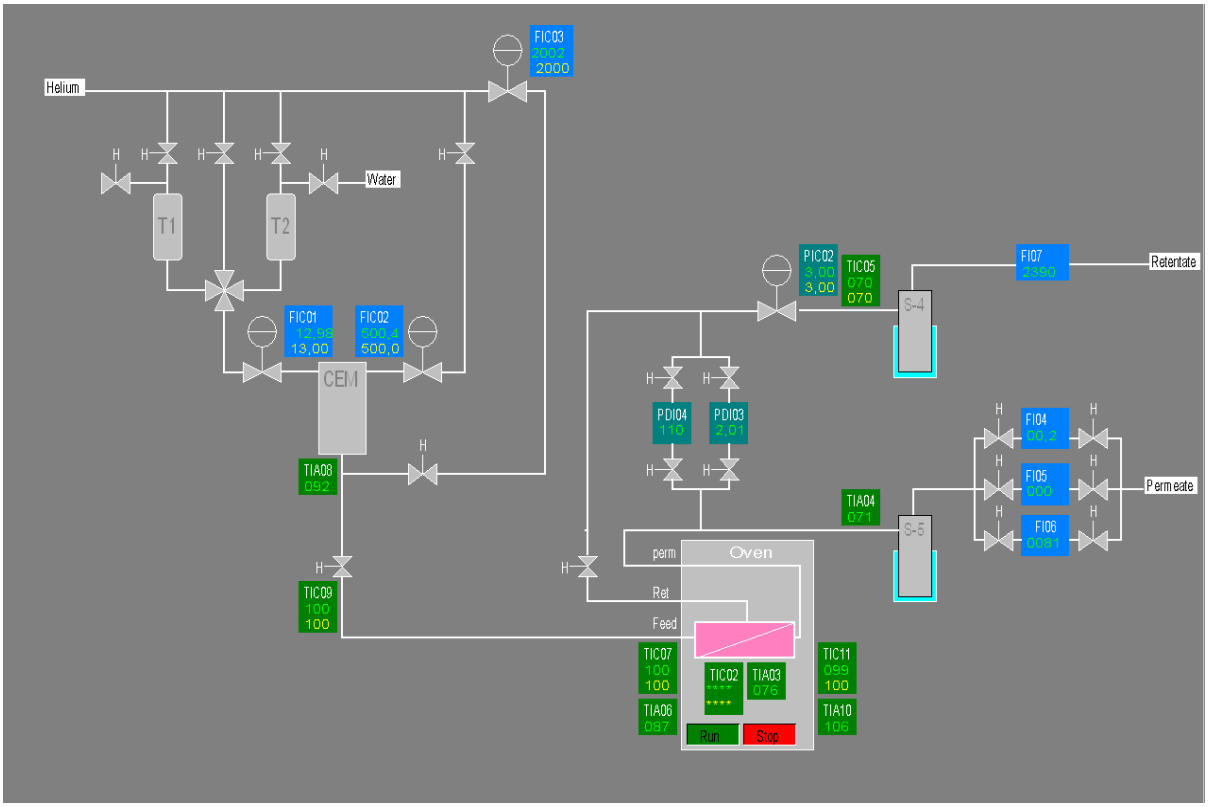

Figure 8.6: Schematic illustration of the permporometry set-up: Flow Indicators (FI); Flow Indicator Controller (FIC); Pressure Indicator (PI); Pressure Indicator Controller (PIC); Temperature Indicator (TI); Temperature Indicator Controller (TIC); Cold Traps (S-4, S-5); Controlled Evaporator Mixer (CEM); Pressure Transducer Indicator (PDI).

8.2.4 Diffusivity set-up

The diffusivity of gases through the SILM cannot only be calculated from the permeability, but it can also be directly measured using a magnetic suspension balance (MSB). We used an MSB (Rubotherm GmbH) to measure the diffusivity of CO_2 in [emim][FAP]. A schematic drawing of this set-up is shown in Figure 8.7.

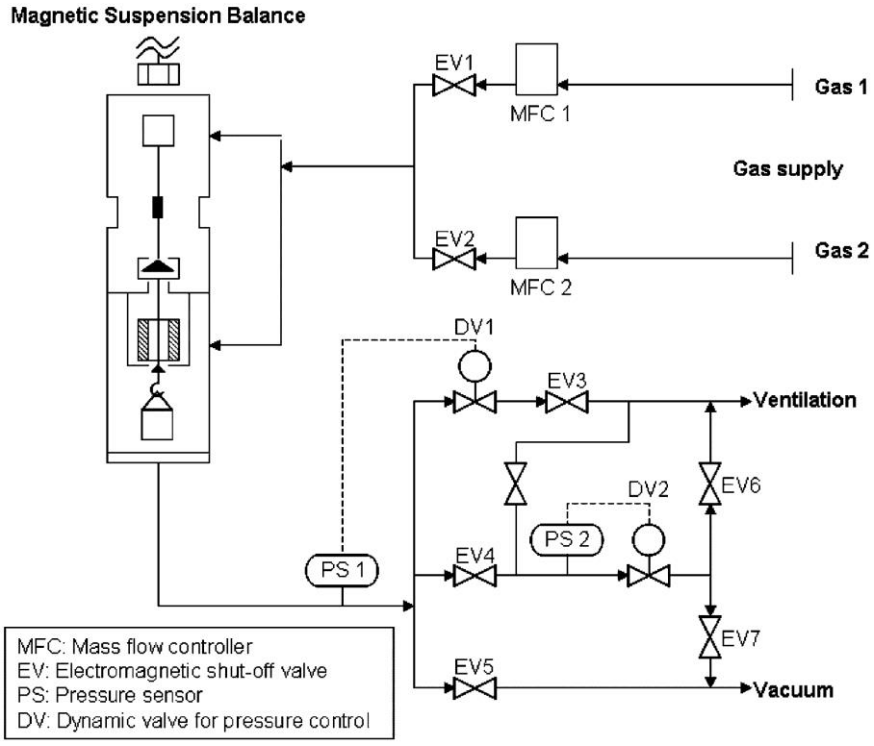

Figure 8.7: Rubotherm set-up to determine the diffusivity of CO_2 in the IL [emim][FAP]

The Rubotherm equipment allows measurement of CO_2 absorption/desorption isotherms in [emim][FAP] by measuring the CO_2 loading upon stepwise pressure increase/decrease at constant temperature. Diffusion coefficients of CO_2 at constant pressure (p) and temperature (T) can be determined by measuring the mass of absorbed CO_2 in [emim][FAP] (m_{CO2}) as function of time, (Figure 8.8). This mass is not similar to the balance reading (m_{bal}), but has to be corrected for the buoyancy effect via:

$$m_{CO_2}(p,T) = m_{bal}(p,T) - m_{sc+s}(0,T) + V_{sc+s} \cdot \rho_{CO_2}(p,T) \qquad \text{Eq.4}$$

where m_{sc+s} is the mass of the total sample container loaded with IL at vacuum conditions, V_{sc+s} is the total volume of the loaded sample container with IL and ρ_{CO2} is the density of CO_2

at the operating conditions. All the measurements in this study were carried out in the static mode in order to minimize the aerodynamic drag forces created by the flowing gases.

If one assumes that i) Fick's law is valid, ii) diffusion is a one-dimensional process (vertical), iii) the diffusion coefficient is independent of gas concentration, iv) equilibrium is established at the gas-liquid interface, v) the thickness of the IL sample and viscosity of the IL are constant during absorption, then the CO_2 diffusivity can be determined using the following diffusion equation, see Figure 8.8:

$$\frac{m_{CO_2}(t)-m_{CO_2}(0)}{m_{CO_2}(\infty)-m_{CO_2}(0)}=1-\frac{8}{\pi^2}\sum_{n=0}^{\infty}\frac{1}{(2n+1)^2}\exp\left\{\frac{-Dt(2n+1)^2\pi^2}{4l^2}\right\} \qquad \text{Eq.5}$$

where m_{CO_2}(t) is the amount of the absorbed CO_2 by the IL [emim][FAP] at time *t*, $m_{CO2}(\infty)$ is the corresponding amount attained theoretically after infinite time (equilibrium), *D* is the diffusion coefficient and *l* is the thickness of the sample (*l*= 0.102 cm). In practice only a limited set of terms was needed to determine the diffusivity using eq (5). In all our calculations the upper bound was set at *n=15*. Furthermore, to minimize the effect of the concentration on the diffusion coefficient, the stepwise pressure increase was limited to 0.1 MPa.

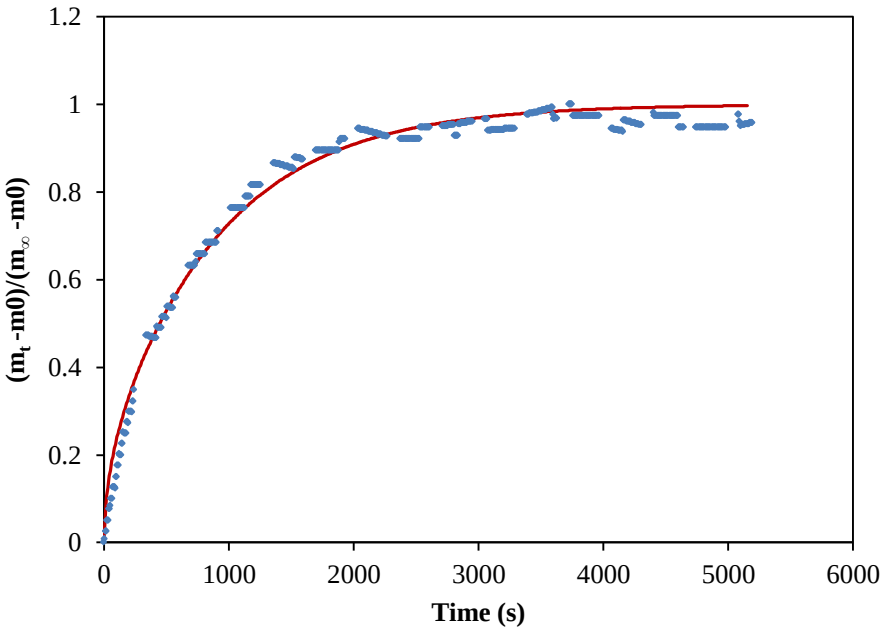

Figure 8.8: The mass of accumulated CO_2 in [emim][FAP] over time at *p* = 0.9 MPa: experimental results (solid dots); calculated results (solid line).

8.3 Results and discussion

8.3.1 Pure gas permeability

The permeability of the gas through a SILM can be explained on the basis of a dissolution-diffusion transport mechanism that consists of two steps: (i) the dissolution of the gas in the IL (impregnated in the γ-alumina layer) and (ii) the gas diffusion across the membrane [20]. The permeabilities of pure He, CH_4, C_2H_6, C_3H_8 and CO_2 through the prepared SILM were measured with the gas permeation set-up, where the temperature was set at 313 K and the transmembrane pressure (Δp) was kept at 0.7 MPa. The results of the single gas permeabilities are presented in Figure 8.9.

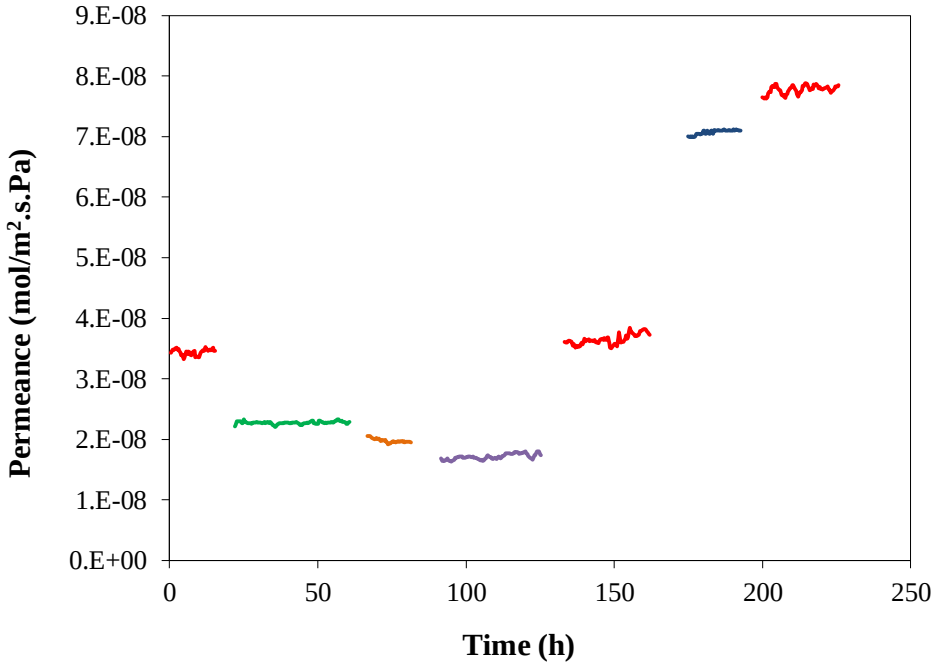

Figure 8.9: Permeance of pure gases through prepared SILM at T= 313 K and Δp = 0.7 MPa: ▲, He; ■, CH_4; ♦, C_2H_6; ×, C_3H_8; ●, CO_2.

From Figure 8.9, it can observed that pure CO_2 shows a much higher permeability through the SILM than the hydrocarbons, which is advantageous for the application of SILMs for gas sweetening. Among the hydrocarbons, CH_4 shows the highest permeability. However, from previous work we know that CH_4 shows the lowest solubility in the IL [emim][FAP] [6]. Because the gas permeability through a SILM corresponds to the product of the gas solubility

and the diffusivity, it can be concluded that the permeation behavior of hydrocarbon gases through a SILM is dominated by the diffusivity of the gases.

The permeability of He was also measured as a reference. After measuring the hydrocarbon permeabilities, the He permeability was determined again and found to be similar to its original value, indicating that no deterioration in the membrane occurred during the experiment. However, it can be seen that He permeance increased after CO_2 permeation through the SILM. This behavior could be attributed to a change in the IL properties as result of the strong interaction with CO_2. Ahosseini et al. [21] reported that viscosity of the IL decreases drastically with CO_2. A lower viscosity of the IL results in higher gas diffusivities, and thus higher gas permeation through the SILM. This may explain the higher permeability of He (compared to its original value) after the CO_2 measurement.
However, it is expected that the permeability of He (after the CO_2 experiment) will decrease, when the CO_2 is released. This was tested by monitoring the amount of CO_2 in the permeate using GC after switching to He. The result is shown in Figure 8.10. It can be noticed that the CO_2 concentration in the He permeance became zero within less than 1 hour, while the He permeability did not change during many hours (Fig. 8.9). This could be attributed to a certain amount of CO_2 remaining dissolved in SILM, still influencing the He permeance through the SILM.

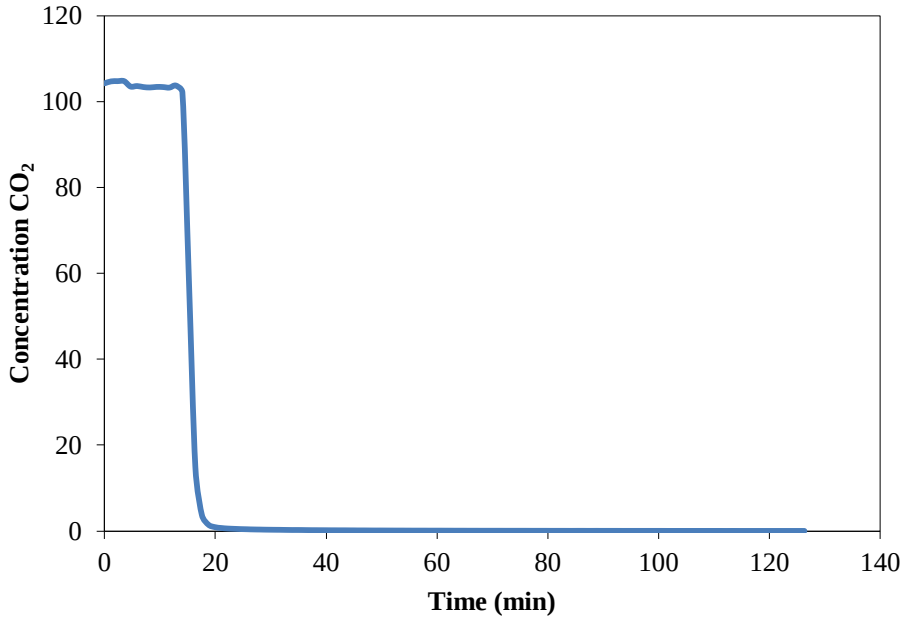

Figure 8.10: Concentration of CO_2 in He permeance over time.

The average values of CO_2, CH_4, C_2H_6 and C_3H_8 permeance through the prepared SILM are listed in Table 8.1.

Table 8.1: Average values of pure gas permeance at T= 313 K. and Δp = 0.7 MPa.

Gas	**CH_4**	**C_2H_6**	**C_3H_8**	**CO_2**
P_i (mol/m^2·s·Pa) × 10^{-8}	2.27	1.96	1.72	7.09

The ideal permselectivity of a SILM (α) can be defined as the ratio of the permeances of pure gases A and B:

$$\alpha_{AB} = \frac{P_A}{P_B} \qquad \text{Eq.6}$$

The ideal permselectivities of CO_2 over the three hydrocarbons are presented in Table 8.2.

Table 8.2: Ideal permselectivity (α_{ideal}) of CO_2/hydrocarbon at T=313 K. and Δp = 0.7 MPa.

	CO_2/CH_4	**CO_2/C_2H_6**	**CO_2/C_3H_8**
α_{ideal}	3.12	3.62	4.12

The ideal permselectivity of CO_2/CH_4 in the prepared SILM with the IL [emim][FAP] was found to be much lower than ideal solubility selectivity for CO_2/CH_4 (S = 9.69) that was found previously in the same IL at same conditions [6]. Instead, the ideal permselectivities of CO_2/C_2H_6 and CO_2/C_3H_8 in the prepared SILM were found to be higher than the ideal solubility selectivities for CO_2/C_2H_6 (S = 2.90) [6] and CO_2/C_3H_8 (S = 1.33) [6] in [emim][FAP]. The ideal permselectivity for CO_2/CH_4 (on basis of pure gas permeability) will be compared next with the mixed gas permselectivity.

8.3.2 Mixed gas permeability

Mixed-gas permeation measurements were performed at a constant temperature of 313 K, a feed pressure of 0.9 MPa and a permeate pressure of 0.2 MPa (Δp = 0.7 MPa) for the binary mixture of CO_2/CH_4 (50/50%, v/v). Table 8.3 shows a comparison between the gas permeation through the SILM for CO_2 and CH_4, when both gases were measured separately and when both gases were mixed. From these measurements the respective permselectivities were calculated.

Table 8.3: Ideal permeance (P_i), mixed gas permeance ($P_{i,mixed}$), ideal permselectivity (α_{ideal}) and mixed permselectivity (α_{mixed}) of CO_2/CH_4 at T= 313 K and Δp = 0.7 MPa.

Gas	P_i **(mol/m^2·s·Pa)**	$P_{i,mixed}$ **(mol/m^2·s·Pa)**
CO_2	7.09 x 10^{-8}	4.04 x 10^{-8}
CH_4	2.27 x 10^{-8}	3.51 x 10^{-8}
	α_{ideal} = 3.12	α_{mixed} = 1.15

It can be clearly noticed that the mixed gas permselectivity for CO_2/CH_4 mixture through the SILM is lower than the ideal permselectivity. One reason could be that the CO_2 interaction with the anion of the IL increases the intermolecular dispersion forces, causing an enhancement of the solubility of CH_4 in the IL compared to the solubility of the pure gas (CH_4) and reduces its own solubility (CO_2) in the IL [22]. Another explanation could be that CO_2 lowers the viscosity of the IL, which leads to an increase in the diffusivity of CH_4. Therefore, the permeability of CH_4 mixed with CO_2 is expected to increase through the SILM compared to the permeability of pure CH_4. That yields to a reduction of the permselectivity of the SILM for CO_2/CH_4.

Thus, even though [emim][FAP] is an excellent alternative absorbent with high CO_2 absorptive capacity and selectivity (S = 9.69), the incorporation of this IL in a SILM is less promising for the removal of CO_2 from natural gas streams, especially because the mixed permselectivity for CO_2/CH_4 is very low (α = 1.15).

8.3.3 Humidity effect on gas permeability

The objective of this work is to use the prepared SILM for removing CO_2 from natural gas. Next to CO_2, natural gas contains other undesirable impurities, such as water [23]. The presence of water in natural gas could have an effect on the permeation behavior of the gases through the SILM. Therefore, the influence of the water presence on the gas permeability through the SILM was tested using the permporometry set-up. Because this equipment cannot handle corrosive gases (such as CO_2), He was used as a feed gas with a temperature of 343 K, a pressure difference of 0.1 MPa and a gas feed flow rate of 500 mL/min. The experiment was performed by switching between humid and dry He gas and vice versa continuously over time, whereby the He permeance was monitored. The performance of the prepared SILM is shown in Figure 8.11.

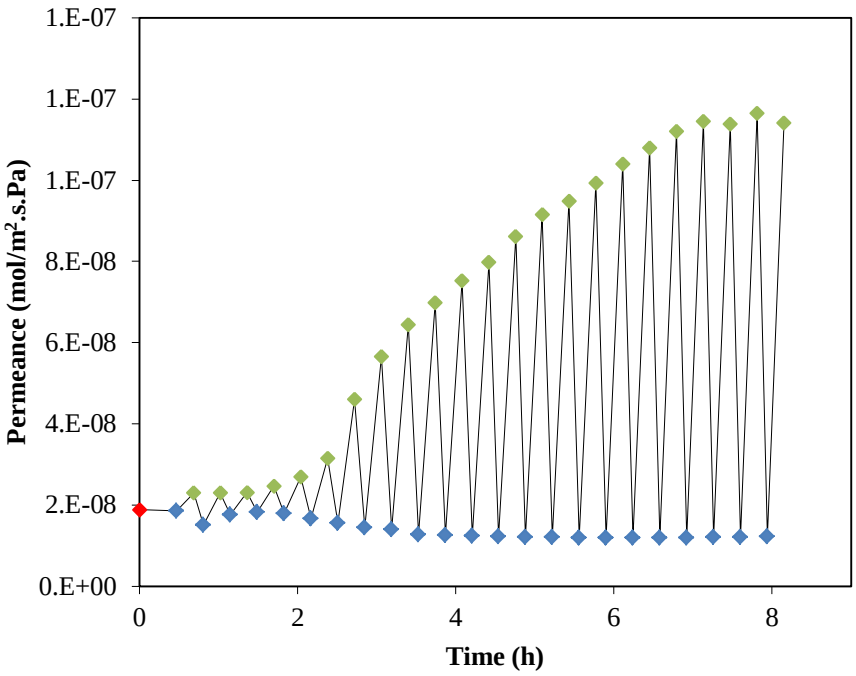

Figure 8.11: He permeance through the prepared SILM: ♦, Initial value, ♦, humid feed gas with 2g/h H_2O, ♦, dry feed gas at T= 343 K and Δp = 0.1 MPa.

It can be noticed from Figure 8.11 that the presence of water vapor in the gas stream decreased the gas permeability of the prepared SILM. Many researchers have explained gas solubility behavior in ILs on basis of the free volume [24, 25]. When a trace amount of water is present in the He gas feed stream, the water will probably occupy some of the free volume in the IL that normally is available for He. This will lead to a reduction in He solubility in the IL and ultimately to a reduction in the He permeance. Further, the formation a thin film of water at the surface of the membrane may be responsible for part of the permeation decrease that was observed.

On the other hand, the He permeance under dry conditions was increased significantly compared to the initial value (Figure 8.11). This increase could be attributed to a chemical degradation effect. It is known that ILs with fluorinated anions, such as [FAP^-], are unstable in the presence of water at high temperatures. They can hydrolyze and form hydrogen fluoride (HF) [26]. Because HF is volatile, it would be removed from the membrane by the gas flow [27]. This HF may not be detectable in the permeate because the concentration is low or because it will react with the support material (alumina). The degradation of IL will result in a decrease of the SILM performance. Therefore, the natural gas stream should be dehydrated before it is fed into the SILM.

8.3.4 Gas diffusivities

For gases that permeate through a liquid membrane via a solution-diffusion mechanism, the diffusivities can be obtained from the measured permeabilities via:

$$P = D_{12} \times S \qquad \text{Eq.7}$$

where P is permeability in mol·m/(m^2·s·Pa), S is the solubility in mol/(m^3·Pa) and D_{12} is the diffusivity in m^2/s of the gas molecule (1) in the IL (2) [20]. The permeability P in Eq. 7 is obtained from the permeabilities in Table 8.1 (given in mol/(m^2·s·Pa)) multiplied by the thickness of the SILM (2.64 µm) and divided by the porosity of the membrane (50%), because gas permeation occurs only through the pores filled with IL. The solubilities S of the different gases in IL at the feed conditions (313 K, 0.9 MPa) in Eq. 7 were obtained from literature data [1, 6, 28] (solubilities given in mole fraction x) and converted to the required units via:

$$S = \frac{x}{(1-x) \cdot \frac{M_{w,IL}}{\rho_{IL}} \cdot p} \qquad \text{Eq.8}$$

where the molecular weight of the IL ($M_{W,IL}$) is 556.16 g/mol, the density of the IL (ρ_{IL}) is 1.69 g/cm^3 and the feed pressure (p) is 0.9 MPa. The diffusivities D_{12} of CO_2, CH_4, C_2H_6 and C_3H_8 in the IL can now be determined using Eq. 7, and are presented in Table 8.4.

In addition, the diffusivity of CO_2 in [emim][FAP] was also directly measured using the Rubotherm set-up. The measured CO_2 diffusivity using the Rubotherm equipment (4.7×10^{-10} m^2/s) at the same conditions is nearly equal to the value obtained from the permeability measurements (4.49×10^{-10} m^2/s).

Because the experimental measurement of gas diffusivities is time-consuming, the Morgan et al. correlation [18] was used to predict gas diffusivities in ILs:

$$D_{12} = 3.7\times10^{-3} \frac{1}{\eta_2^{0.59} V_1 \rho_2^2} \qquad \text{Eq.9}$$

where D_{12} is the diffusivity in m^2/s of the gas molecule (1) in the IL (2), η_2 is the viscosity of the IL, ρ_2 is the density of the IL, and V_1 is the molar volume of the solute (gas) at normal boiling point [10, 29]. The predicted diffusion coefficients of the various gases in [emim][FAP] are also reported in Table 8.4.

Table 8.4: Experimental and predicted diffusivities (*D*) of various gases in [emim][FAP] at *T*=313 K, including the liquid molar volumes of the gas (V_{gas}), the gas solubilities in [emim][FAP] (*S*) and the gas permeabilities (*P*).

Gas	V_{gas} (cm^3/mol)	*S* (mol/m^3.Pa)	*P* (mol.m/m^2.s.Pa)	Experimental *D* (m^2/s)	Predicted *D* (m^2/s)
CO_2	34.00 [10]	8.24E-4 [1]	3.70E-13 [this work]	4.49E-10	4.77E-10
CH_4	35.54 [29]	0.78E-4 [28]	1.21E-13 [this work]	15.6E-10	4.63E-10
C_2H_6	46.15 [29]	2.54E-4 [6]	1.06E-13 [this work]	4.15E-10	3.51E-10
C_3H_8	74.87 [29]	5.41E-4 [6]	0.95E-13 [this work]	1.76E-10	2.16E-10

From Table 8.4 it can be concluded that the experimentally determined diffusivity of CO_2 in [emim][FAP] coincides with the predicted value. However, the prediction of the hydrocarbon diffusivities in [emim][FAP] is deviating from the prediction using the correlation, but follows the same trend as the experimentally obtained diffusivities ($D_{CH_4} > D_{C_2H_6} > D_{C_3H_8}$). This trend was to be expected, because other researchers observed a same trend (decreasing diffusivity with increasing solute size) for gas diffusion in other ILs [9, 18].

Table 8.4 also shows that the experimentally obtained diffusivity of CH_4 is much higher than the predicted value. Two possible explanations can be given. It could be that not all transport takes place via the solution diffusion mechanism (in the pores filled with IL), but via the Knudsen diffusion mechanism instead (in empty pores or defects). Knudsen diffusion is inversely proportional to the gas molecular weight and thus expected to be highest for CH_4 compared to other gases (CO_2, C_2H_6 and C_3H_8). However, the initial membrane check with He showed no sign of these extra pores. Secondly, the correlation has been fitted to data measured on a SILM in a different porous structure and a different set-up using dissimilar circumstances, which may also lead to deviating predictions, although a similar systematic error for all gases measured would be expected.

The high diffusivity of CH_4 compared to CO_2 nevertheless explains why the permselectivity of mixed CO_2/CH_4 is so much lower than the solubility selectivity of CO_2/CH_4, even though [emim][FAP] shows preferential absorption of CO_2 over hydrocarbons. Thus, kinetic effects can significantly alter thermodynamic equilibrium results, and have to be taken into account during design of dynamic processes.

8.4 Conclusions

A SILM consisting of a α-alumina support with two top γ-alumina layers impregnated with the IL [emim][FAP] was prepared and its potential for gas sweetening was evaluated. The pure gas permeability of various natural gas components (CO_2, CH_4, C_2H_6 and C_3H_8) through this SILM were determined at a trans-membrane pressure of 0.7 MPa and temperature of 313 K. The following trend was observed: $P_{CO_2} > P_{CH_4} > P_{C_2H_6} > P_{C_3H_8}$. The mixed gas permselectivity of CO_2/CH_4 (50/50%, v/v) was found to be much lower ($\alpha = 1.15$) than the ideal permselectivity ($\alpha = 3.12$). The performance of the SILM was negatively affected by the presence of water. Diffusivities of the pure gases (CO_2, CH_4, C_2H_6 and C_3H_{10}) were determined experimentally and predicted using a suitable model correlation, which reproduced the CO_2 behavior well, but could not describe the diffusivities of the hydrocarbons quantitatively, although the trend was correctly predicted. CH_4 showed a much higher diffusivity than CO_2, which explains why the permselectivity of a binary CO_2/CH_4 mixture is so much lower than the solubility selectivity of pure CO_2 and CH_4. Thus, even though [emim][FAP] is an excellent alternative absorbent with high CO_2 absorptive capacity and selectivity ($S = 9.69$), the incorporation of this IL in a SILM as a unit operation is less promising for the removal of CO_2 from natural gas streams, because the permselectivity for CO_2/CH_4 mixtures is much lower.

8.5 References

[1] M. Althuluth, M.T. Mota-Martinez, M.C. Kroon, C.J. Peters, Solubility of Carbon Dioxide in the Ionic Liquid 1-Ethyl-3-methylimidazolium Tris(pentafluoroethyl)trifluoro phosphate, Journal of Chemical & Engineering Data, 57 (2012) 3422-3425.

[2] M. Althuluth, M.C. Kroon, C.J. Peters, Solubility of Methane in the Ionic Liquid 1-Ethyl-3-methylimidazolium Tris(pentafluoroethyl)trifluorophosphate, Industrial & Engineering Chemistry Research, 51 (2012) 16709-16712.

[3] J.L. Anderson, J.K. Dixon, J.F. Brennecke, Solubility of CO_2, CH_4, C_2H_6, C_2H_4, O_2, and N2 in 1-Hexyl-3-methylpyridinium Bis(trifluoromethylsulfonyl)imide: Comparison to Other Ionic Liquids, Accounts of Chemical Research, 40 (2007) 1208-1216.

[4] G. Hong, J. Jacquemin, M. Deetlefs, C. Hardacre, P. Husson, M.F. Costa Gomes, Solubility of carbon dioxide and ethane in three ionic liquids based on the bis{(trifluoromethyl)sulfonyl}imide anion, Fluid Phase Equilibria, 257 (2007) 27-34.

[5] M.T. Mota-Martinez, M. Althuluth, M.C. Kroon, C.J. Peters, Solubility of carbon dioxide in the low-viscosity ionic liquid 1-hexyl-3-methylimidazolium tetracyanoborate, Fluid Phase Equilibria, 332 (2012) 35-39.

[6] M. Althuluth, M.T. Mota-Martinez, A. Berrouk, M.C. Kroon, C.J. Peters, Removal of Small Hydrocarbons (Ethane, Propane, Butane) from Natural Gas Streams using the Ionic Liquid1-Ethyl-3 -methylimidazolium Tris(pentafluoroethyl)trifluorophosphate, The Journal of Supercritical Fluids, 90 (2014) 65-72.

[7] J.L. Anthony, E.J. Maginn, J.F. Brennecke, Solubilities and Thermodynamic Properties of Gases in the Ionic Liquid 1-n-Butyl-3-methylimidazolium Hexafluorophosphate, The Journal of Physical Chemistry *B*, 106 (2002) 7315-7320.

[8] S. Raeissi, C.J. Peters, A potential ionic liquid for CO_2-separating gas membranes: selection and gas solubility studies, Green Chemistry, 11 (2009) 185-192.

[9] R. Condemarin, P. Scovazzo, Gas permeabilities, solubilities, diffusivities, and diffusivity correlations for ammonium-based room temperature ionic liquids with comparison to imidazolium and phosphonium RTIL data, Chemical Engineering Journal, 147 (2009) 51-57.

[10] Y. Hou, R.E. Baltus, Experimental Measurement of the Solubility and Diffusivity of CO2 in Room-Temperature Ionic Liquids Using a Transient Thin-Liquid-Film Method, Industrial & Engineering Chemistry Research, 46 (2007) 8166-8175.

[11] D. Camper, C. Becker, C. Koval, R. Noble, Diffusion and Solubility Measurements in Room Temperature Ionic Liquids, Industrial & Engineering Chemistry Research, 45 (2005) 445-450.

[12] M. Gonzalez-Miquel, J. Bedia, C. Abrusci, J. Palomar, F. Rodriguez, Anion Effects on Kinetics and Thermodynamics of CO_2 Absorption in Ionic Liquids, The Journal of Physical Chemistry *B*, 117 (2013) 3398-3406.

[13] S.S. Moganty, R.E. Baltus, Diffusivity of Carbon Dioxide in Room-Temperature Ionic Liquids, Industrial & Engineering Chemistry Research, 49 (2010) 9370-9376.

[14] J.B. Tang, W.L. Sun, H.D. Tang, M. Radosz, Y.Q. Shen, Enhanced CO_2 absorption of poly(ionic liquid)s, Macromolecules, 38 (2005) 2037-2039.

[15] C. Wang, H. Luo, D.-e. Jiang, H. Li, S. Dai, Carbon Dioxide Capture by Superbase-Derived Protic Ionic Liquids, Angewandte Chemie International Edition, 49 (2010) 5978-5981.

[16] D. Camper, J.E. Bara, D.L. Gin, R.D. Noble, Room-Temperature Ionic Liquid−Amine Solutions: Tunable Solvents for Efficient and Reversible Capture of CO_2, Industrial & Engineering Chemistry Research, 47 (2008) 8496-8498.

[17] E.D. Bates, R.D. Mayton, I. Ntai, J.H. Davis, CO_2 Capture by a Task-Specific Ionic Liquid, Journal of the American Chemical Society, 124 (2002) 926-927.

[18] D. Morgan, L. Ferguson, P. Scovazzo, Diffusivities of Gases in Room-Temperature Ionic Liquids: Data and Correlations Obtained Using a Lag-Time Technique, Industrial & Engineering Chemistry Research, 44 (2005) 4815-4823.

[19] H. Yang, Z. Xu, M. Fan, R. Gupta, R.B. Slimane, A.E. Bland, I. Wright, Progress in carbon dioxide separation and capture: A review, Journal of Environmental Sciences, 20 (2008) 14-27.

[20] J.J. Close, K. Farmer, S.S. Moganty, R.E. Baltus, CO_2/N_2 separations using nanoporous alumina-supported ionic liquid membranes: Effect of the support on separation performance, Journal of Membrane Science, 390–391 (2012) 201-210.

[21] A. Ahosseini, E. Ortega, B. Sensenich, A.M. Scurto, Viscosity of n-alkyl-3-methyl-imidazolium bis(trifluoromethylsulfonyl)amide ionic liquids saturated with compressed CO_2, Fluid Phase Equilibria, 286 (2009) 72-78.

[22] D.G. Hert, J.L. Anderson, S.N.V.K. Aki, J.F. Brennecke, Enhancement of oxygen and methane solubility in 1-hexyl-3-methylimidazolium bis(trifluoromethylsulfonyl) imide using carbon dioxide, Chemical Communications, (2005) 2603-2605.

[23] R.W. Baker, K. Lokhandwala, Natural Gas Processing with Membranes: An Overview, Industrial & Engineering Chemistry Research, 47 (2008) 2109-2121.

[24] R. Babarao, S. Dai, D.-e. Jiang, Understanding the High Solubility of CO_2 in an Ionic Liquid with the Tetracyanoborate Anion, The Journal of Physical Chemistry *B*, 115 (2011) 9789-9794.

[25] M.S. Shannon, J.M. Tedstone, S.P.O. Danielsen, M.S. Hindman, A.C. Irvin, J.E. Bara, Free Volume as the Basis of Gas Solubility and Selectivity in Imidazolium-Based Ionic Liquids, Industrial & Engineering Chemistry Research, 51 (2012) 5565-5576.

[26] R. Quinn, J.B. Appleby, G.P. Pez, Hydrogen sulfide separation from gas streams using salt hydrate chemical absorbents and immobilized liquid membranes, Separation Science and Technology, 37 (2002) 627-638.

[27] P. Scovazzo, J. Kieft, D.A. Finan, C. Koval, D. DuBois, R. Noble, Gas separations using non-hexafluorophosphate [PF6] anion supported ionic liquid membranes, Journal of Membrane Science, 238 (2004) 57-63.

[28] M. Althuluth, M.C. Kroon, C.J. Peters, Solubility of Methane in the Ionic Liquid 1-Ethyl -3-methylimidazolium Tris(pentafluoroethyl)trifluorophosphate, Industrial & Engineering Chemistry Research, 51 (2012) 16709-16712.

[29] B.E. Poling, J.M. Prausnitz, J.P. O'Connell, The Properties of Gases and Liquids, fifth ed., McGraw-Hill, New York, (2001).

Chapter 9

Conclusions & Recommendations

9.1 Conclusions

Ionic liquids (ILs) are promising solvents for natural gas sweetening, especially the IL 1-ethyl-3-methylimidazolium tris(pentafluoroethyl) trifluorophosphate ([emim][FAP]). It is shown that CO_2 is more soluble in this particular IL than in any other IL sharing the same cation. The main reason is that the anion of this IL is highly fluorinated. Another feature is the large anion size is large which results, compared to other fluorinated ILs, to a higher stability with respect to moisture and air. This study also showed that [emim][FAP] is thermally stable at temperatures up to 600 K, consequently, it can withstand the operating temperatures (300 – 400 K) normally involved in conventional natural gas sweetening processes. An additional feature that may benefit the application of the selected IL is its extremely low vapor pressure with the consequence that no contamination of the gas stream will occur. Furthermore, [emim][FAP] showed a significant decrease in viscosity with a slight increase in temperature, which can be an advantage for the gas mass transfer. It is well known that the gas diffusion in the IL is related inversely with viscosity of the IL (chapter 3).

For better judgment of the applicability of [emim][FAP] in natural gas sweetening processes, the solubility of CH_4 in this IL was determined. The results showed that this IL is a good solvent for natural gas sweetening, because it combines a high CO_2 solubility with a low absorption capacity for CH_4, as indicted by the high solubility selectivities achieved ($S_{CO2/CH4}$ = 5.77 to 11.58), depending on the operating conditions. The solubilities of both CO_2 and CH_4 were found to increase with pressure and decrease with increasing temperature. Further, an increase in temperature has a large influence on the CO_2 solubility in [emim][FAP], while for CH_4 the influence on its solubility is small. This difference in solubility behavior is can beneficial for the separation process (chapter 4).

In natural gas sweetening, the loss of small hydrocarbons such as C_2H_6, C_3H_8 and C_4H_{10} to the CO_2-rich stream is a concern. It is desirable to maintain these compounds in the CH_4-rich stream, because of their value. Therefore, the solubility in [emim][FAP] of these small hydrocarbons that could be present in the raw natural gas were investigated as well. It was found that the solubility of small hydrocarbons in the IL [emim][FAP] increases with increasing hydrocarbon chain length: $CH_4 < C_2H_6 < C_3H_8 < CO_2 < C_4H_{10}$. Further, it was established that an increase in hydrocarbon chain length decreases the maximum achievable solubility because of the occurrence of liquid-liquid immiscibility at higher concentrations of

the hydrocarbon. The maximum achievable gas solubility was nearly to 27.5% mol, 22.5 mol%, 15.0 mol% for C_2H_6, C_3H_8 and C_4H_{10}, respectively at temperature ~ 293 K. Enthalpies of absorption of the small hydrocarbons and also CO_2 in [emim][FAP] were found to be relatively low, resulting in lower energy costs for regeneration. The enthalpies of absorption of small hydrocarbons increased with increasing chain length of the hydrocarbons, which is consistent with their solubility behavior. Maximum selectivities for CO_2 removal from small hydrocarbons are achieved at lower temperatures, and found to be higher than selectivities observed for other ILs and physical solvents. For example, at a temperature of 333 K, the separation ratios of CO_2/C_2H_6 are 2.67, 2.20 and 1.82 for [emim][FAP], [hmim][Tf_2N] and Genosorb1753, respectively. This confirms that [emim][FAP] is a promising candidate absorbent that can compete with commercial physical solvents for gas sweetening processes (chapter 5).

The Peng-Robinson Equation of State (PR-EoS), combined with quadratic mixing rules, has been used to correlate the experimental gas solubility data accurately over a wide temperature range (293K- 363K) and pressures up to 11 MPa. This research established that the experimental data of all binary mixtures hydrocarbon + [emim][FAP] could be accurately correlated by using only one linearly temperature-dependent binary interaction parameter with an absolute average deviation (*AAD*) less than 1%, while, on the other hand, the solubility data of the binary mixture CO_2 + [emim][FAP] required two binary interaction parameters to yield an *AAD* of less than 3%. Without a temperature dependency of the binary parameters the correlation is poor (chapter 6).

The absorption behavior of the heavier aliphatic hydrocarbons and aromatic hydrocarbons (benzene, toluene, ethylbenzene and xylene, collectively called BTEX) in [emim][FAP] IL has been studied. This information is of utmost importance, because of the severe problems that BTEX may cause in the sulfur recovery unit, during liquefying, and in emissions. It was observed that the solubility of the BTEX compounds in [emim][FAP] is high. For this reason, this IL is a good solvent to reduce the concentration of BTEX components present in the gas stream for the sweetening process. Obviously, these compounds should be recovered from the acid gas stream before this stream can be forwarded to the sulfur recovery plant, in order to protect the catalyst bed in the sulfur recovery step from coking to be caused by BTEX components (chapter 7).

A technology that has attracted practical interest is the use of supported ionic liquid membranes (SILMs) for gas sweetening as a potentially cost-effective technology. To explore this technology, [emim][FAP] was impregnated successfully in the γ-alumina layer of a tubular porous asymmetric membrane. The pure gas permeability of natural gas components, such as CO_2, CH_4, C_2H_6 and C_3H_8 were tested through the SILM at a trans-membrane pressure of 0.7 MPa and a temperature of 313 K. The following trend of pure gas permeabilities was observed for the SILM in this study: $P_{CO2} > P_{CH4} > P_{C2H6} > P_{C3H8}$. In addition, the mixed gas permeability and permselectivity for the binary mixture of CO_2/CH_4 (50/50%, v/v) were also measured The mixed gas permselectivity (α = 1.15) was found to be much lower than the ideal permselectivity (α= 3.12). It was established that the performance of the SILM was negatively affected by the presence of water, which component is generally present in natural gas. Therefore, dehydration of the natural gas stream is necessary before it is fed to the SILM. Even though [emim][FAP] is an excellent alternative absorbent with high CO_2 absorptive capacity, the incorporation of this IL in a SILM is less promising for the removal of CO_2 from natural gas streams, because the permselectivity for CO_2/CH_4 is low. The gas separation process depends on thermodynamics (solubility) and kinetics (gas diffusivity). Therefore, it is important to optimize the process such that the best gas separation conditions in terms of both thermodynamic and kinetic constraints (chapter 8).

9.2 Recommendations

In this study, solubilities in [emim][FAP] of the natural gas components CO_2, C_2H_6, C_3H_8, C_4H_8, hexane, heptane, benzene, toluene, ethylbenzene and *o*-xylene have been measured. However, one most important component is missing in the research: H_2S, the reason is that, besides of safety regulations, Cailletet facilities cannot handle this component as mercury is in direct contact with the sample. Because in the near future natural gases with elevated concentrations of H_2S have to be treated, it is extremely important to make facilities available that allows safe experimental work on systems with large concentrations of H_2S involved. Availability of these data is beneficial for an optimum design of gas sweetening facilities.

In this study, solubilities of natural gas components have been measured separately in [emim][FAP], i.e. in binary mixtures, and from these measurements the solubility selectivities have been determined. However, the presence of CO_2 or any other compound could affect the CH_4 solubility and vice versa. This may have the consequence that

solubilities of individual components in mixed gases could be different than the solubilities of pure gases as were measured in this work. As a consequence, this also means that the selectivities might be affected. Ramdin *et. al* [1] have recently shown that the real selectivity of CO_2/CH_4 in ILs didn't differ significantly from the ideal CO_2/CH_4 selectivity in the same ILs. However, Hert *et al.* [2] observed that in a mixture of CO_2 and CH_4 an enhanced CH_4 solubility in the IL [hmim][Tf_2N] occurred in comparison to the solubility of pure CH_4 in the same IL. Consequently, it is of major interest to investigate the solubility of mixed gases in [emim][FAP] in future studies.

It was found that the CO_2 absorption in [emim][FAP] is strongly pressure dependent. Therefore, this IL is favorable for the bulk removal of CO_2 at high CO_2 partial pressure, i.e. at high CO_2 concentrations. This process can be followed by amine-based absorption technology to reduce the CO_2 concentration in the natural gas to a suitable level to avoid corrosion and hydrate formation during transportation. In this scenario, the energy requirement through the whole process could be much lower than in case of using only amine-based technology. This can be explained as follows: IL regeneration can be performed by successive depressurizations and the majority of CO_2 will be removed in this step. Thus, the feed gas in the amine-based absorption technology will contain low a CO_2 concentration. For this reason, the heat energy input required to regenerate the amine solvent will be significantly lower.

One of the main challenges in the application of [emim][FAP] in natural gas sweetening, is its sensitivity to water. It is known that the fluorinated ILs can hydrolyze and form HF at higher temperatures. Therefore, the natural gas stream should be dehydrated before it is introduced into the absorption process. Alternatively, the absorption process should be operated at temperatures low enough to avoid hydrolyzing of the IL. The latter approach also has the advantage of an enhanced CO_2 absorption in [emim][FAP]. According to short-term scanning TGA measurements, [emim][FAP] exhibited a good thermal stability. However, to evaluate the thermal stability of [emim][FAP] more accurately, which is important for industrial applications, the long-term thermal stability, i.e. over multiple cycles of absorption/desorption, is necessary to perform.

One of the main problems arising from the use of amine-based solvents for natural gas sweetening is corrosion. Some studies have shown that ILs have ability to corrode some metals and alloys, especially at high temperatures. Therefore, if [emim][FAP] is considered

as an alternative absorbent in natural gas sweetening, its corrosion properties should also be tested.

The incorporation of the selected IL in a supported ionic liquid membrane (SILM) showed a low permselectivity for CO_2/CH_4. This observation was unexpected as the same IL showed a high solubility selectivity for CO_2/CH_4. For this reason, it is necessary to use a technique to investigate the probability of defects or empty pores in such a liquid membrane in any future studies. Practically, it is hard to achieve CO_2 absorption in conventional columns or SILMs filled with such viscous ILs due to a high mass-transfer resistance and low absorption rate. It was found that the diffusion coefficients of CO_2 in [emim][FAP] near ambient temperature is in the order of 4.5×10^{-6} cm^2/s, which is slower than CO_2 diffusion in traditional solvents ($\sim1\times10^{-5}$ cm^2/s) [3]. Therefore, it is recommended to use a technology that achieves a high mass transfer for such viscous solvents.

Rotating packed beds (RPB) are designed to generate high-gravity forces to form thin liquid films or tiny liquid droplets with the purpose to enhance the mass transfer between gas and liquid. The structure of a typical countercurrent RPB is illustrated in Figure 9.1.

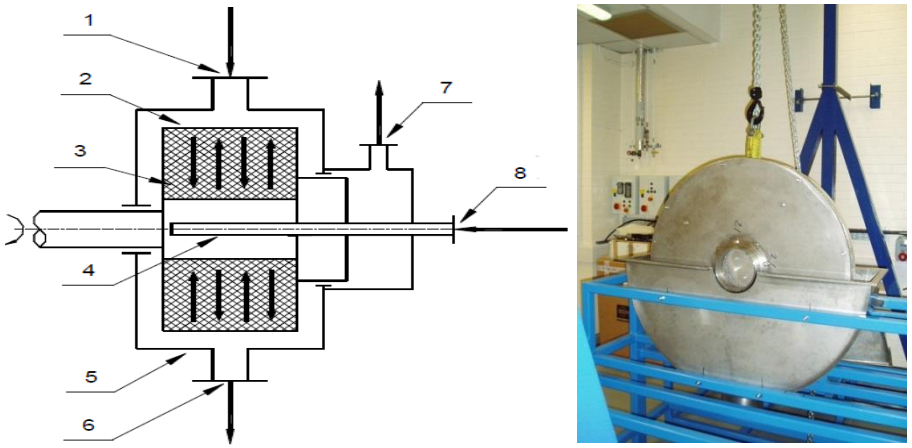

Figure 9.1: The structure of a countercurrent RPB: (1) gas inlet; (2) rotor; (3) packing; (4) liquid distributor; (5) shell; (6) liquid outlet; (7) gas outlet; (8) liquid inlet [4].

Zhang *et al*. [4] reported that the mass transfer coefficient in the RPB is at least one to two orders of magnitude higher than that in a conventional packed tower. As a result, this technology requires much less packing material, leading to a reduction of the size of the equipment (Figure 9.2). Thus, the (RPB) is a compact facility that could compete with the much larger conventional absorption columns. Because of their smaller size, this kind of facilities can be particularly useful in off-shore applications.

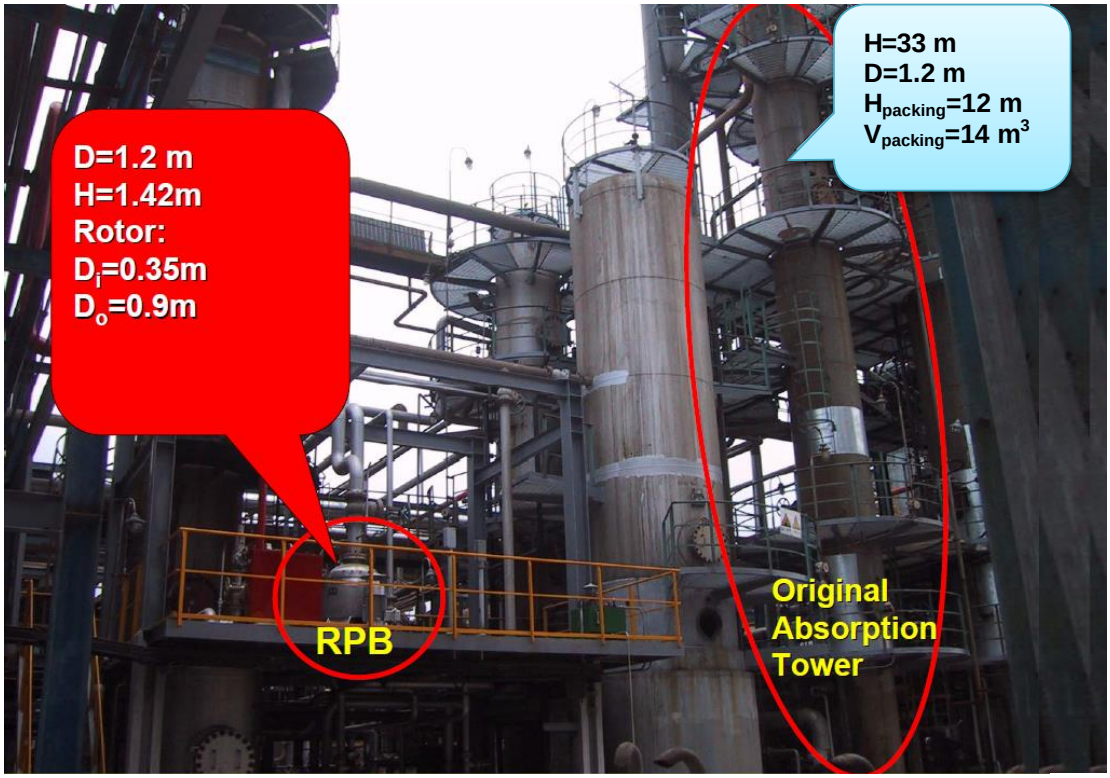

Figure 9.2: Traditional amine absorption tower versus rotating packed bed (RPB) absorption unit [5].

An additional feature is that much less of expensive ILs is needed for the RPB technology. It would be highly recommended to investigate the incorporation of selected ILs in a RPB absorber.

9.3 References

[1] M. Ramdin, A. Amplianitis, T.W. de Loos, T.J.H. Vlugt, Solubility of CO_2/CH_4 gas mixtures in ionic liquids, Fluid Phase Equilibria, 375 (2014) 134-142.

[2] D.G. Hert, J.L. Anderson, S.N.V.K. Aki, J.F. Brennecke, Enhancement of oxygen and methane solubility in 1-hexyl-3-methylimidazolium bis(trifluoromethylsulfonyl) imide using carbon dioxide, Chemical Communications, (2005) 2603-2605.

[3] S.-Y. Horng, M.-H. Li, Kinetics of Absorption of Carbon Dioxide into Aqueous Solutions of Monoethanolamine + Triethanolamine, Industrial & Engineering Chemistry Research, 41 (2001) 257-266.

[4] L.-L. Zhang, J.-X. Wang, Y. Xiang, X.-F. Zeng, J.-F. Chen, Absorption of Carbon Dioxide with Ionic Liquid in a Rotating Packed Bed Contactor: Mass Transfer Study, Industrial & Engineering Chemistry Research, 50 (2011) 6957-6964.

[5] J. Chen, The Recent Developments in the HiGee Technology, Green Process Engineering and the European Process Intensification Conference, (2009).

Abbreviations

The following abbreviations have been used for some chemicals and for cations and anions of various ionic liquids:

Chemicals

DEA	diethanolamine
MEA	monoethanolamine
MDEA	methyldiethanolamine
TEGMME	triethylene glycol monomethyl ether

Cations

[emim]	1-ethyl-3-methylimidazolium
[bmim]	1-butyl-3-methylimidazolium
[hmim]	1-hexyl-3-methylimidazolium
[2empy]	2-methyl-N-ethylpyridinium

Anions

$[Tf_2N]$	bis(trifluoromethylsulfonyl)amide
$[PF_6]$	hexafluorophosphate
$[BF_4]$	tetrafluoroborate
[FAP]	tris(pentafluoroethyl)trifluorophosphate
$Et[SO_4]$	ethylsulfate

About the Author

Mamoun A. M. Althuluth was born on 15th December 1983 in Nablus, Palestine. After finishing his high school studies, he started his undergraduate studies in Chemical Engineering at An-Najah National University in Palestine. In June 2007, he got his BSc degree in Chemical Engineering, his graduation project titled "Preparation of Activated Carbon and its Application in Textile Wastewater Treatment". After graduation he joined the UNESCO-IHE Institute for Water Education in The Netherlands to prepare his MSc with a MEDRC scholarship. He got his MSc degree with distinction in Water Supply Engineering from UNESCO-IHE in 2009. His MSc thesis entitled “Development of Particulate/ Colloidal Fouling Indicators in Sea Water Reverse Osmosis Plants”. After that he worked for a couple of months as a researcher in the Water Treatment Technology group at UNESCO-IHE. Thereafter, he moved to the United Arab Emirates and joined the Petroleum Institute (PI), Abu Dhabi. He was appointed as a Research/ Teaching assistant in the Chemical Engineering Department. In 2010, he was funded by the Gas Research Center (GRC) at the PI to start a collaborative project with Delft University of Technology and was continued at Eindhoven University of Technology. In 2014, at the ADNOC Research & Development Academic Conference (ADRAC) he was awarded the R&D Hay Bin Yaqdhan award

List of publications

Journal publications

[1] M. Althuluth, M.T. Mota-Martinez, M.C. Kroon, C.J. Peters, Solubility of Carbon Dioxide in the Ionic Liquid 1-Ethyl-3-methylimidazolium Tris(pentafluoroethyl)trifluor phosphate, *J. Chem. Eng. Data*, 57 (2012) 3422-3425.

[2] M. Althuluth, M.C. Kroon, C.J. Peters, Solubility of Methane in the Ionic Liquid 1-Ethyl-3-methylimidazolium Tris(pentafluoroethyl)trifluorophosphate, *Ind. Eng. Chem. Res.*, 51 (2012) 16709-16712.

[3] M.T. Mota-Martinez, M. Althuluth, M.C. Kroon, C.J. Peters, Solubility of carbon dioxide in the low-viscosity ionic liquid 1-hexyl-3-methylimidazolium tetracyanoborate, *Fluid Phase Equilib.*, 332 (2012) 35-39.

[4] M. Althuluth, M.T. Mota-Martinez, A. S. Berrouk, M.C. Kroon, C.J. Peters, Removal of Small Hydrocarbons (Ethane, Propane, Butane) from Natural Gas Streams using the Ionic Liquid 1-Ethyl-3-methylimidazolium Tris(pentafluoroethyl)trifluorophosphate, *J. Supercrit. Fluids*, 90 (2014) 65-72.

[5] M.T. Mota-Martinez, M. Althuluth, A. Berrouk, M.C. Kroon, C.J. Peters, High pressure phase equilibria of binary mixtures of light hydrocarbons in the ionic liquid 1-hexyl-3-methylimidazolium tetracyanoborate, *Fluid Phase Equilib.*, 362 (2014) 96-101.

[6] M. Althuluth, A. S. Berrouk, M. C. Kroon and C. J. Peters, Modeling Solubilities of Gasses in Ionic Liquids Using the Peng-Robinson Equation of State, *Ind. Eng. Chem. Res.* 53 (2014) 11818-11821

[7] M. Althuluth, J.P. Overbeek, H.J. Wees, L.F. Zubeir, W.G. Haije, A. Berrouk, C.J. Peters, M.C. Kroon, Natural Gas Purification Using Supported Ionic Liquid Membrane, *J. of Membr. Sci.*, (2014). Under review.

[8] M. Althuluth, N. R. Rodriguez, C.J. Peters, M.C. Kroon, Solubility and Separation of Heavy Hydrocarbons from Natural Gas using the Ionic Liquid 1-Ethyl-3–methylimidazolium Tris(pentafluoroethyl) trifluorophosphate, *Fluid Phase Equilib.* (2014). Submitted.

Oral/Poster Presentations

[1] M. Althuluth, M.T. Mota-Martinez, M.C. Kroon, C.J. Peters, Solubility of Carbon Dioxide in the Ionic Liquid1-Ethyl-3-methylimidazolium Tris(pentafluoroethyl)trifluoro phosphate, **Poster**: 13th European Meeting on Supercritical Fluids, (ISASF) 9-12 October (2011), The Hague, The Netherlands.

[2] M. Althuluth, M.C. Kroon, C.J. Peters, Gas Sweetening Using the Ionic Liquid 1-Ethyl-3-methylimidazolium Tris(pentafluoroethyl)trifluorophosphate. **Oral**: The 3rd Asian-Pacific Conference on Ionic Liquids and Green Processes (APCIL'12), 19-25 September 2012, Beijing, China.

[3] M. Althuluth, A. S. Berrouk, M. C. Kroon and C. J. Peters, Gas Sweetening Using the Ionic Liquid 1-Ethyl-3-methylimidazolium Tris(pentafluoroethyl)trifluorophosphate: Experiments and Modeling. **Poster** : 9th European Congress of Chemical Engineering, (ECCE9), 21-25 April (2013), The Hague, The Netherlands.

[4] M. Althuluth, A. S. Berrouk, M. C. Kroon and C. J. Peters, Removal of small hydrocarbons (ethane, propane) from natural gas streams using the ionic liquid 1-ethyl-3-methylimidazolium tris(pentafluoroethyl) trifluorophosphate. **Poster**: 13th International Conference on Properties and Phase Equilibria for Products and Process Design, (PPEPPD13), 26-30 May (2013), Iguazu Falls, Argentina – Brazil.

[5] M. Althuluth, A. S. Berrouk, M. C. Kroon and C. J. Peters, Solubility of aromatics compounds (BTEX) from Natural gas in the Ionic Liquid 1-Ethyl-3-methylimidazolium Tris(pentafluoroethyl) trifluorophosphat , **Oral**: 2nd ADNOC Research and Development Conference ADRAC 2013. 24-26 February (2014), Abu Dhabi, UAE

[6] M. Althuluth, A. S. Berrouk, M. C. Kroon and C. J. Peters, Natural gas purification using supported ionic liquid membrane, **Oral**: 2nd International Conference on Ionic Liquids in Separation and Purification Technology, (ILSEPT), 29-2 July (2014), Toronto, Canada.

[7] M. Althuluth, A. S. Berrouk, M. C. Kroon and C. J. Peters, Separation Performance of [emim][FAP] in Natural Gas Sweetening. **Poster**: European Symposium on Applied Thermodynamics, (ESAT), 6-9 July (2014), The Eindhoven, The Netherlands.

Acknowledgements

I would like to thank my promoter, Prof. Cor Peters for providing me the opportunity to have an excellent experience in the field of the thermodynamics. I would like to thank him for his scientific advice, assistance and encouragement during my research. He has given me the freedom to pursue various topics. He has giving me the opportunity to interact and share knowledge with experts in various fields by giving me the chance to attend many national and internationals scientific conferences.

I am deeply thankful to my co-promoter, Prof. Maaike Kroon for her guidance and inspiration throughout this study. I am deeply grateful for her insightful discussions and suggestions on my manuscripts.

I would like to thank Prof. Thijs Vlugt and Prof. Theo de Loos for giving me the opportunity to perform part of my experiments at the thermolab at Delft University of Technology. I would also like to thank the staff and my colleagues in Process & Energy Department at Delft University for their help and support during my stay: Eugene, Leslie, Ilona, Michel, Alondra, Mahinder, Mohammad, Mariette, Sara, Jessica, Somayeh, Sergio, Stevia, Albert and Sayee.

I would also like to thank my colleagues in the Separation Technology Group at Eindhoven University of Technology for their warm welcoming and support from the moment that I joined till the last day: Adriaan, Dries, Wilko, Caroline, Pleunie, Mark, Laura, Dannie, Patricia, Ferdinand, Vignesh, Panos, Jordi, Blanca, Sona and Ali. Caroline and Pleunie are highly appreciated for your administrative support. I would like to thank my colleague Mayte who was working with me in the project "ionic liquids for CO_2 separation" for her support and ideas that she has shared with me throughout work. I would also like to express my deep appreciation to Dr. Marisa for her help and suggestions while I was writing my thesis. I am also very thankful to Lawien for useful discussions and translating my summary into Dutch. I would like to thank Nerea for her help in the liquid-liquid measurements.

I would also like to thank people of Chemical Engineering Department at the Petroleum Institute- Abu Dhabi for their suggestions, discussions and support during the period that I spent there: Dr. Abdallah Berrouk, Sabbir, Yasser, Dileep, Emad, Salah. I would also like to thank Sibi and Sreeja for their administrative support.

I would like to thank the people of Sustainable Process Technology at Energy & Research Center, the Netherlands where the last part of my PhD research was carried out, especially Dr. Wim Haije, Johan and Hans for scientific meetings, discussions and valuable suggestions.

I would like to express my sincere thanks to the Gas Research Center of the Petroleum Institute in Abu Dhabi, UAE for their financial support to carry out this research.

Last but not least, thanks to my family and friends for their motivation and support throughout my study.

Mamoun Althuluth

Eindhoven, 2014